



universität
wien

DISSERTATION

Titel der Dissertation

Templated Polymer Nanostructures – Chemical Sensors towards Cu(II) Ions and TiO₂ Nanoparticles

Verfasserin

Sadia Zafar Bajwa

angestrebter akademischer Grad

Doktorin der Naturwissenschaften (Dr. rer. nat.)

Wien, 2012

StudienKennzahl lt. Studienblatt: A091419

Dissertationsgebiet lt. Studienblatt: Chemie

Betreuer: Univ.-Prof. Mag. Dr. Peter A. Lieberzeit

Preface

This work has been done in the group of Chemical Sensors and Optical Molecular Spectroscopy from July 2008 till March 2012 under the supervision of Univ. Mag. Prof. Dr. Peter A. Lieberzeit at the Department of Analytical Chemistry, University of Vienna, Währingerstraße 38, 1090-Vienna, Austria.

Dedicated To My Parents

Zafar Hussain Bajwa

and

Shaheen Zafar Bajwa

Acknowledgements

In compilation of this dissertation, many persons and their help remained at my back and I am glad to have opportunity to acknowledge them by this life time document. First, I have to admit the fact that without the advice, support, and help of my research advisor *Univ. Prof. Dr. Peter A. Lieberzeit*, this work would never have realized in to a PhD dissertation. His ideas, guidance, friendly attitude, discussions, and feedback motivated me towards the progress of this research project. The first day when I entered in the group, my knowledge about the versatile field of molecular imprinting and chemical sensors was very preliminary. He helped me in laying and carrying out this project and above all guiding me at difficult but key moments of my work. I offer hearty thanks to him for always being there to look for academic and other issues. Here, I cannot forget to thank *O. Univ. Prof. Dr. Franz L. Dickert* for accepting me as a coworker in this group. I will remember him especially for his kindness towards my children. Furthermore, I want to thank ex and present colleagues of this group for their friendship, pleasant company, helpful discussions and valuable tips in the course of experimental work.

I must not forget to gratitude the Higher Education Commission (HEC) of Pakistan for granting scholarship that enabled me to pursue this PhD project in Austria. This scholarship brought me a splendid experience to meet and intermingle with persons belonging to different parts of the world with diverse culture and traditions. This not only enhanced my academic and research exposure but social experience as well. Further, I want to thank Austrian Exchange Service (ÖAD) for regulating scholarship matters between me and HEC.

I have to give a debt of gratitude to my parents, for their love, prayers, and efforts. They encouraged me to believe in myself and to achieve high goals. I greatly mean the love and support of my all brothers though thick and thin, always and especially during my stay here in Vienna.

Very importantly, I am greatly indebted to my kind husband *Dr. Muhammad Rauf*. Only because of his patience, sacrifices, and encouragement; I have been able to complete this dissertation. Finally, I cannot forget my very sweet and beautiful children, *Seerat Rauf* and *Abdul-Nafey Rauf*. Heartiest thanks to my family for their love and making my life so complete and shinning.



Sadia Zafar Bajwa
March, 2012

Table of Contents

PREFACE.....	I
ACKNOWLEDGEMENTS.....	III
<u>CHAPTER 1</u>	
INTRODUCTION.....	1
1.1 CHEMICAL SENSORS.....	1
1.2 COMPONENTS	2
1.3 CHARACTERISTICS	3
1.4 ACOUSTIC WAVE SENSORS	6
1.4.1 SURFACE ACOUSTIC WAVE (SAW) DEVICES	6
1.4.2 BULK ACOUSTIC WAVE (BAW) DEVICES.....	8
1.5 MOLECULAR IMPRINTING (MIP).....	10
1.5.1 APPLICATIONS	11
1.6 STATE OF THE ART LITERATURE OVERVIEW	12
<u>CHAPTER 2</u>	
Cu(II) IONS SENSOR LAYERS.....	17
2.1 INTRODUCTION.....	17
2.1.1 PROBLEM STATEMENT	17
2.2 MATERIALS AND STRATEGIES.....	19
2.2.1 FABRICATION OF DEVICES	19
2.2.2 SETUP OF MASS SENSITIVE MEASUREMENTS	23
2.2.3 MEASURING SETUP FOR CONDUCTANCE MEASUREMENTS	24
2.2.4 DESIGN OF ION-SELECTIVE POLYMERS	25
2.2.5 PREPARATION OF POLYMERS COATINGS	27
2.3 RESULTS AND DISCUSSION.....	30

2.3.1	AFM STUDIES OF DEVICES.....	30
2.3.2	BASIC SENSOR SIGNALS	31
2.3.3	SENSOR CHARACTERISTICS	39

CHAPTER 3

CHARACTERIZATION OF COPPER-IMPRINTED NVP POLYMER **46**

3.1	INTRODUCTION.....	46
3.2	EXPERIMENTAL WORK	46
3.3.	RESULTS AND DISCUSSION.....	46
3.3.1	CHARACTERIZATION OF PRE-POLYMER MIXTURE BY IR SPECTROSCOPY.....	46
3.3.2	CHARACTERIZATION OF PRE-POLYMER MIXTURE BY UV/VIS SPECTROSCOPY.....	51
3.3.3	INFLUENCE OF COUNTER ION ON IMPRINTING	52
3.3.4	INFLUENCE OF COUNTER ION ON SENSOR RESPONSE	54
3.3.5	DYNAMIC RANGE.....	55
3.3.6	RESPONSE TIME OF SENSOR LAYER	56
3.3.7	STOICHIOMETRIC ASSESSMENT OF IMPRINTING	56
3.3.8	INFLUENCE OF POLYMERIZATION SOLVENT.....	58
3.3.9	EFFECT OF COATED LAYER HEIGHT	60
3.3.10	REPRODUCIBILITY	62
3.3.11	AGING OF SENSOR DEVICE	63
3.3.12	SELECTIVITY STUDIES	64
3.3.13	REAL WATER SAMPLES	74
3.4	CONCLUSION	75

CHAPTER 4

TITANIUM DIOXIDE NANOPARTICLES IMPRINTING **77**

4.1	INTRODUCTION.....	77
4.1.1	PROBLEM STATEMENT	78
4.2	METHODS AND STRATEGIES.....	79

4.2.1	SYNTHESIS OF TITANIA NANOPARTICLES	79
4.2.2	SYNTHESIS OF Ti SOL GEL THIN FILMS	80
4.2.3	SYNTHESIS OF POLYURETHANE	80
4.2.4	PREPARATION OF NANOPARTICLE SUSPENSION	80
4.2.5	IMPRINTING STRATEGIES.....	81
4.2.6	MOISTURE CONTROL SETUP.....	83
4.2.7	AFM CHARACTERIZATION PROTOCOL.....	83
4.3	RESULTS AND DISCUSSION.....	84
4.3.1	TITANIUM DIOXIDE NANOPARTICLES (Ti NPs)	84
4.3.2	SURFACE IMPRINTING AND WASHING WITH ACIDIC MEDIUM.....	85
4.3.3	SURFACE IMPRINTING AND WASHING WITH SODIUM DODECYL SULFATE SOLUTION....	88
4.3.4	SURFACE IMPRINTING AND WASHING WITH ISOPROPANOL	88
4.3.5	DIRECT IMPRINTING AND WASHING WITH ACIDIC MEDIUM	90
4.3.6	MECHANICAL AGITATION EMPLOYING SURFACE IMPRINTING.....	95
4.3.7	INFLUENCE OF HEAT	96
4.3.8	INFLUENCE OF HUMIDITY.....	99
4.3.9	DESIGNING TITANIUM DIOXIDE TEMPLATE CAVITIES.....	102
4.3.10	BEHAVIOR OF NANOPARTICLES IN WATER	103
4.4	CONCLUSION	104
	ABSTRACT.....	106
	ABBREVIATIONS.....	109
	REFERENCES.....	111
	CURRICULUM VITAE.....	122

1. Introduction

This dissertation deals with the development of chemical sensors for the detection of divalent copper ions, and the fabrication of polymeric substrates with titanium dioxide imprinted cavities. An insight into necessary theoretical concepts, background, and relevant literature overview are given in this chapter.

1.1 Chemical Sensors

Chemical sensors have become an essential part of analytical science and also everyday life within the last few decades.^{1,2} The advancement of technology aroused the need for artificial sensing devices capable of working in a defined environment and it led to the invention of chemical sensors. The term *sensor* was coined during 1970s and since then hundreds of chemical sensors have been documented. Various definitions of chemical sensors have emerged as different views exist about their components and end use. Generally, a chemical sensor is a (small) device capable of continuously monitoring concentrations of chemical constituents in liquids or gases and converting this information in real time to an electrical or optical signal.³ According to IUPAC,⁴ a chemical sensor is a device that transforms chemical information, ranging from the concentration of a specific sample component to total composition analysis, into an analytically useful signal. In a nutshell, a chemical sensor is a device which responds to a particular analyte in a selective way through a chemical reaction and can be used for the qualitative or quantitative determination of the analyte. It is capable of translating chemical information into electrical signals and responds quickly to chemical quantities. It maintains not only its activity over a long period of time but also it is sensitive enough to detect low concentration values of analytes.

Moreover, usually small sample volumes with little/no efforts for sample pre treatment are required for the operation of chemical sensors.

1.2 Components

A chemical sensor usually comprises of two basic components; a chemical or molecular recognition system i.e. a receptor, and a physiochemical transducer.⁵ The typical arrangement of a chemical sensor is outlined in Figure 1.1.

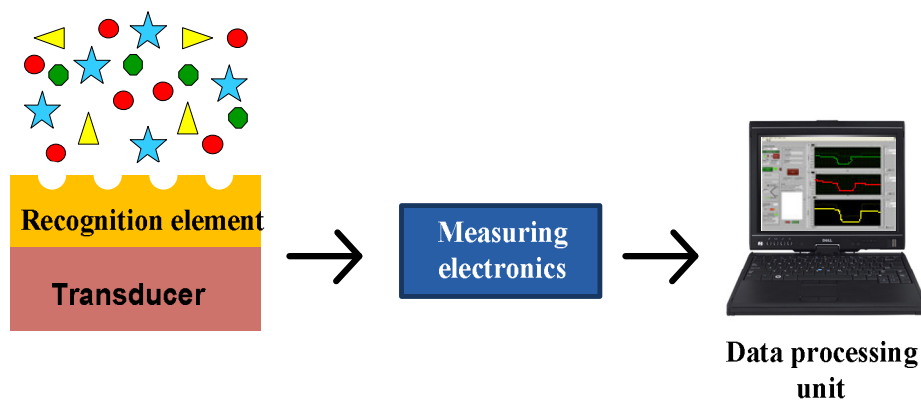


Figure 1.1: Schematic presentation of the basic components of a typical chemical sensor.

The *receptor*, in most of the cases, is a thin layer that is capable of responding selectively to a particular substance in its surrounding. The analyte is recognized on the basis of its size/dimension, chemical properties, etc. so, the term molecular recognition is used to describe this behavior of receptor layer. The process of interaction of the receptor with analyte goes on till it approaches an equilibrium state that could be either an interaction equilibrium state or a chemical reaction equilibrium state. In the former case, phenomena such as adsorption, ion exchange, and liquid-liquid extraction take place at the interface of analyte and receptor. In the latter case any chemical reaction

occurring at the surface is responsible for the recognition information. The physical or chemical changes resulting by the interaction of the analyte with the receptor are very often non electrical in their origin. A transducer translates these non electrical information into electrical quantity i.e. voltage, current, resistance, or frequency. This translation makes the basis of classification of transducers e.g. energy conversion transducer generates voltage or electric potential (electromotive force) as a measure of the quantity that is required to be measured. Some other types include limiting current transducer in vacuum photo tube and flame ionization detector, resistive transducer in Figaro sensor.⁶ In some sensors the receptor itself acts as a transducer e.g. metal oxide semi conductor sensors. These change electrical conductivity when come in contact with gases and this conductivity change is itself a measurable electrical signal. In most cases, both receptor and transducer are separate entities e.g. mass sensitive sensors in which the receptor is a thin sensitive layer whereas a piezoelectric quartz crystal acts as a transducer.

1.3 Characteristics

The performance of a chemical sensor depends upon several static and dynamic parameters which decide its efficiency towards a particular application. These parameters are listed below;

Sensitivity: It is the measure of the sensors response towards the designed analyte and refers to the change in the amount of sensor signal with the change of concentration of the target substance. Sensitivity of the sensor directly depends upon many factors like receptor and transducer materials, operating conditions, viscosity, and temperature of the measurement medium etc.

Selectivity: It refers to the degree to which a chemical sensor can distinguish target analyte from other species in the sample matrix and especially the substances of related structures. It is the measure of the contribution of the analyte concentration to the total sensor signal as compared to the contribution of concentration of other compounds. It largely depends upon the physical and chemical nature of the analyte and the type of receptor.

Reversibility: This parameter is interwoven with aforementioned factors and refers to the regeneration of the measured sensor signal to its original value or baseline conditions, when the target analyte is removed or washed off. This shows that the analyte is not bound to the sensor irreversibly. Along with operating conditions, reversibility is strongly influenced by the nature and extent of analyte/transducer interactions, kinetics and or thermodynamics of the sensing reaction.

Detection limit: This factor is also of prime importance and is the lowest value of a concentration that can be measured by the sensor under given conditions. Generally, a good sensor can respond to the concentration of analyte as low to ppb levels. It directly depends upon the type of receptor and transducer employed and the electronics if circuitry is involved in the built of sensor, in question.

Response time: It is the amount of time required to establish full scale output from zero concentration to a change in concentration of the analyte. In other words, how long a sensor signal takes time to establish equilibrium value towards a definite concentration. Generally, sensors with short response time are favoured for practical applications. Like other characterising parameters, response time is also affected by the operating conditions and physical factors.

Dynamic range: It is a set of concentration values ranging from the lowest limit to the upper value that can be detected with precision and accuracy. It is necessary for a sensor to cover a wide dynamic range to be applied for practical use.

Drift: It is a slow and stable change of the sensor response under given operating conditions and is determined by linear fitting of the experimental data points. Low amount of drift shows the stability of sensor signal and reveals its reliability.

Stability: It is the ability of a sensor to maintain its activity for a certain period of time. Usually, drift values are employed to determine the stability of a chemical sensor.

Ruggedness: The performance of a chemical sensor can also be affected by operating physical parameters e.g. temperature, humidity, viscosity etc. For practical applications a chemical sensor is considered appropriate if it can also work in harsh environments.

In a nutshell a chemical sensor which generates fast, sensitive, selective, precise, and accurate response with low drift, high signal to noise ratio and wide dynamic range is preferred. The chemical sensor should be small, cost effective, longterm stable, with good shelf life, and be able to work in harsh environments. All above factors decide its reliability for commercial use.

In the present research work, chemical sensors are designed employing quartz crystal microbalances (QCM), periodic microelectrodes (PME) device as the transducers, whereas nanostructured imprinted layers are used as the receptor materials. Thus, in coming sections, mass transducers and imprinting strategy are being described in detail.

1.4 Acoustic Wave Sensors

Acoustic wave sensors are so named because their detection mechanism in such sensors involves generation of a mechanical or acoustic wave. The acoustic wave propagates through/on the surface of the material. Changes in the characteristics of the propagation path affect the velocity and/or amplitude of the wave. These can be monitored by measuring the frequency or phase characteristics of the device and can then be correlated to the corresponding physical quantity being measured. All acoustic wave devices and sensors use a piezoelectric substrate to generate the acoustic waves.

In 1880, Pierre Curie and Jacques Curie observed that when certain dielectric crystals (those containing a polar axis) are subjected to an applied mechanical stress, an equivalent electric potential is generated in its response.⁷ This phenomenon was named as piezoelectricity and such materials were called as piezoelectric materials e .g. Ceramic, Quartz and Rochelle salt, etc. One year after the discovery of P. Curie and J. Curie, in 1881 Gabriel Lippmann applied basic principles of thermodynamics and proved piezoelectric effect mathematically and experimentally. The reverse of this phenomenon is called as inverse piezoelectric effect. Here, an electric field is applied across the material which causes mechanical distortion e.g. if high frequency alternating current is applied to a piezoelectric material, an ultrasonic wave of the same frequency can be generated.

1.4.1 Surface Acoustic Wave (SAW) Devices

As the name manifests, in such devices oscillation phenomenon is confined to the surface only. SAW transducers are produced from ST-cut quartz plates on which periodic microelectrodes are printed. The schematic diagram of typical microelectrodes patterned on a piezoelectric substrate is presented in Figure 1.2. When an alternating current is applied to the contact pads, an electric

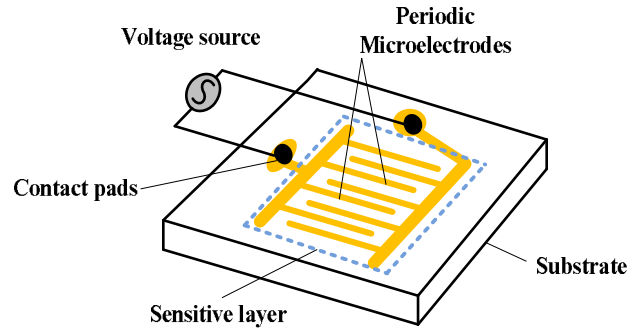


Figure 1.2: Schematic illustration of a surface acoustic wave device.

field is established between spatially periodic electrodes. Particles within the piezoelectric crystal are displaced and a surface acoustic Rayleigh wave is generated at one of the comb electrodes. It subsequently travels along the surface of the transducer until it interacts with the other electrode. This triggers an alternating voltage, which can be electrically quantified. Acoustic terminations are designed at each end of the piezoelectric material to absorb the bidirectionally launched surface acoustic waves. This concept of generation of electric field lines is illustrated in Figure 1.3.

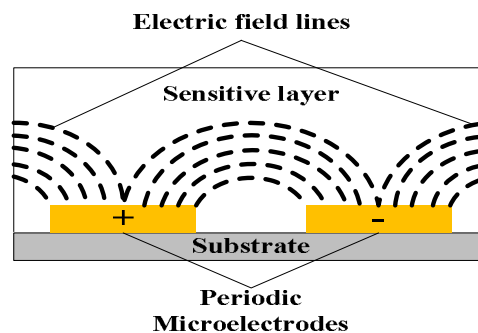


Figure 1.3: A conceptual view of waves generated at the surface of microelectrodes patterned on a piezoelectric substrate.

The frequency range of SAW transducers ranges from 50MHz and several GHz⁸ implying increased sensitivity towards mass sensing compared to other

piezoelectric materials. The main drawback of SAW devices is that normal SAWs can not be used in the liquid phase owing to excessive damping of the surface wave.⁹ After 1980s, SAW devices began to be used in electronics and telecommunications, chemical sensing and biomedical applications. Since then hundreds of papers have been published on different aspect of microelectrodes. Other than physical interpretation, interdigital capacitors are employed commonly for the detection of organic solvents vapours,¹⁰ humidity,¹¹ etc. The recent application of periodic electrodes are in the field of biology e.g. detection of bio species,¹² glucose, and urea,¹³ etc.

1.4.2. Bulk Acoustic Wave (BAW) Devices

The name implies that acoustic waves are generated in whole bulk of the material. The typical example that prevails in literature for such kinds of devices is quartz crystal microbalance (QCM). Graphical illustration of a 10MHz quartz with dual electrode geometry is given in Figure 1.4.

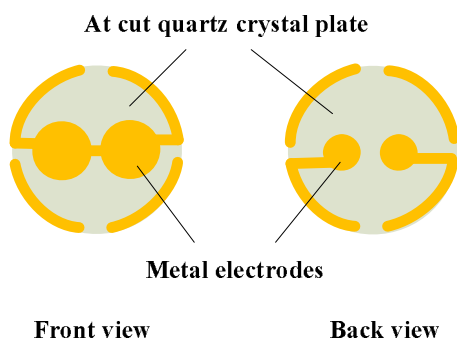


Figure 1.4: Schematic depiction of a 10MHz quartz crystal microbalance.

In this device the mass of the analyte is detected as the change in fundamental frequency of the quartz crystal resonator. The QCM resonates in the thickness shear mode (TSM) and are commonly used under vacuum, in gas phase, and liquid environments. It can measure mass densities down to a level of below

$1\mu\text{g}/\text{cm}^2$. A typical quartz crystal microbalance device consists of AT-cut quartz plate with metal electrodes on both the front and the back sides. This patterning of electrodes depends upon the configuration of analyte and the sensing medium. It makes the resonator thicker in the centre than at the rim and renders the displacement field to the centre of crystal by a mechanism called energy trapping.¹⁴ The oscillator circuit is employed to drive the resonator that usually operates in the time and frequency control mode. The QCMs of frequency range 10-20MHz are usually used in sensor applications whereas commercially available QCMs exhibit fundamental frequencies up to 50MHz, but at this point the crystal plates are too thin and therefore, suffer mechanically instability. Inherently, the resonance frequency of the QCM depends on temperature and pressure. There has been remarkable progress in the development of QCM principle in sensitive devices for the detection and concentration measurements of specific molecules in gaseous and liquid media.¹⁵ Historically, first studies in this regard were sought by the National Bureau of Standards (U.S.) in the early 1920's.¹⁶ In 1929, Bell Labs in collaboration with NBS delivered four complete temperature-controlled 100kHz oscillators to NBS. These oscillators were used as the national primary standard of radio frequency. Since the late 1950's quartz plate resonators have been used as sensitive microbalances for thin films adhered to the surface. Until 1980, only a few publications were documented regarding the use of QCM in chemistry or material science and mostly research work was done in the field of astrology and physics. During the same period it was shown that the QCM can function as a sensor even if immersed in water, other liquids or solutions. This discovery led to a rapid increase in the number of publications in chemistry, chemical engineering, and sub-disciplines as analytical, surface, material, and electrochemistry.

1.5 Molecular Imprinting (MIP)

In nature recognition is determined by directed, non-covalent interactions that define exact positions of the reaction partners in space. Several fields of chemistry aim at exploiting such interactions in the artificial systems; one of those is molecular imprinting. Here, a highly cross-linked polymer is synthesized in the presence of a template (usually the analyte-to-be or a structure analogue). Removal of the template from the matrix after polymerization leaves behind recognition sites within the material that can selectively re-incorporate the target compound of interest. The first type of imprinting is the covalent interaction or pre-organized approach that was mainly developed by Wulff and Sarhan.¹⁷ The template and monomer are linked to one another prior to polymerization. For actually achieving recognition sites, these covalent bonds have to be cleaved in the final polymer. The second type of imprinting interactions was developed by Mosbach and co-workers.¹⁸ It is the non-covalent or self assembly approach and the pre-arrangement between the template and monomer(s) is based on non-covalent interactions. The third approach is based on semi-covalent or sacrificial spacer interactions⁴ which is in fact a combination of the aforementioned approaches. Here, covalent interactions first arrange template and monomer and then non-covalent binding determines the recognition ability of the synthesized polymer.

Both in nature and chemical sensors, all types of interactions, be it non-polar, π - π , dipolar/hydrogen bonding etc. are employed. A variety of monomers and crosslinkers are available to suit the target analyte. The polymer matrices produced in this way exhibit favorable chemical, mechanical and thermal stability.

Molecularly imprinted polymers can be synthesized by a wide range of polymerization reactions including free radical polymerization,¹⁹

electropolymerization,²⁰ polyaddition,²¹ inorganic polymer systems,²² etc. For larger analytes, e.g. bio-species, surface imprinting into thin films and nanoparticles has substantial advantages. The approach has already led to many successful MIPs towards a range of analytes including e.g. *Escherichia coli* bacteria,²³ erythrocytes,²⁴ yeast cells,²⁵ TMV.²⁶

1.5.1 Applications

The pre-dominant advantage of the MIPs is versatility in terms of the analyte and the number of publications dealing with molecular imprinting protocols has increased to more than 800 per year since last three decades.²⁷ Imprints have been documented for formaldehyde,²⁸ toluene,²⁹ nicotine,³⁰ indoleacetic acid,³¹ carbohydrates,³² dengue virus,³³ albumin,¹⁹ etc. to only name a few. Hence, this strategy is a mean to design a large variety of receptors that are simple, cost effective, robust, stable, and straight forward. Now-a-days, the main focus of this area is material designing for bio species and the first reported such polymer deals with the detection of bacteria.³⁴ An innovative strategy towards bioorganisms imprinting is the stamping of these species over a polymeric substrate. The resulting imprints after the removal of stamps keep memory of the stamped organisms.³⁵ Template-directed preparation of nanoparticles is another novel and recent area of interest. A model compound can be employed during the preparation of nanoparticles and later particles are washed thoroughly to remove the template. This approach has decisive advantage of manifold increased sensitivity, offering larger surface area as compared to the imprinted polymer films.³⁶ The application of characteristic sequence as the template is also documented to trace the presence of microorganism e.g. dengue virus.³⁷ A very efficient sensor is reported for the detection of dengue virus choosing pentadecapeptide as the model protein and immobilizing it with poly acrylic acid.

In short, molecular imprinting strategy is an avenue to simple-to-operate, cost effective, robust, and precise sensors for a variety of analytes. New research areas are being introduced within its realm dealing with not only different imprinting protocols, nature of analytes but also with different varieties of transducers.

1.6 State of the Art Literature Overview

Metal ion detection:

Metal ions especially heavy metal ions have potential impact on the human health and environment. Therefore, sensitive and accurate methods of their detection are widely required and sought. Many laboratory based detection methods have developed including atomic absorption spectrometry (AAS),³⁸ inductively coupled plasma-atomic emission spectroscopy (ICP-AES),³⁹ flow injection,⁴⁰ electrochemistry,⁴¹ liquid chromatography,^{42,43} inhibition-based enzymatic assays,⁴⁴ solid-phase extraction,⁴⁵ and immunoassay.⁴⁶ In addition to the above mentioned ones, a range of strategies based on indicators have been developed for the detection of metal ions. In this regard, for colorimetric and fluourometric determination, several chromophore and flourophore dyes have been reported in the literature. One interesting example is the determination of 10 metal ions Ca(II), Mg(II), Cd(II), Hg(II), Co(II), Zn(II), Cu(II), Ni(II), Al(III), and Ga(III) by utilizing the common receptor 8-hydroxyquinoline attached to the conjugated flourophores. The whole sensor consequently is highly susceptible to the change in fluorescence depending upon bonding with metal ions.⁴⁷ Pattern recognition methods are adopted to evaluate the analytical utility of the sensor arrays. The identification accuracy is found ranging between 96-100% for these arrays. Another approach is colorimetric determination involving the color change due to the reaction of target metal ion with gold nanoparticles bearing modified surfaces.⁴⁸ Gold

nanoparticles are fabricated by sodium citrate as the metal ion reductant and the surface passivant. Later gold nanoparticles are functionalized symmetrically by various agents like DNA etc. to produce color change due to the interaction of metal with DNA.⁴⁹ Another work is about the synthesis of gold nanoparticles $13.6 \pm 0.4\text{nm}$ in diameter, functionalized with 11-mercaptoundecanoic acid and aggregated in the presence of Hg(II), Pb(II) and Cr(II) ions by ion template chelation process. Changes in the absorption spectra of particles are studied with Hyper Rayleigh Scattering (HRS) of the aggregate solution.⁵⁰ Another novel approach explains the synthesis of gold and silver nanoparticles utilizing naturally occurring bifunctional antioxidant gallic acid. These nanoparticles are exposed to Pb(II) solutions leading to limits of detection (LoD) in the micromolar range in presence of other metal cations in water. This is attributed to the unique coordination behavior of Pb(II) ions with flexible bond length and geometry that allows for the formation of a stable supramolecular complex producing plasmon coupling and an observable color change. Ca(II), Cu(II), Cd(II), Hg(II), Mg(II), Ni(II), and Zn(II) interact only with lesser numbers of ligands leaving the nanoparticles isolated so no spectral change is observed under the experimental conditions.⁵¹

Metal ions can interact with thiol groups via sulfur-metal interactions to give rise to stable complexes. A thin film of thiolated chitosan has been synthesized that can response selectively towards Hg(II) metal ions.⁵² When this film is exposed to the metal ions, it causes changes in film thickness that is investigated using spectroscopic ellipsometer and measuring refractive indices. Although this is more responsive to Hg(II) but also shows sensitivity towards Ni(II), Cr(III), and Cr(IV).

A colorimetric fiber for the heavy metal ions detection and adsorption is synthesized aminating polyacrylonitrile fiber with ethylenediamine. This fiber

is functionalized with 4-(2-pyridylazo)-1,3-benzenediol (PAR) for the reaction with metal ions. The metal ion is detected via investigating colorimetric properties and the limit of detection is described to be 1×10^{-6} mol/l for Pb(II) ions.⁵³ An interesting example of metal ion detection is found in a US patent where melanin is extracted and coated over gold electrodes of QCM. Melanin is isolated from *Thea sinensis* Linn and 5.3ng thick (0.38pmol) film is spread over the gold electrodes. Melanin acts as chelator towards metal ions and binding affinity is checked for various metal ions. For Hg(II) the LoD is 0.005ppm while for Mn(II), Pb(II), Cd(III) and Cr(III) it exhibits high sensitivities from 350Hz/ppm to 2500Hz/ppm.⁵⁴ Another study of metal ion detection by QCM is reported by synthesizing bipyridinium derivative and coating over front electrodes of QCM. Frequency variations are observed for Cd(II), Hg(II) and Pb(II) ranged between 10^{-4} and 10^{-2} M in strength. The response to Hg(II) is demonstrated significantly higher in comparison to other interfering analytes.⁵⁵

Another approach utilized three dyes 1,4-dihydroxyanthracene-9,10-dione, 3-hydroxy-2-naphthoic acid, and methyl-3-hydroxy-2-naphthoate as ligands for the interaction with metal ions and their subsequent measurement. MeOH:water (4:1) mixture is used as solvent of these dyes. In this paper ketone, hydroxyl, and carboxyl groups are explained to bind metal ions. The ligand properties of these dyes are investigated by UV/VIS absorption, fluorescent emission, HOMO/LUMO energy levels and job's method for evaluating electron distribution densities.⁵⁶ A study describes antibody based sensors for the detection of heavy metal ions. Two immunosensor format microwell KinExA™ 3000 are employed and four different monoclonal antibodies specific for chelated complexes of Cd(II), Co(II), Pb(II), and U(IV) ions and are incubated with these complexes. The KinExA format results in to 10–1000fold greater sensitivity because of affinity differences between monoclonal antibodies and immobilized metal–chelate complex. The

analytical method is applied to ground water samples spiked with Cd(II) and the mean analytical recovery of added Cd(II) is reported to be $114.25 \pm 11.37\%$. In another investigation various analytical reagents are trapped in cellulose film and among these, films modified with 1-(2-pyridylazo)-2-naphthol (PAN) are produced by dissolving cellulose film and PAN in ionic liquid 1-butyl-3-methylimidazolium chloride and then precipitating with water. Later, these are employed to determine Zn(II), Mg(II), and Ni(II) colorimetrically and LoD are reported at the 10^{-6} mol/l level.⁵⁷ A novel way to detect metal ions in aqueous solution is studied developing thin, colored films of chitosan and poly(allylamine) (PAH) cross-linked with hexamethylene 1,6-di(aminocarboxysulfonate) (HDACS). These films exhibit selective detection of metal ions due to the thickness and or color changes. Chitosan and HDACS films are selective towards Cr(IV) binding whereas PAH-HDACS shows preference for both Cu(II) and Cu(I) salts.⁵⁸

Nanoparticles:

Nanotechnology has emerged during the last two decades due to the interesting physiochemical properties of nanoparticles that are very different from bulk materials. The most notable feature of nanoparticles is high surface-area-to-volume ratio where the behavior of atoms present at the surface dominates over those inside the particle. Moreover, the size of particles falls in the range where quantum effects play more important role than in bulk materials. Owing to extensive research and development in the realm of nanoscience, it is not straightforward to review published work however most documented papers are related to metal (Au,⁵⁹ Ag,⁶⁰ Pt,⁶¹ FePt,⁶² CdTe,⁶³ etc.) and metal oxide nanoparticles (TiO₂,⁶⁴ ZrO₂,⁶⁵ CeO₂,⁶⁶ FeO,⁶⁷ CuO, NiO,⁶⁸ etc.) with some recent reports about chitosan nanoparticles.⁶⁹

In 1972, Fujishima and Honda discovered the phenomenon of photocatalytic splitting of water on a TiO₂ electrode under ultraviolet (UV) light.⁷⁰ Since

then, numerous efforts have been devoted to the research of TiO_2 materials. In addition to nanoparticles this includes also mesoporous and nanoporous materials,⁷¹ aerogels,⁷² opal and photonic materials⁷³ and nanosheets⁷⁴. A part of the published material accounts for the structural properties of nanoparticles as anatase, rutile, etc. and effect of various physical and chemical parameters over the synthesis and stability of these structures are demonstrated.⁷⁵ The thermodynamic stability of many nanoparticle phases is also often investigated.

Despite increasing research and development in nanoscience and exhaustive reports about nanoparticles, their types, properties and applications, still no study has contributed towards the imprinting of nanoparticles or fabrication of their nano cavities. The second part of this dissertation deals with the fabrication of titanium dioxide nano voids on different polymeric substrates to give forth transducer that could be potentially applied to take up nanoparticles reversibly. Thus, to the best of our knowledge, for the first time a polymeric receptor usable to detect titanium dioxide nanoparticles is reported in the present dissertation.

2. Cu(II) Ions Sensor Layers

2.1 Introduction

Metals play a very important role in our daily life and their presence is necessary for many physiological and biochemical mechanisms.⁷⁶ Copper is one of the trace metals that have high biological and environmental significance and the effects exerted by its presence, efficiency, and deficiency in food and water are recent topics of health research.⁷⁷ The excessive intake of copper is declared toxic by nutritionists and one may suffer from abdominal pain, cramps, nausea, diarrhea, vomiting, and liver damage. The copper toxicity in the presence of low zinc level can even cause serious problems like schizophrenia, senility, etc. The Institute of Medicine at the National Academy of Sciences established 10mg as the tolerable level of copper nutrient in food⁷⁸ while World Health Organization (WHO) has recommended 2mg/l as the safer limit of copper ions in drinking water.⁷⁹

2.1.1 Problem Statement

From the abovementioned, it is clear that sensitive and selective determination of copper, especially in water, is of substantial economic and ecological interest. There are some already established analytical methods for this purpose, e.g. anodic stripping voltammetry,^{80,81} AAS,^{82,83} liquid chromatography,^{84,85} ICP,⁸⁶ X-ray fluorescence,⁸⁷ etc. These analytical techniques are sophisticated, sometimes involving complicated operating methods and often require sample preparation or pretreatment, so there is a pressing need to develop a measurement system that is simple, robust, cost effective, and precise.

Ion imprinting is a recent field within the domain of molecular imprinting. In 1976 for the first time, Nishide et al described ion template effect during the synthesis of a chelating polymer.⁸⁸ Afterwards, it gained importance and among some examples of successful MIP include poly(4-vinylpyridine) crosslinked with 1,4-dibromobutane,⁸⁹ diethyl vinyl phosphonate and acrylic acid with *N,N*-methylene diacrylamide,⁹⁰ chitosan with epichlorohydrin,⁹¹ 1-vinyl-2-pyrrolidone and divinyl benzene,⁹² poly(4-methyl-4-vinyl-2,2-bipyridine) copolymers with divinyl benzene,⁹³ copper(II) methacrylate complexes with water, pyridine, and 4-vinylpyridine,⁹⁴ seed emulsion polymerization of styrene, butylacrylate and methacrylic acid in water,⁹⁵ double imprinting of copper employing chitosan succinate,⁹⁶ organic inorganic hybridization with sucrose and polyethylene glycol.⁹⁷

In the MIP area, most of the published documents about ion imprinting deals with the synthesis, characterization of ion imprinted polymers/resins and or their adsorption studies instead of the development of real sensor devices.⁸⁸⁻⁹⁸ However, examples of published papers where QCM is used as the transducer are rare. One of the documents describes the surface complexation of the metal ions at thiodisuccinic acid functionalised self-assembled monolayer (SAM) modified electrodes on 10MHz AT-cut quartz resonators.⁹⁹ Another paper reported imprinted polymer matrices coated on the mass sensitive microbalance for the determination of copper metal ions in waste water.¹⁹ Here, methacrylic acid is crosslinked with triethylopropane trimethacrylate in the presence of copper ions under ultraviolet light and the sensitivity of QCM-IP device is reported to be below 100Hz against 0.1mM copper. Another published QCM sensor for Cu(II) ions detection involves imprinted sol gel synthesis. The sensitivity in this case is reported to be 350HZ for 0.1mM Cu(II) ions with less selectivity (250Hz for Zn(II) ions).¹⁰⁰

For the development of copper sensor by ion imprinting, the polymer matrices with improved sensitivity, selectivity, in addition to the experimental manipulation involving different kinds of transducers are required. This chapter deals not only with the synthesis but also the screening of copper ion imprinted polymers using different ligands as β -cyclodextrin, polyvinylphenol and N-vinyl-2-pyrrolidone. A systematic study is carried out to address the influence of ligand upon copper ion imprinting whereas further insight in to the binding mechanism is provided by IR and UV/VIS spectrometry. As ion imprinting into polymer matrices is a challenging task owing to small ionic radii and the absence of geometric fit. Furthermore, imprinting protocol has to consider closely related ionic radii, chemical and physical properties of the target and interfering ions. This issue is addressed studying varying complexabilities of functional monomers. Thus synthesized ion-imprinted polymer can reproduce coordination number, size and geometry of that complex. Sensor properties are exploited and validated employing two different types of transducers, QCM and PME. One of the synthesized polymers (using N-vinyl-2-pyrrolidone) yields about 650Hz and 750 μ S sensitivity at 1mM concentration of Cu(II). The selectivity was found to be double than the effect caused by interfering bivalent ions and three times against monovalent ions. This sensor studies explains the first practical applicability of the imprinted layers for the determination of copper in real water samples.

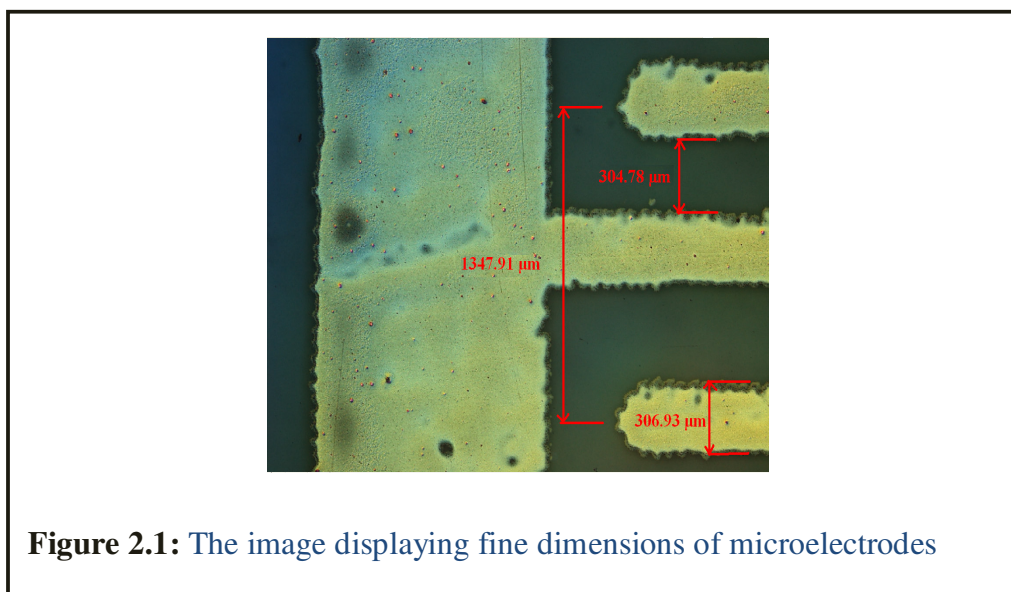
2.2 Materials and Strategies

2.2.1 Fabrication of Devices

Electrode Design for Quartz Crystal Microbalance (QCM): A dual electrode design was developed with two electrodes on the front face and two on the rear face for quartz crystal microbalance with 14mm in diameter. The

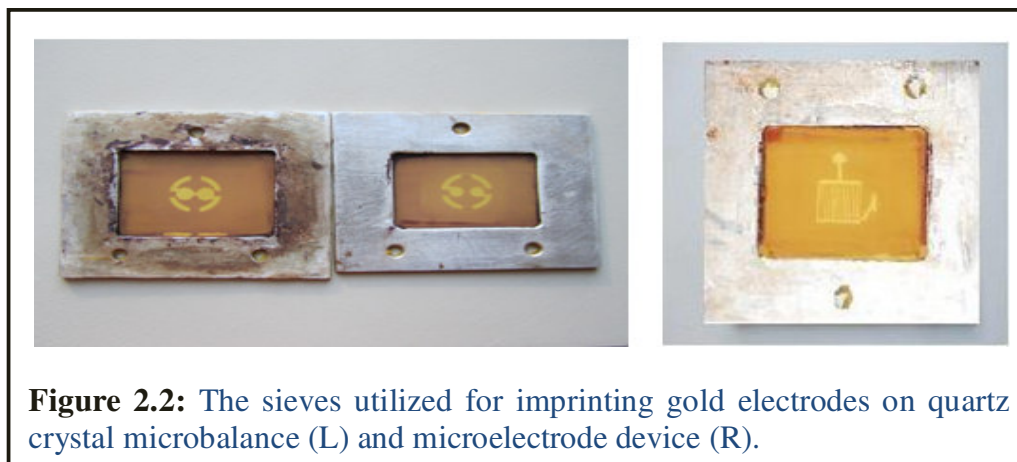
electrodes on the front side were larger in diameter (5mm) and connected to one another and to the electrical ground. The ones on the opposite side were kept smaller (4mm), separated, and connected to the phase of the respective channel. This geometry compensates for the non-specific effects by temperature fluctuation, viscosity changes, etc. without the loss of appreciable sensitivity. This design was utilized for imprinting electrodes over quartz crystal microbalance sheets.

Electrode Design for Periodic Microelectrodes (PME) Device: The structure of prepared PME is shown in Figure 2.1. Microelectrodes with



periodic geometry was designed with 9 conducting fingers at each electrode, respectively. Each finger was $\sim 300\text{--}310\mu\text{m}$ in width (α) and 7.6mm in length while the gap between two fingers was adjusted to be $\sim 304\mu\text{m}$. Spatial period was calculated as $\lambda = 4\alpha = 1224\mu\text{m}$ whereas total sensitive area available for coating polymer layers was $7 \times 12\text{mm}$. Thus the meander length of PME was calculated as $L = 2 \times 9 \times 7 = 126\text{mm}$.

Preparation of Metallic Sieves for Electrode Screen Printing: The sieves employed to cast electrodes imprints on QCM substrates, and microelectrodes on glass substrates, are displayed in Figure 2.2. To fabricate these sieves, a



cloth of 21 μ m mesh size was tightly glued on a metallic frame. A uniform layer of a UV sensitive polymer (Azocol[®] Poly-Plus S from KIWO) was coated on this screen and kept in a dark, dust free chamber at 30-40°C for half an hour till found dry. The desired electrode design was printed in black color on a transparent sheet and fixed on the glass plate in a UV chamber (UV-Belichtungsgerät 1, 220V, isel-automation, Germany). The fabricated sieve was placed on the electrode design in a way so the sketch was in the middle of sieve. The UV chamber was closed and the sensitive layer on the sieve was exposed to UV light for 30 seconds. Finally, the sieve was washed with warm water to remove unhardened polymer and to obtain the final electrode design.

Imprinting of Electrodes: AT-cut Quartz crystal sheets of 10MHz fundamental frequency (purchased from Great Microtama Industries, Surabaya, Indonesia) were chosen for the mass sensitive measurements whereas the conductometric investigations were carried out utilizing glass plates, roughly of 4.4cm x 5.1cm dimension. Either of the devices, quartz sheet or glass plate, was placed on to a Teflon block and affixed with a

vacuum pump. Then relevant sieve was fixed over the device according to the Figure 2.3.

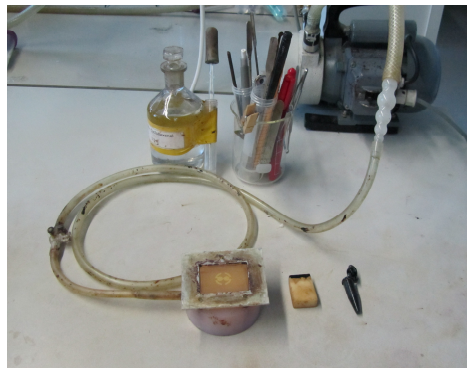


Figure 2.3: The setup employed for imprinting of gold electrodes on transducers.

A smooth and uniform layer of gold past was spread over the sieve using the regular strokes of a sharp rubber edge. This resulted into casting of the electrode image over the device. Then devices were baked in an oven to remove the organic residues. QCM sheets were heated at 400°C for 4 hours and PME plates were placed in the oven at 530°C for 3 hours. A similar procedure was followed for the imprinting of gold electrodes on the rear side of quartz sheets. Figure 2.4 displays QCM sheets along with PME device.

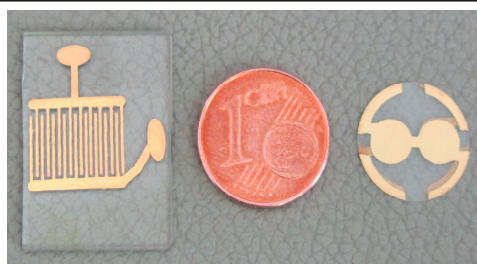


Figure 2.4: Microelectrodes device with periodic electrode patterns (L) and quartz crystal microbalance sheets (R) with dual electrode geometry.

Preparation of Devices: Quartz crystal sheets were taken out of the oven, cooled in the air, and washed with acetone. These were directly utilized for coating the polymer films to carry out mass sensitive measurements, whereas PME devices were further finished before performing sensor measurements. The electrical connections of devices were built by electroplating contact pads with 1M solution of $\text{CuSO}_4 \cdot 5\text{H}_2\text{O}$ at 6V (Votcraft®).

2.2.2 Setup of Mass Sensitive Measurements

Measuring Cell: Mass sensitive measurements were carried out by mounting the quartz sheets into a specially designed cell that is displayed in Figure 2.5.

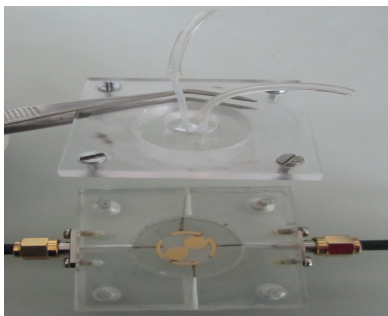


Figure 2.5: Measuring cell with QCM adjusted inside.

This cell had four electrical connections and consisted of following parts; a holder to support the QCM, a cap for the inflow and outflow of solutions, a base to support quartz holder and a lid to tighten the cap. The former two were composed of PDMS (polydimethylsiloxane) while the latter two parts were of PMMA (polymethylmethacrylate). The quartz sheet was adjusted in the cell in a way that larger and coated electrodes faced the liquid phase above it while smaller electrodes remained in the air facing electrical connections of the cell base. During measurements this arrangement ensured reduced conductivity and electric field effects due to the formation of field lines.

Experimental Setup:

The measurement assembly arranged for the mass sensitive investigations is shown in Figure 2.6. The inlet and outlet of the measuring cell were

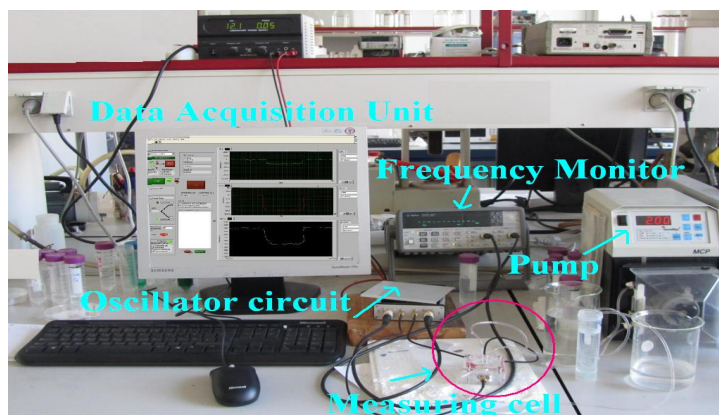


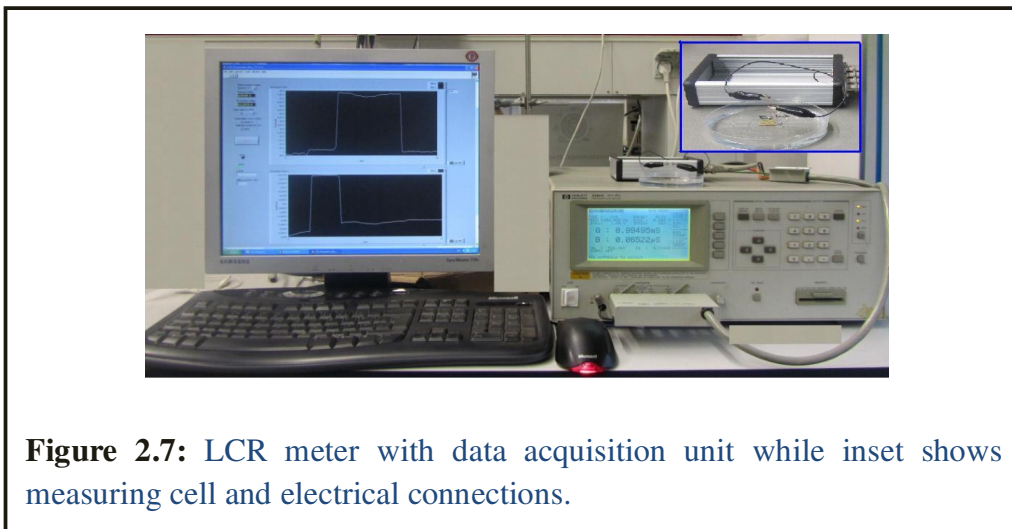
Figure 2.6: Measuring setup to monitor frequency shifts.

connected to the test solution and waste sources with the help of tubing (0.5mm diameter). The liquid was pumped in to the cell with the help of a pump (ISMATEC MCP V5.2) maintained at the flow rate of 2ml/min during all measurements. For QCM measurements, electrical connections were made and the measuring cell was connected with a DC power supply to the oscillator circuit that was further connected to an Agilent 53131A 225MHz Universal Counter for frequency monitoring. The circuit was attached to an input DC voltage source that was maintained at 12V, 60mA. The frequency counter was connected to a PC unit with especially designed software for the data acquisition and storage. All mass changes were observed as frequency shifts by the software. All measurements were carried out at $25 \pm 2^\circ\text{C}$.

2.2.3 Measuring Setup for Conductance Measurements

The experimental setup for measuring conductance signals is displayed in

Figure 2.7. The periodic microelectrode device was dipped in a cell



containing 50ml test solution and electrically connected to an Inductance LCR meter (Hp 4284A). It was ensured during all measurements that device surface was fully immersed into the test liquid to obtain optimal response. The LCR-Meter was read out by a PC with custom-made software to monitor sensor signals generated by PME device. All measurements were carried out at $25 \pm 2^\circ\text{C}$.

2.2.4 Design of Ion-Selective Polymers

All the chemicals and reagents were purchased from Merck and Sigma-Aldrich in the highest available purity. De-ionized water was used for the rinsing purpose and as a solvent. Stock solutions were prepared by dissolving defined amounts of the respective metal in the de-ionized water. These stock solutions were diluted as required for further use.

The synthesis procedures of Cu(II) ion-imprinted polymers are described below. For the sake of interpretation, these polymers systems are notated as Cu(II)-IPI, Cu(II)-IPII, Cu(II)-IPIII. In all these polymers $\text{CuCl}_2 \cdot 2\text{H}_2\text{O}$ was added as the source of Cu(II) ions.

Synthesis Protocol for Cu(II)-IPI:

3mg of $\text{CuCl}_2 \cdot 2\text{H}_2\text{O}$ were dissolved in 50 μl of methanol (MeOH) and 200 μl of tetrahydrofuran (THF). Afterwards, 1mg of β -cyclodextrin was added in 50 μl of dimethylformamide (DMF) and added to the copper solution to develop a Cu(II) complex with β -cyclodextrin. To synthesize polyurethane, 10mg of polyvinylphenol (PVP) and 150mg of diphenyl 4,4'-diisocyanate (DPDI) were dissolved in 200 μl of THF. This pre-polymer solution was purged with N_2 and heated at 70°C for 30 minutes in a water bath till the onset of gel point. Out of this polymer mixture, 50 μl were mixed with the solution containing metal complex and 300 μl of THF to yield the ion-imprinted polymer. To prepare the film for mass measurement, 60 μl of imprinted polymer mixture were diluted with 40 μl of THF to obtain the required layer height in the range of 400nm. A reference polymer was prepared and diluted exactly the same way except the addition of copper, but including β -cyclodextrin.

Synthesis Protocol for Cu(II)-IPII:

In a further approach, Cu(II) ion-imprinted polymer was designed following the synthesis procedure of Cu(II)-IPI, leaving out β -cyclodextrin. To synthesize polymer, 3mg of $\text{CuCl}_2 \cdot 2\text{H}_2\text{O}$ were dissolved in 50 μl of MeOH and 200 μl of THF. Polyurethane was prepared with 70mg of PVP, 80mg of DPDI, in 200 μl of THF. After purging with N_2 and heating at 70°C, 50 μl were mixed with metal ion solution. The resulting mixture was diluted with 300 μl of THF to make a stock solution of the imprinted polymer. Finally, 60 μl of imprinted polymer were dissolved in 40 μl of THF to coat the device with required film layer height. A reference polymer was prepared and diluted exactly the same way but without adding copper.

Synthesis Protocol for Cu(II)-IPIII:

Finally, a free radical polymerization approach was adopted and 1-vinyl-2-pyrrolidone (NVP) as the functional monomer, ethylene glycol dimethyl methacrylate (EGMA) as the crosslinker, and Cu(II) as the template were chosen. 3mg of $\text{CuCl}_2 \cdot 2\text{H}_2\text{O}$ were directly dissolved in 300mg of NVP hence it was used both as a complexing agent and a solvent. This solution was sonicated for 30 minutes. 30mg out of this Cu(II)-NVP complex were transferred to another reaction vial and 60mg of EGMA, 3mg of 2,2'-azo-bis-isobutyronitrile, 500 μl acetonitrile (AcN) as solvent and porogen, were added. This reaction mixture was again sonicated for half an hour to ensure complete mixing of all ingredients. The pre polymer mixture was kept under UV for 45 minutes to polymerize. It was directly employed for coating polymer layers on the devices without any dilution. A reference polymer was prepared exactly the same way excluding the addition of copper.

2.2.5 Preparation of Polymers Coatings

To achieve the homogenous polymer surface for the mass sensitive measurements, the quartz crystal sheet was cleaned with acetone and mounted on a spin coater as shown in Figure 2.8. 5 μl out of the respective diluted

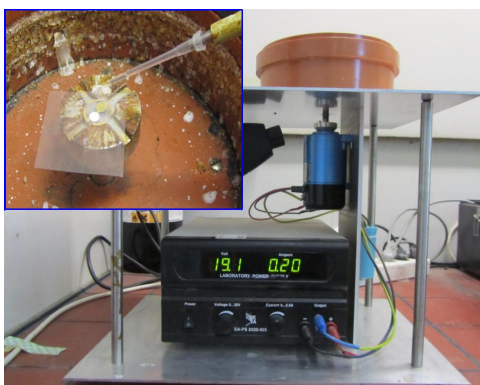


Figure 2.8: Picture displaying the spinner and coating procedure.

polymer were spin-coated on one of the quartz sheet electrodes, at a speed of 2000-3000 rpm for nearly 45 seconds. After sufficient drying the polymer film was masked and the other electrode surface was coated with the same quantity of imprinted polymer. The aforementioned polymer film thickness was calculated comparing the resonance frequencies before and after the film coating on a network analyzer. Figure 2.9 shows network analyzer (ENA series of Agilent Technologies model no. E5062A, along with QCM sheet.

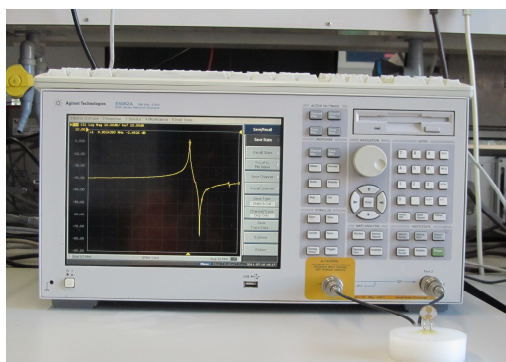
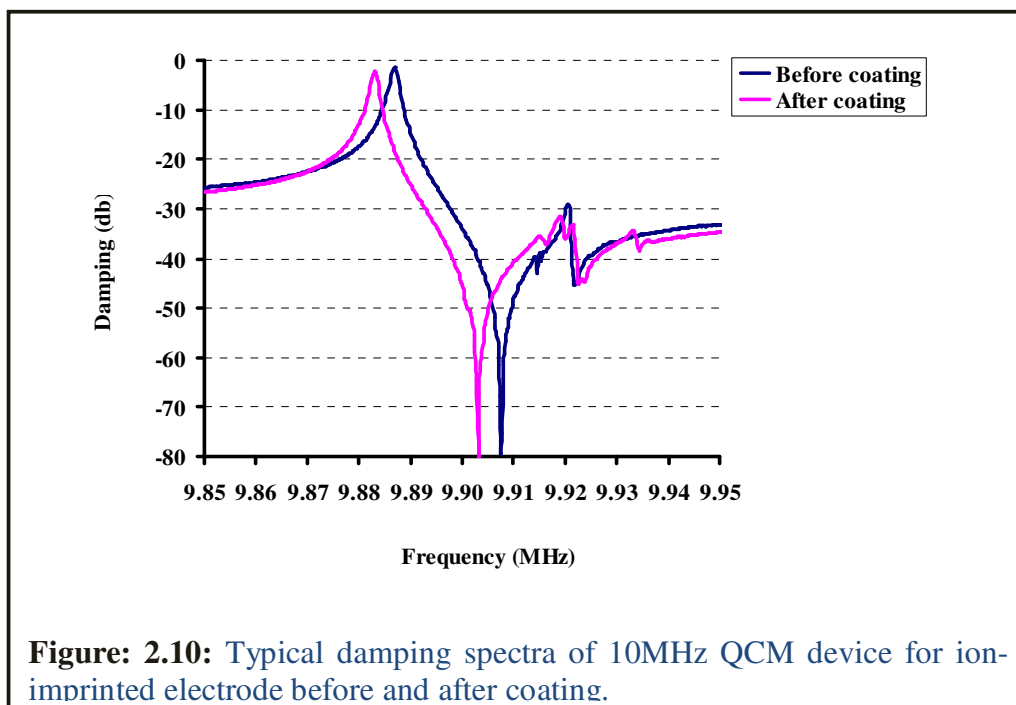


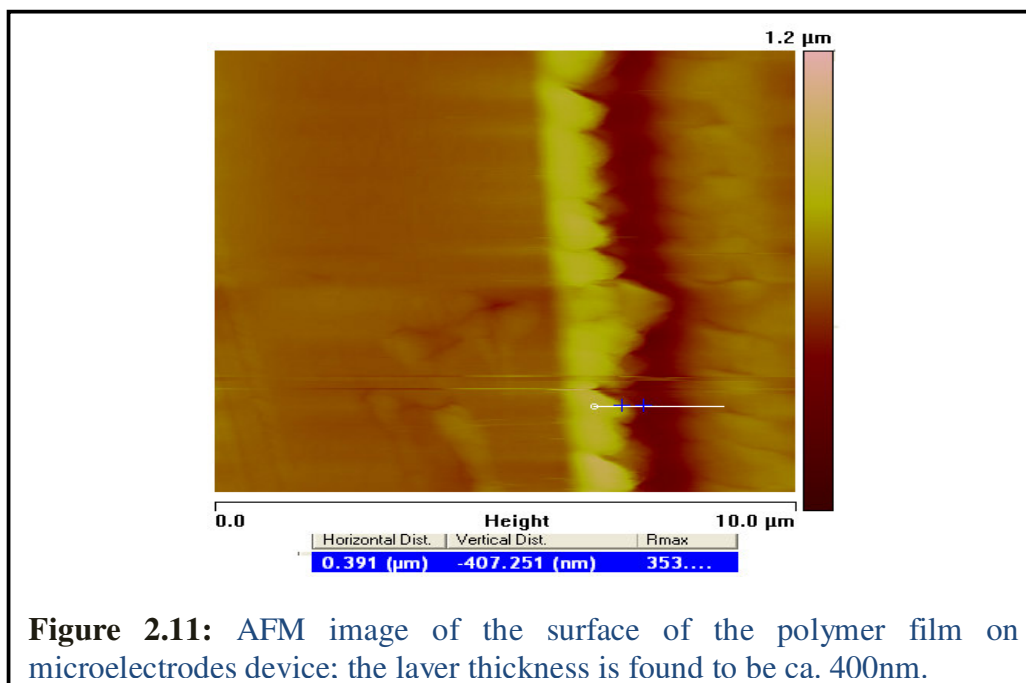
Figure 2.9: QCM mounted to a network analyzer.

One of the each representative damping spectra obtained before and after coating the polymer film, are displayed in Figure 2.10. To conduct mass sensitive experiments, QCM devices were coated with the polymer layers of equal thickness i.e. $400 \pm 30\text{nm}$ that corresponds to the resonance frequency difference of 10kHz.

PME devices were also spin- or drop-coated. In the case of Cu(II)-IPI and Cu(II)-IPII, 10 μl were spread on the surface of device and then spun at the speed of 1000-2000 rpm for 2 minutes. For coating Cu(II)-IPIII, 10 μl were just spread to ensure complete coverage of microelectrodes. Afterwards, the device was placed directly under UV for 25-35 minutes to complete polymerization. The layer height of the polymer film in this case was



confirmed by recording AFM images on a VEECO Nanoscope IVa AFM/STM system. Section analysis revealed layer heights; one of the representatives is displayed in Figure 2.11.

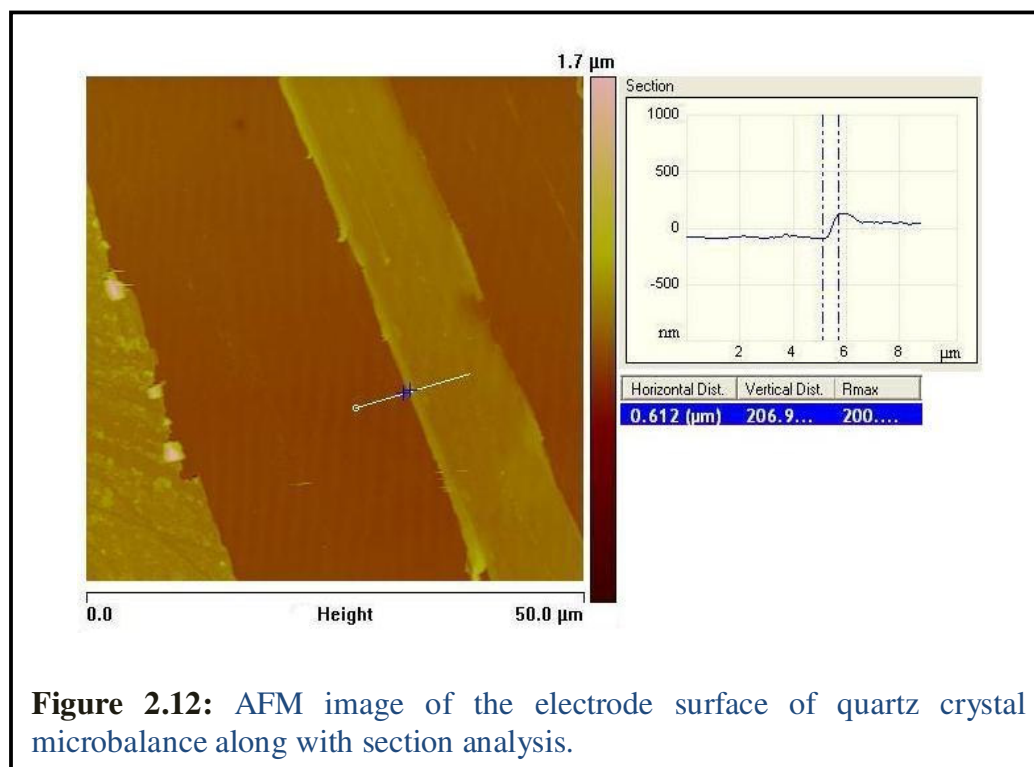


The film thickness on the surface of microelectrodes is found to be ca. 400nm. After coating, devices were cured overnight at room temperature. To remove the template copper, devices were immersed in 100ml of de-ionized water for 24 hours at room temperature. Gentle stirring ensured complete removal of the template ions. After measurements, devices were washed several times with water and stored at room temperature until next use.

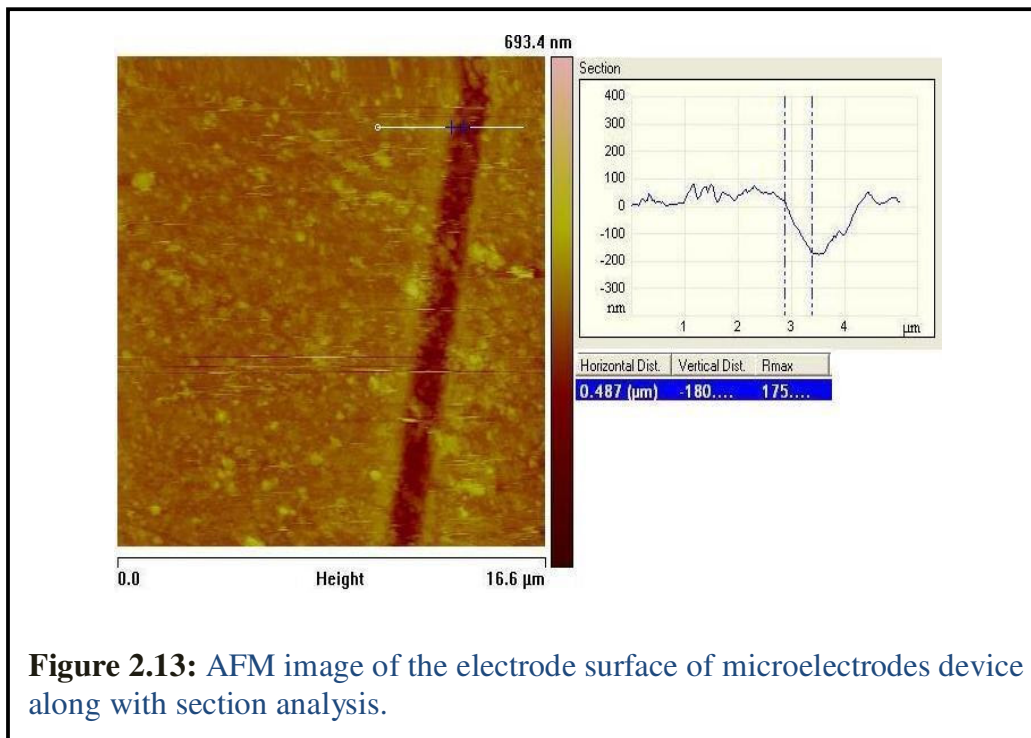
2.3 Results and Discussion

2.3.1 AFM Studies of Devices

The thickness of gold layer over electrodes of QCM and PME devices was verified by scratching it and recording the surface images by AFM. The section analysis of a typical AFM image for the QCM gold layer is presented in Figure 2.12. This manifests that about 200nm of gold is deposited on the QCM surface.



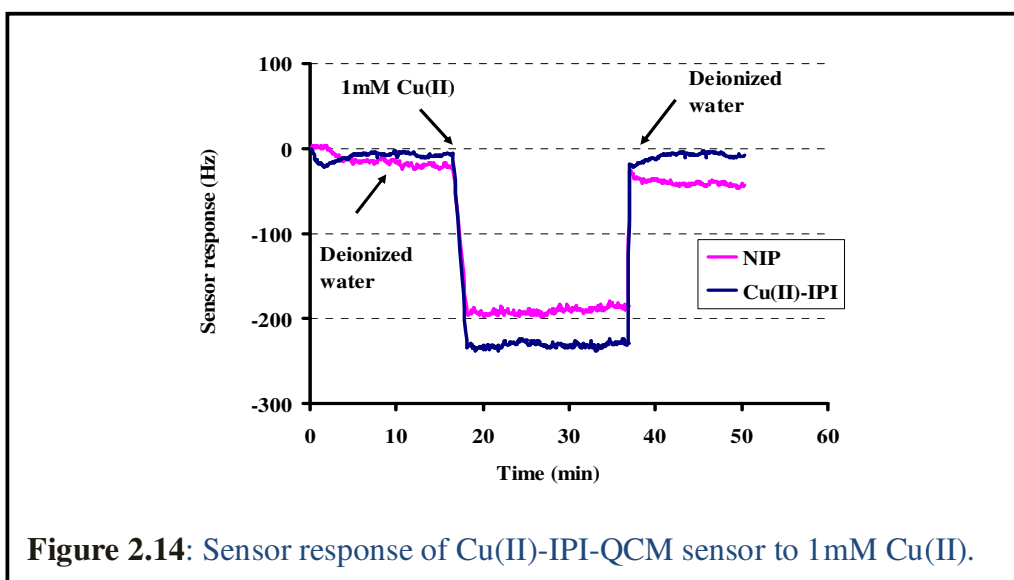
The gold thickness bears more significance for the microelectrodes device as it is directly related to the generation of electric field lines. A respective AFM picture is displayed in Figure 2.13 that reveals the gold layer of the electrode is ca. 180nm thick.



2.3.2 Basic Sensor Signals

(i) Mass sensitive measurements

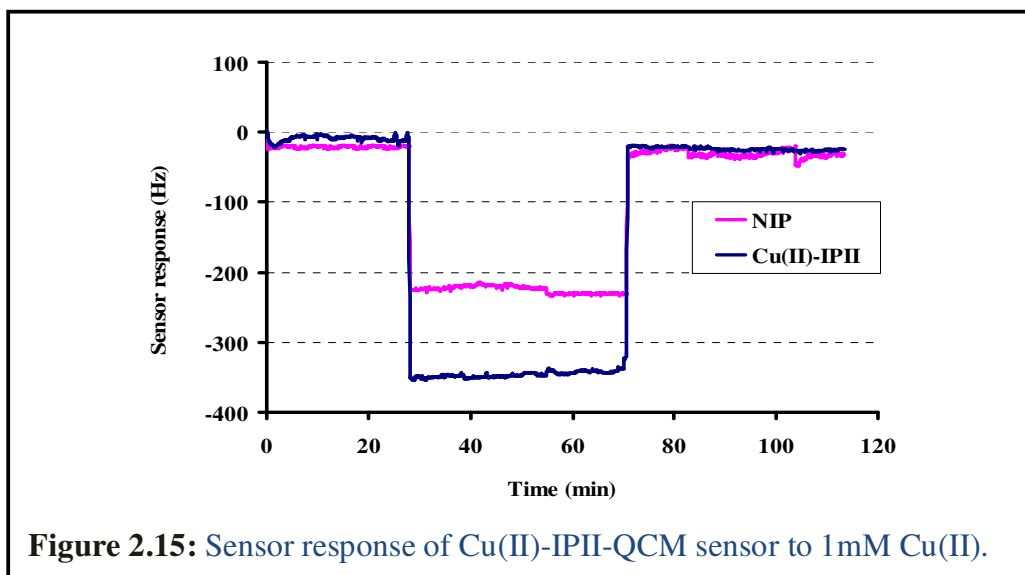
Foremost of all, it was important to ensure the existence of required interaction sites in the imprinted polymer films. The mass sensitive response for Cu(II)-IPI is presented in Figure 2.14. To record all mass sensitive responses, the quartz crystal sheets, prepared and coated by section 2.2.4 and 2.2.5 were washed thoroughly with de-ionized water in order to remove the template ions and unpolymerized residues from the film surface. These were mounted in the measuring cell (section 2.2.2). First, de-ionized water is



flushed into the cell to maintain the equilibrium between the aqueous phase and the layer surface and also serves to remove template ions. After a constant sensor base line has been observed, 1mM Cu(II) solution is pumped in to the cell. As soon as the metal ions approach the film surface, the frequency gradually decreases due to the incorporation of metal ions into cavities. The imprinted polymer shows frequency shifts up to $231 \pm 3\text{Hz}$, soon after flushing copper solution in to the cell. The non-imprinted one also causes a considerable decrease of basic frequency i.e. $190 \pm 13\text{Hz}$. Thus a net sensor response of $40 \pm 5\text{Hz}$ is obtained. After some time, the system was switched to de-ionize water. The frequency reverted to its original value due to desorption of the metal ions from the cavities. These changes prove the reversibility of the QCM-IPI sensor. For designing Cu(II)-IPI, β -cyclodextrin is used as the functional monomer or ligand and to bind divalent copper ions coordinatively. Cyclodextrins are macrocyclic glucose oligomers with hydrophobic cavities, the ability for molecular recognition and the formation of host guest complexes¹⁰¹ including metals as hosts.¹⁰² The significant response on the IIP of 231Hz manifests the ability of β -cyclodextrin to act as a ligand for Cu(II) ions and to generate cavities for their reversible

recognition but the considerable response of non-imprinted polymer film consolidates the presence of unreacted β -cyclodextrin in the polymer matrix. β -cyclodextrin has ability to capture metal ions so it happens actually during the injection of copper and non-imprinted electrode has showed influential frequency shift.

In the same way, Cu(II)-IPII system was also examined and the results obtained are depicted in Figure 2.15.



This polymer system proves more efficient for the copper ion binding and the response is almost 100Hz larger than in the case of β -cyclodextrin-Cu(II) complexed polymer system. The device signal exhibits the general features of an appreciable sensor response e.g. stability and complete reversibility. However, again the non-imprinted polymer layer yields pronounced effects, for this polymer matrix $225 \pm 5\text{Hz}$ and $346 \pm 5\text{Hz}$ are frequency shifts arising from non-imprinted and imprinted layers respectively, hence obtaining $121 \pm 9\text{Hz}$ as the net sensor response.

The sensor signals generated by the non-imprinted and imprinted layers of Cu(II)-IPIII system are presented in Figure 2.16. The ion-sensitive layer

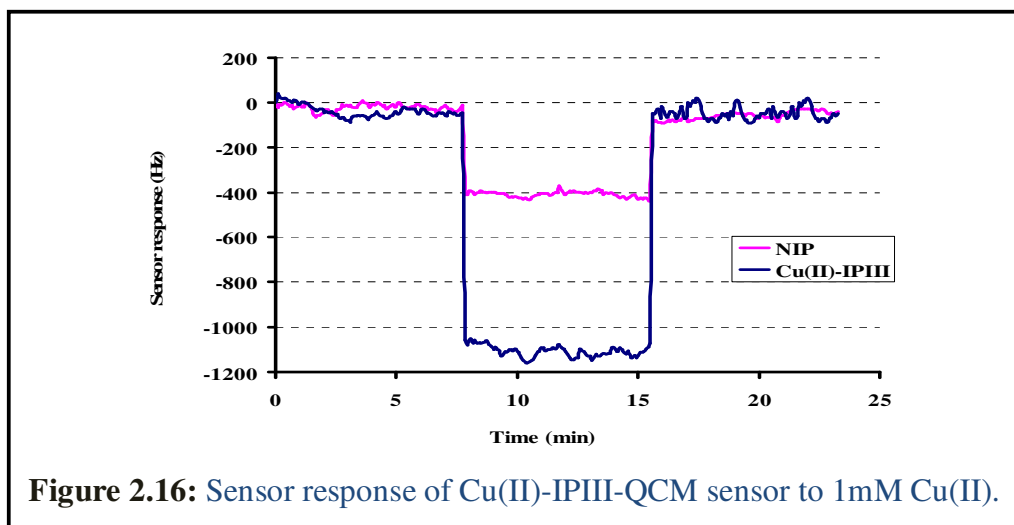


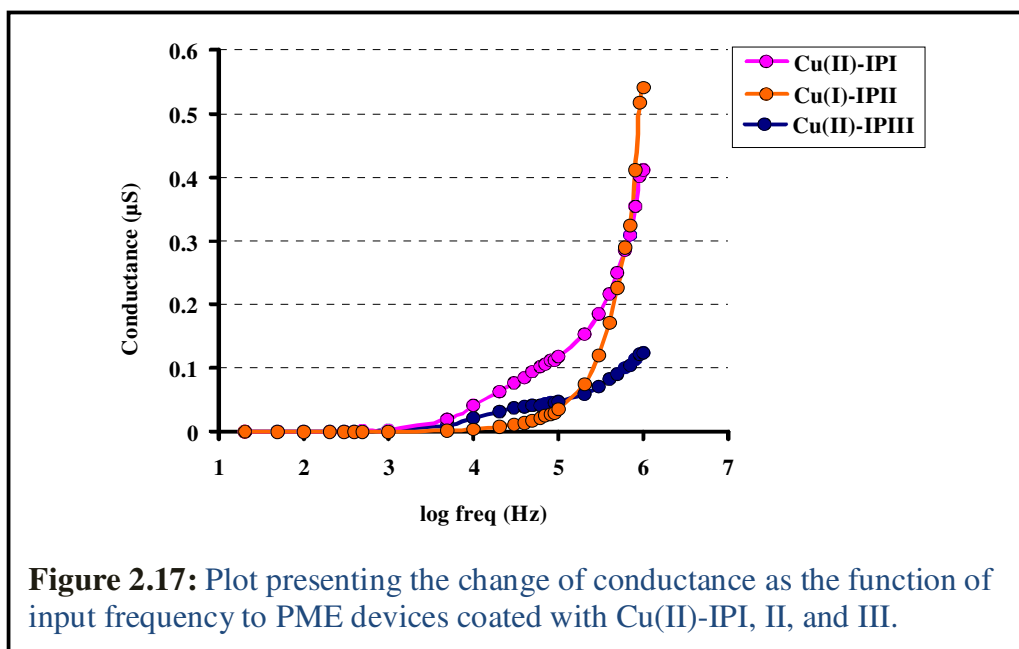
Figure 2.16: Sensor response of Cu(II)-IPIII-QCM sensor to 1mM Cu(II).

results in a decrease of $1100 \pm 25\text{Hz}$ in basic frequency, with $408 \pm 13\text{Hz}$ being response from the non-imprinted polymer layer hence yielding $698 \pm 25\text{Hz}$ as the net imprinting effect. The order of imprinting efficiency deduced from Figure 2.14-2.16 therefore is $\text{Cu(II)-IPIII} > \text{Cu(II)-IPII} > \text{Cu(II)-IPI}$.

Irrespective of the polymer chemistry and consequent efficiencies of the imprinted polymers, generally, the sensor responses of IP-I, II, and III possess three main characteristics. **First**; these polymer layers confirm the presence of the Cu(II) ion sensitive interaction sites in the imprinted layers. If the polymer is imprinted with copper then it is able to recognize it. **Second**; the signals generated by the imprinted layers are reversible. **Third**; the signals produced by the layers are stable and no loss of mass is observed switching the system from and to the de-ionized water. So, these imprinted polymer layers fulfill essential basic parameters of a chemical sensor.

(ii) Conductometric measurements

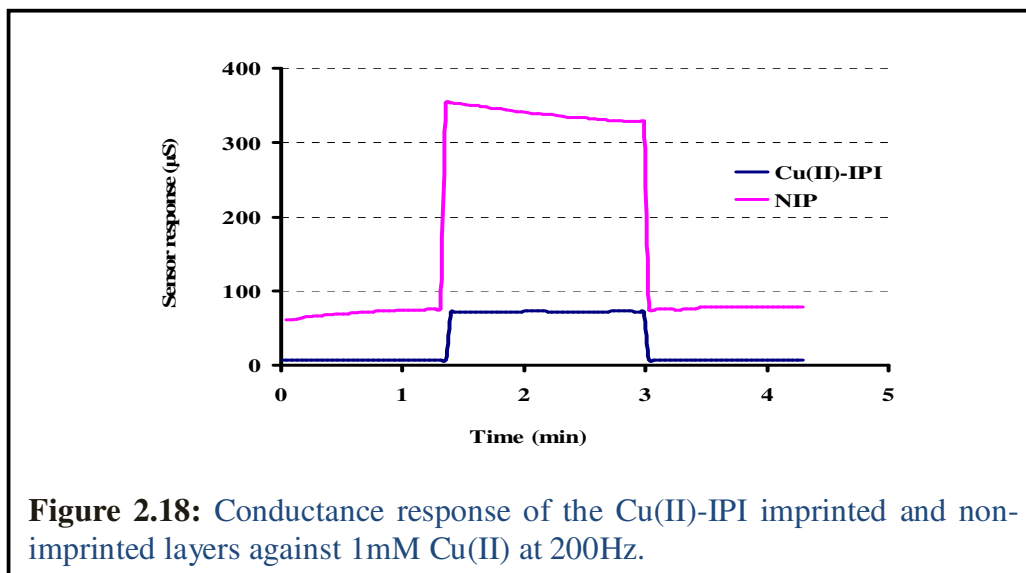
First of all, the appropriate frequency to carry out sensor experiments has to be determined in the frequency range from 20Hz to 1MHz. Figure 2.17 shows a plot of $\log f$ versus conductance, for the imprinted polymer films in the air.



It reveals two important points; first, changing the frequency input of these devices, conductance is increased i.e. impedance decreased. Secondly, at lower frequencies, this increase of conductance is almost negligible as to that at high frequencies. Of course, at higher frequencies conductance increases strongly, because the device is mainly a capacitor. Therefore, lower frequencies should be suitable to reveal changes introduced by the analyte binding.¹⁰³ In light of the appreciable conductance response at lower frequencies, 200Hz was selected as the working frequency for further experiments.

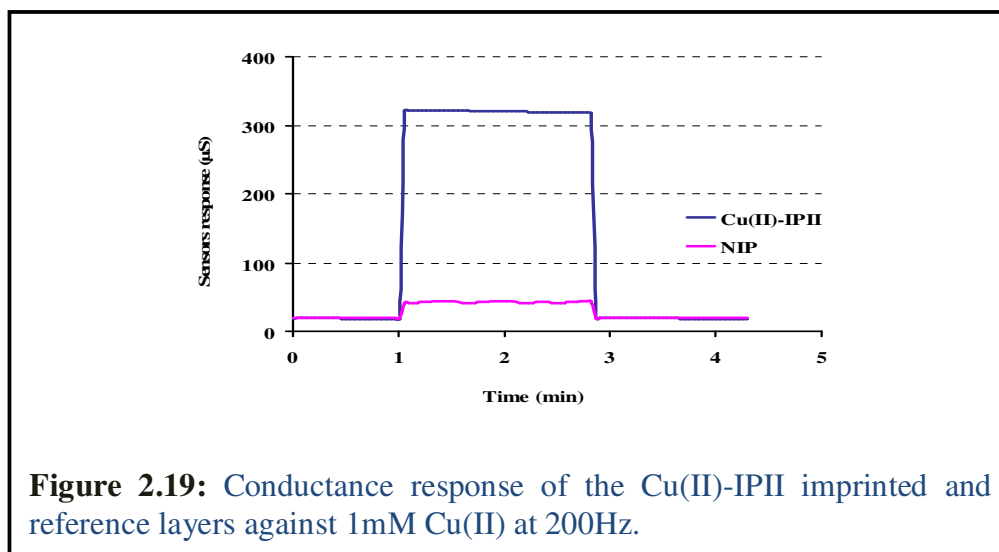
To carry out conductance measurements, PME devices coated with imprinted polymers were washed with distilled water to generate the respective cavities. Thus, these layers were assumed to be responsible for generating conductance signals for rebinding Cu(II) ions in the IIP-cavities. The reference PME device with a non-imprinted polymer (NIP) coating was recorded in the same way as Cu(II)-IP. The net response of the respective imprinted polymer is evaluated by calculating the difference in conductance before and after

rebinding of the template. So, sensor signal in these experiments is actually the conductance shift in response to the addition of a known amount of the analyte, at a certain frequency. Figure 2.18 displays the basic sensor signals of



PME device coated with NIP and Cu(II)-IPI. The uncoated device shows a huge conductance response of $1451 \pm 20 \mu\text{S}$ when immersed in 1mM Copper. This modification of the uncoated microelectrodes surface by the non- and imprinted- polymer causes interesting alteration in conductance properties of the devices. In case of the reference polymer film, the device shows conductance response of $339 \pm 8 \mu\text{S}$ whereas for imprinted polymer layer $72 \pm 0.2 \mu\text{S}$ response is observed. The behavior of imprinted layer is also contrary to the usual behavior as it exhibits masked conductance response in water and undergoes a small shift when the system is switched to the ionic medium. This surprising behavior of the reference and imprinted polymer can be ascribed to the presence of β -cyclodextrin as the functional monomer. It is a multidentate ligand, hence it can contribute a larger number of electrons to enhance the electric field around the microelectrodes. Consequently, for the non-imprinted polymer layers increased conductance is observed even in de-

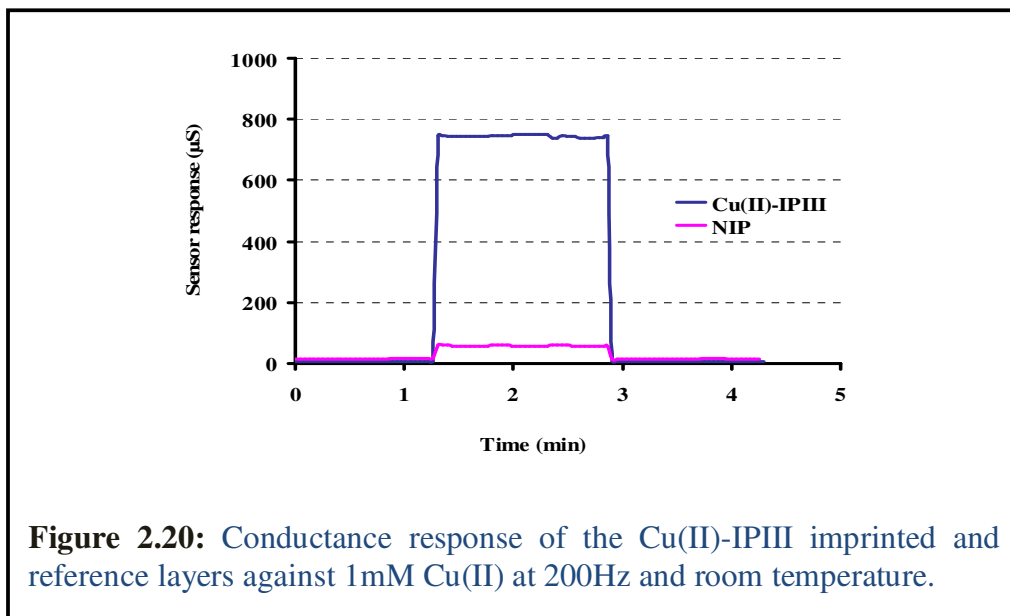
ionized water i.e 70.1 μ S. When copper solution is flushed to the non-imprinted layer, complexation happens that reduces the total number of electrons available for the conductance. Thus a decrease of sensor signal is observed. The sensor behavior of imprinted layer further strengthens this assumption, because during imprinting all electrons of β -cyclodextrin undergo complexation. Therefore, the layer in water undergoes almost negligible change of conductance owing to the unavailability of electrons. When ions are leached out of the imprinted layer and the device is immersed in copper ions solution, the small value of conductance reveals strong binding of Cu(II) ions with β -cyclodextrin to yield complex. This restricted conductance of the imprinted polymer is no wonder as already reported documents justify the strong complexation between the two and copper ions can even cease the movements of polymer chains.³¹ The performance of Cu(II)-IPII is also examined carrying out conductance measurements and the response is illustrated in Figure 2.19.



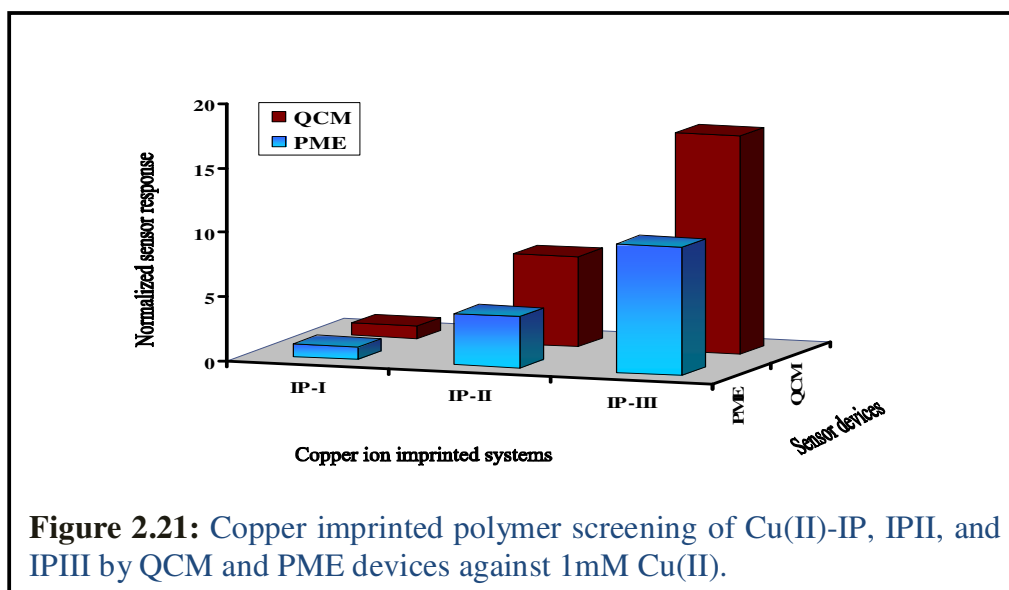
The polymer completely covers the electrodes with a 400nm thick film, which efficiently shields large parts of the electric field from the surrounding solution. This makes them rather insensitive to the changes in ionic strength

finally yielding the small conductance changes as seen in Figure. 2.19. The Cu(II)-IPII coated microelectrodes show a pronounced increase of the conductance value i.e. $320\mu\text{S}$ in 1mM ionic medium in contrast to IP-I. This can be attributed to the presence of interaction sites in the polymer network that support Cu (II) ions present in the surrounding medium. The successful regeneration of the sensor response is also a manifestation of efficient mass transport of copper ions across the imprinted polymer film.

The conductance response of Cu(II)-IPIII is also recorded and is depicted in Figure 2.20 revealing an appreciable conductance response up to $745\mu\text{S}$ for the ion-sensitive layer and a shift of $44\mu\text{S}$ for the reference layer.



Considering the PME sensor responses presented in Figure 2.18-2.20 the same order of imprinting efficiency can be deduced as obtained in the case of mass sensitive measurements. Figure 2.21 summarizes the copper imprinting efficiency of synthesized polymers for QCM and PME devices, respectively showing that indeed vinylpyrrolidone more efficiently binds copper ions within the polymer matrix, than polyvinylphenol, or the cyclodextrin leading

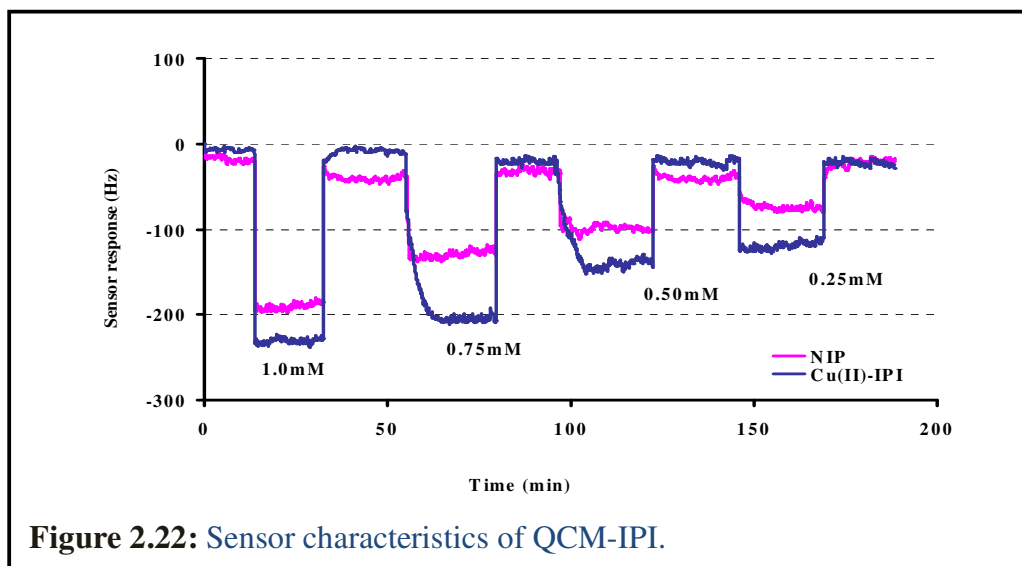


to large sensor responses. However, the exact binding mechanism needs further elucidation, which can be found in chapter 3 (FT-IR).

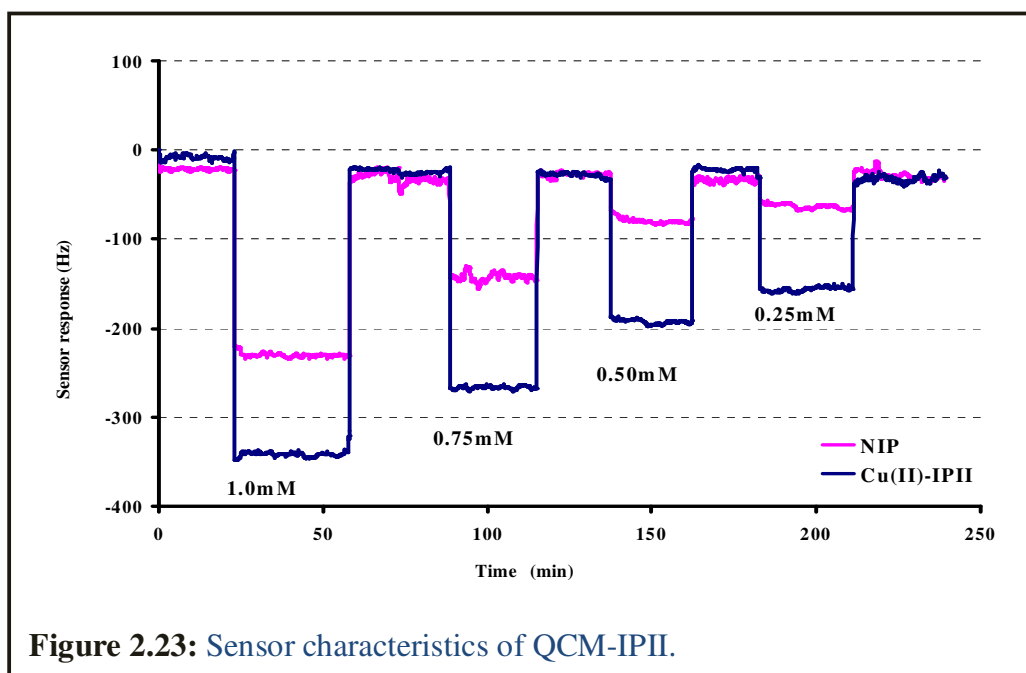
2.3.3 Sensor Characteristics

(i) QCM Sensors:

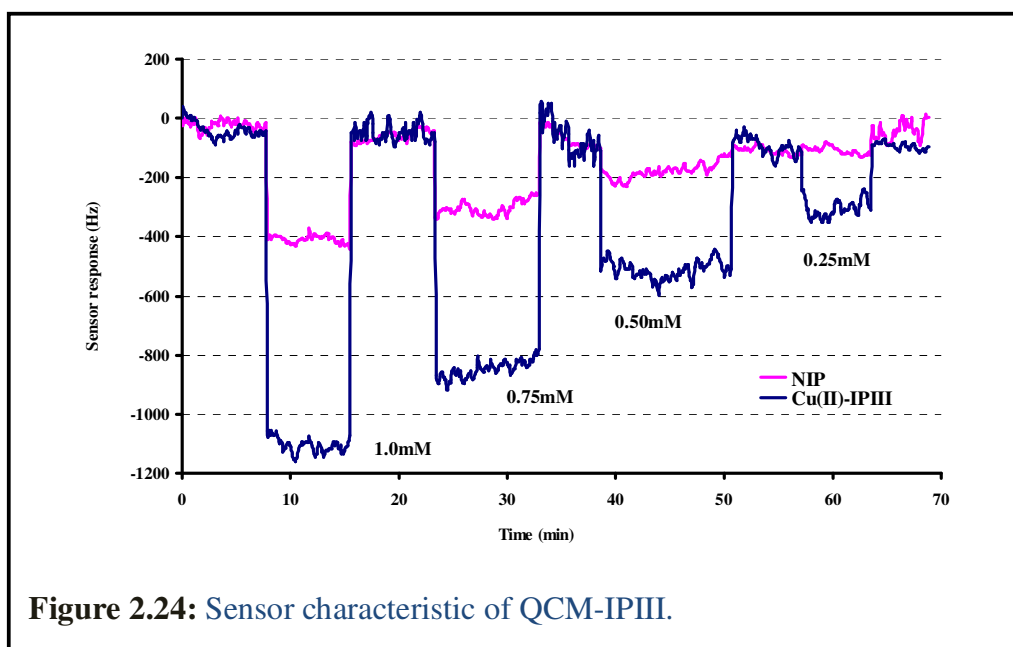
Generally, all the imprinted polymer layers showed increased responses increasing concentration of the analyte. Figure 2.22 presents respective



frequency behavior of IPI towards different concentrations of Cu(II). This unambiguously depicts that also the non-imprinted layer contributes considerably to the overall response of the device obviously due to the hydroxyl groups of β -cyclodextrin. At any of the concentrations used, the only minute additional effect of the imprinted polymer further corroborates the conclusions drawn from the microelectrodes results. Figure 2.23 illustrates

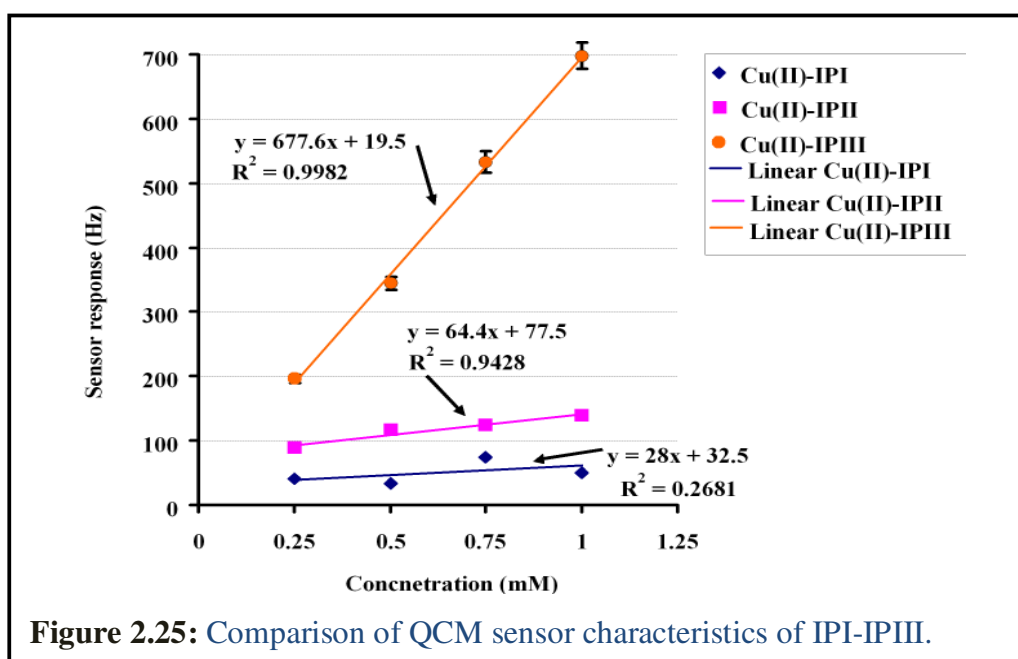


the response of reference and imprinted layer for the polyphenol-based polymer Cu(II)-IP11 in the same way as before. Again, the sensor responses depend on the analyte concentration and the difference between the imprinted polymer and the non-imprinted reference material is larger, contrary to the case of the cyclodextrin copolymer. Furthermore, the noise on the MIP is lower thus indicating lower charge fluctuation and hence increased binding of copper by the material. Finally, Figure 2.24 summarizes the results obtained by the MIP based on the Cu(II)-NVP complex. It can be observed that for the same concentration of copper, IP11 yields by far the largest frequency shifts. The rationale behind this sensor response could be coordinative binding



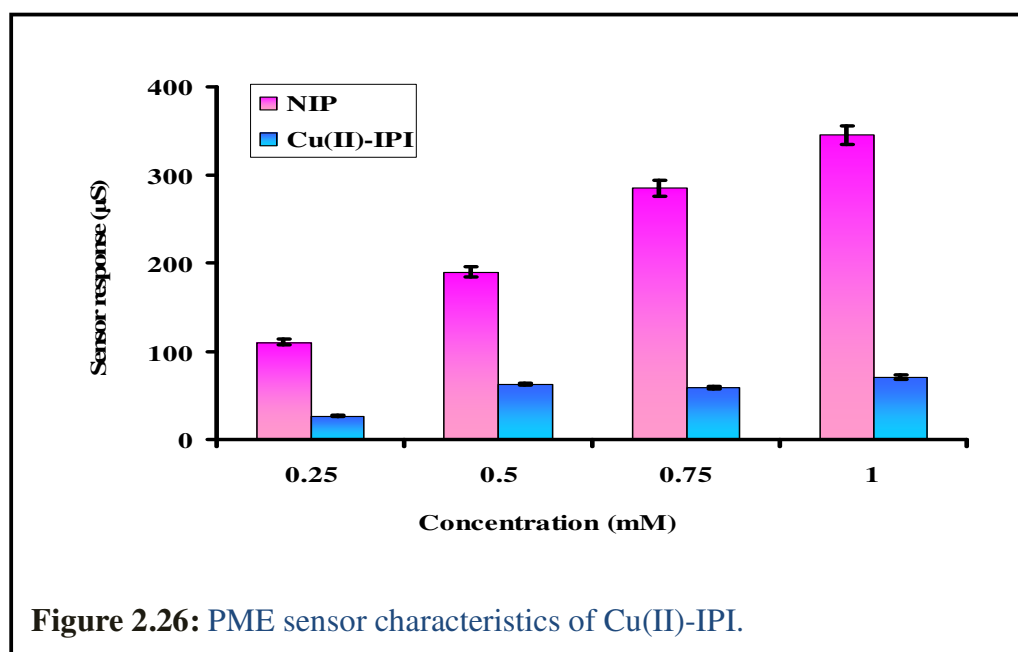
between the copper ion and the N-vinyl-2-pyrrolidone in the polymeric matrix. From the data presented in Figure 2.22-2.24, the following conclusions can be derived: at lower concentrations, the share of non-imprinted layers towards net frequency shift is small as compared to the response at high concentrations so that at small ionic strength the whole response can be attributed to the activity of imprinted layer only. The responses observed on the non-imprinted side also suggest that a certain threshold concentration of ions has to be reached before the frequency shifts can be observed. Therefore, non-specific binding has to be taken into account.

Figure 2.25 compares the sensor characteristics. Obviously, IPIII leads to the highest sensitivity on the QCM sensors, followed by IPII. IPI finally does not show statistically significant sensitivity towards Cu(II).

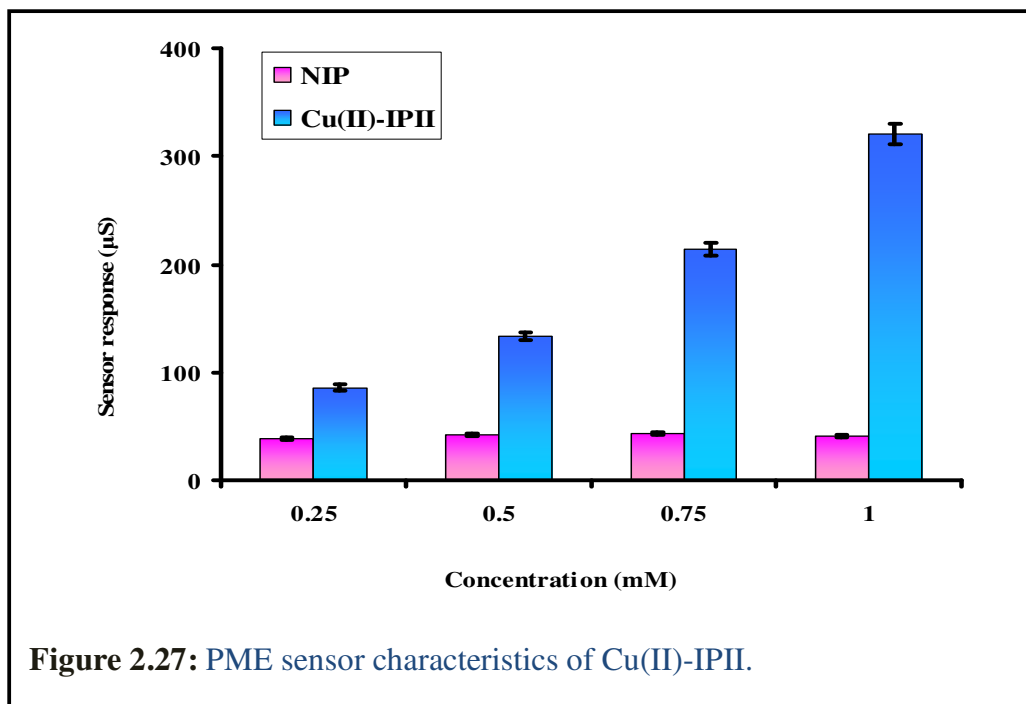


(ii) PME Sensors:

Figure 2.26 presents the sensor characteristics for Cu(II)-IPI film yielding conductance shifts between 35 μ S and 75 μ S.

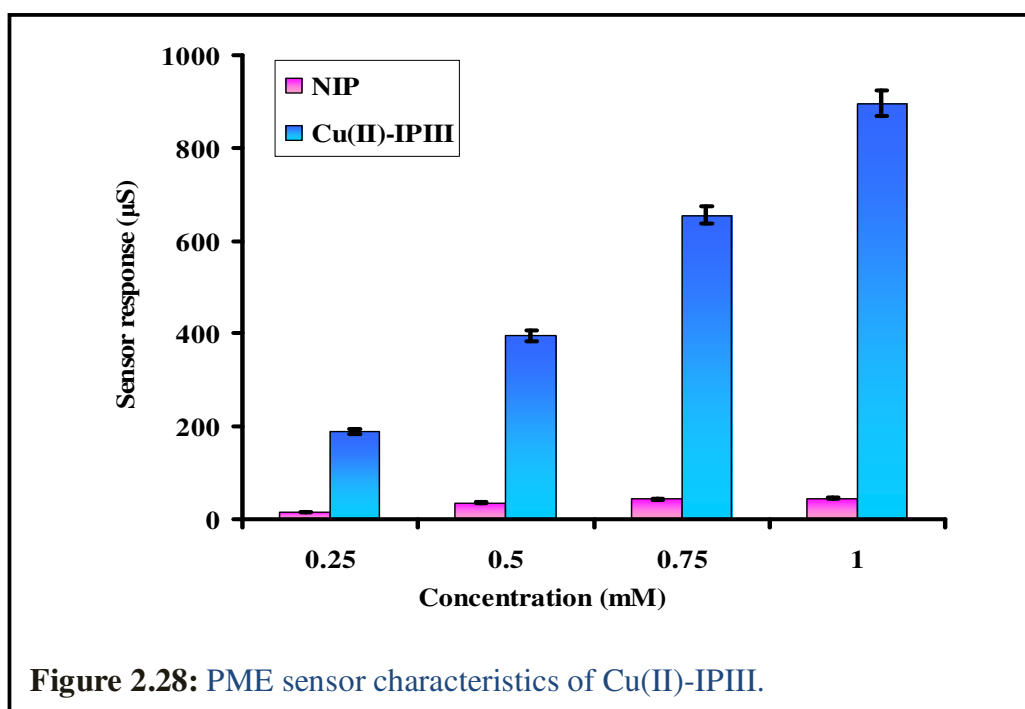


In all cases, the reference polymer gives rise to higher conductance shifts than the imprinted polymer. The sensor behavior in the case of Cu(II)-IPII polymer is depicted in Figure 2.27. Here, the performance of sensor is

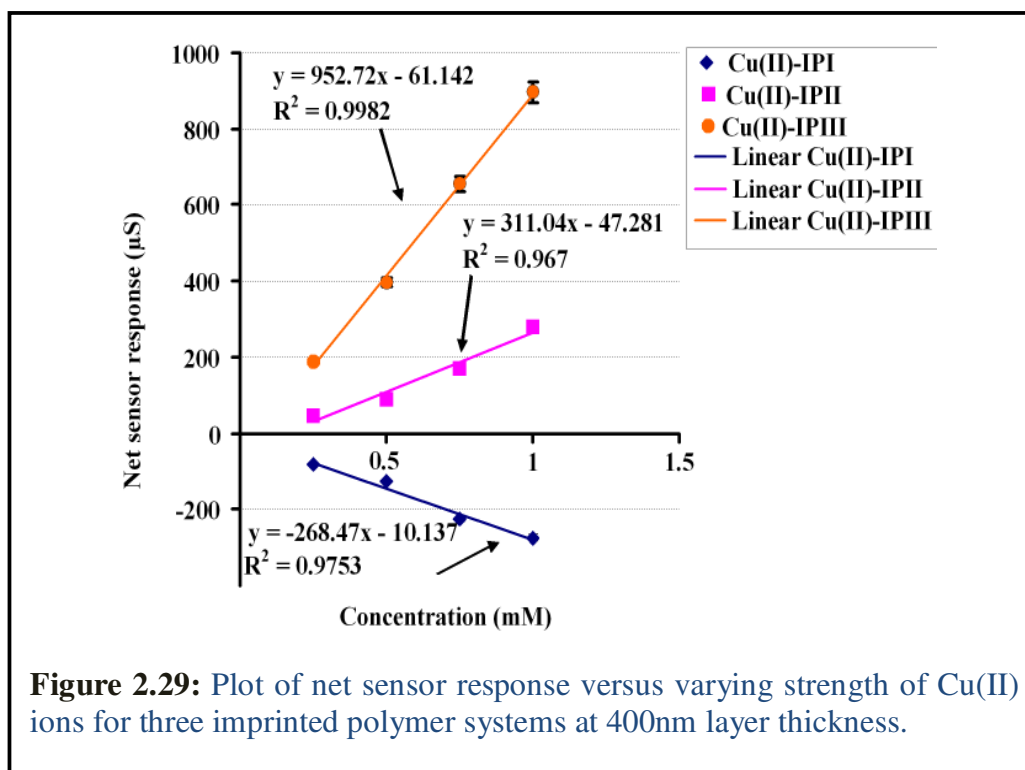


improved also in that way the MIP yields higher sensor responses than the NIP and the conductance is shifted to 350 μS. The NIP exhibits constant minor responses indicating that the layer on the PME device is almost impermeable and thus masks its surface. On the other hand, the ion-imprinted polymer contains cavities that can host copper ions. Therefore, it generates a significant signal against the copper ions.

Finally, Figure 2.28 shows the conductance profile of Cu(II)-IPIII for the same region of copper concentration. For this polymer composition the reference polymer again almost masks the device, whereas imprinted film yields substantial shifts. Figure 2.29 again compares the conductance sensor characteristics of the polymers including the respective linear obtained from regression.



Overall, it reflects the same order in binding strength for the polymers as



during the mass sensitive measurements: i.e. N-vinyl-2-pyrrolidone is most suitable for the ion imprinting of Cu(II) with linear increase of the conductance shift as a function of the analyte concentration. Again, one can assume that copper forms a complex with this monomer that is then further polymerized. In other words the polymer matrix contains cavities that correspond to the structure of this coordination complex rather than only depending on the atomic radius of copper as compared to the polymers where β -cyclodextrin and polyvinyl phenol are utilized for the copper imprinting.

3. Characterization of Copper-Imprinted NVP Polymer

3.1 Introduction

The screening methods described in chapter two substantiate N-vinyl-2-pyrrolidone as a suitable functional monomer for imprinting copper. It is imperative to establish further optimization of the designed sensor. In this chapter spectroscopic and sensor characterization of Cu(II)-IPIII polymer is explained in detail.

3.2 Experimental work

The preparation of sensor devices remained the same as already described in chapter 2, except the sensitive layers are additionally exposed to different concentrations of NiCl_2 , CoCl_2 , ZnCl_2 , and NaCl , in addition to CuCl_2 . For this purpose, stock solutions of 1M concentration were prepared and further solutions were made by appropriate dilution. For studying counter ion effect on the imprinted layers, solutions of CuCl_2 , CuSO_4 , $\text{Cu}(\text{NO}_3)_2$ and $\text{Cu}(\text{Ac})_2$ were used, while real water samples were spiked with CuCl_2 solution to make 1mM solution strength in total. The specific details of other experiments are provided in the relevant sections.

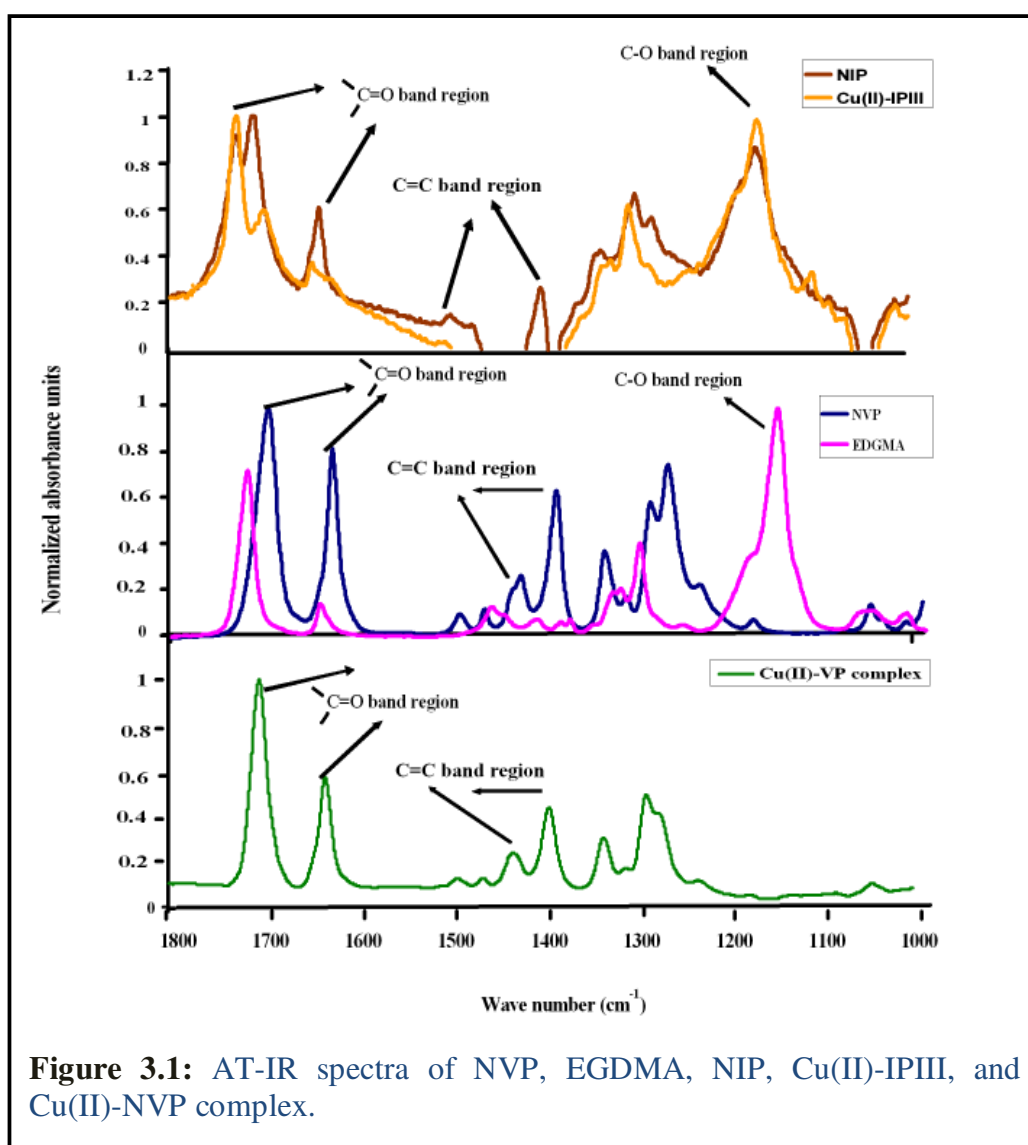
3.3. Results and Discussion

3.3.1 Characterization of Pre-polymer Mixture by IR Spectroscopy

The analysis of the functional monomer, cross linker, pre-polymer non-imprinted, and divalent copper ion-imprinted solutions are carried out by IR spectroscopy, because the non-covalent approach of the imprinting in this case most probably involves the formation of a coordination complex between

3. Characterization of Copper-Imprinted NVP Polymer

the template species and the functional monomer. The development and stability of this complex does not only influence the architecture of interaction sites and their distribution within the polymer matrix but also the recognition capabilities.¹⁰⁴ A Perkin Elmer system 2000 FT-IR Spectrophotometer was employed to study copper complexation and its immobilization into the polymer matrices. To record spectra, ATR (attenuated total reflection) mode was applied. 5 μ l of test solution were dropped onto the diamond crystal in the ATR cell. The respective IR spectra are displayed in Figure 3.1.



3. Characterization of Copper-Imprinted NVP Polymer

NVP exhibits prominent signals from $3100\text{--}3000\text{cm}^{-1}$ due to the aryl type C-H stretch bands of the ring and the vinyl group attached to the ring. Further of them appear at 2880 cm^{-1} due to the saturated CH_2 stretching modes of the vinyl group (not shown in Figure 3.1). Furthermore, the spectrum shows characteristic peaks at 1693cm^{-1} and 1624cm^{-1} that are ascribed to the stretching vibrations of the carbonyl group in literature.¹⁰⁵ The bands appearing from 1500cm^{-1} to 1400cm^{-1} region are due to C=C bond vibrations of the vinyl group while for C-N bond signals are observed at 1280cm^{-1} and 1262cm^{-1} .

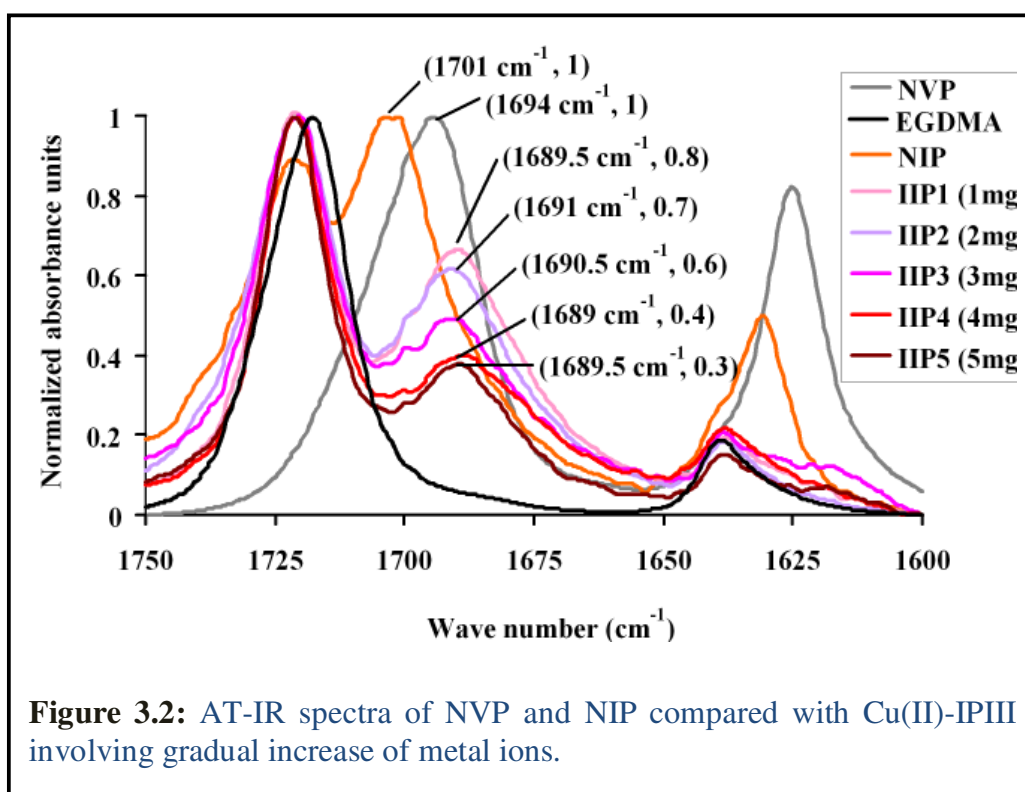
In EGDMA, the region from 3000cm^{-1} to 2835cm^{-1} corresponds to the symmetric and anti symmetric stretch of CH_2 bonds and saturated C-H bonds of the compound (not shown in Figure 3.1). The typical signal for carbonyl group appeared at 1717cm^{-1} in the spectrum. The strongest signal in IR spectrum is observed at 1143cm^{-1} due to C-O bond stretch.

When comparing the monomers, Cu(II)-VP complex and pre-polymers, a range of differences are observed, as can be seen in Figure 3.1. First one belongs to the activity of carbonyl group. The ion-imprinted pre polymer solution shows a red shift to 1689cm^{-1} with a small shoulder at 1637cm^{-1} as compared to N-vinyl-2-pyrrolidone (1693cm^{-1}). This red shift and splitting of the spectral band indicate the interaction of metal ion with the carbonyl group of functional monomer,¹⁰⁶ whereas NIP shows a blue shift to 1701cm^{-1} for corresponding carbonyl band that represents increased rigidity of the ring.¹⁰⁷ Furthermore, the presence of carbonyl signals in Cu(II)-VP complex solution spectrum confirms existence of the same structure in ion-imprinted polymer mixture. Region II indicates decreased intensity of C=C band of the vinyl group in both the reference and ion-imprinted polymers as compared to the monomer, cross linker, and complex solution. This clearly confirms that the presence of copper does not impair polymerization. Region III corresponds to

3. Characterization of Copper-Imprinted NVP Polymer

C–O bond vibrations of the crosslinker and does not show any significant changes for NIP and IIP indicating that copper does not interact with EGDMA.

To further investigate the interactions of copper metal ion with the carbonyl group of N-vinyl-2-pyrrolidone, five ion-imprinted polymers were synthesized with increasing amounts of metal ranging from 1.0 to 5.0mg, respectively, followed by IR analysis. Figure 3.2 shows the outcome:

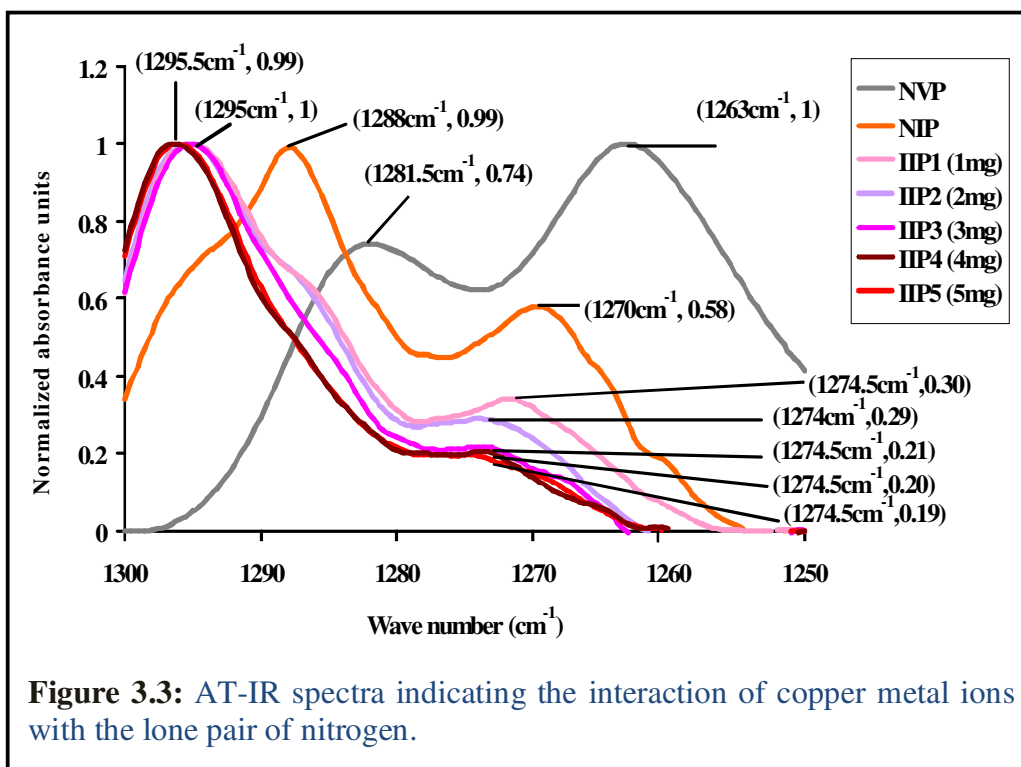


evidently, the carbonyl band of monomer shifts from 1695cm⁻¹ to 1690cm⁻¹ as the result of its complexation with copper (red shift), whereas for NIP this band lies at 1701cm⁻¹ (blue shift). The intensity of the carbonyl signal decreases gradually with increasing amount of the metal from IIP1 to IIP5 indicating its interaction with the carbonyl group of NVP. For the reference polymer no such behavior can be observed. Therefore, the binding mechanism

3. Characterization of Copper-Imprinted NVP Polymer

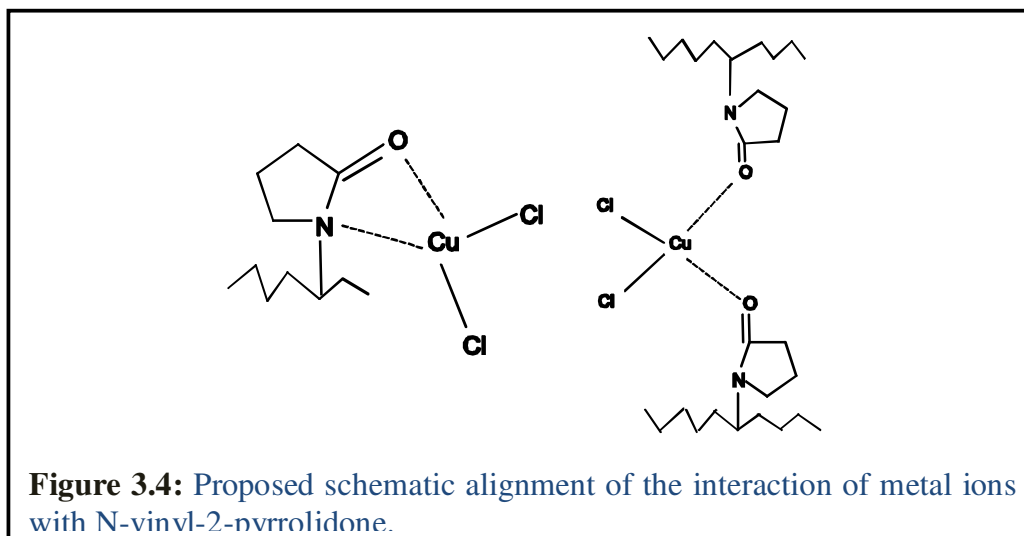
between the MIP and the copper is achieved via coordination between the metal and the carbonyl group via $\text{Cu}\cdots\text{O}\cdots\text{C}$ linkage.

The spectroscopic analysis pointed out another area of major chemical changes undergoing in the pre-polymer solution, namely the signals for C–N bond vibration. The summary of all relative changes is shown in Figure 3.3. The C–N signal of NVP undergoes a blue shift for the addition of copper,



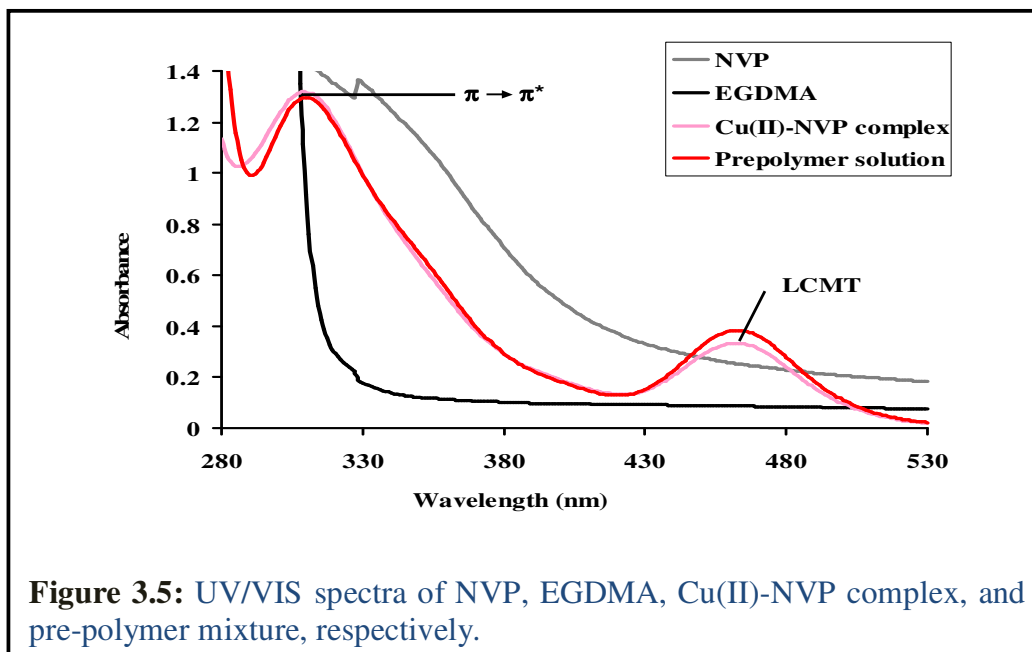
whereas the same shift is less pronounced for the reference polymer. This means that copper metal ions not only interact with the oxygen of the carbonyl group of NVP but also with the lone pair of its nitrogen atom. It is known that NVP is a bidentate ligand so based on IR spectroscopic findings it can be inferred that the divalent copper reacts coordinatively to the oxygen and nitrogen of the same/different monomer molecule.

The schematic models concluded after IR investigations are depicted in Figure 3.4.



3.3.2 Characterization of Pre-polymer Mixture by UV/VIS Spectroscopy

UV-spectrometry also allows for following the coordination phenomena. Figure 3.5 summarizes spectra of the monomer, cross linker, pre-polymer



mixture and Table 3.1 presents the spectral characteristics.

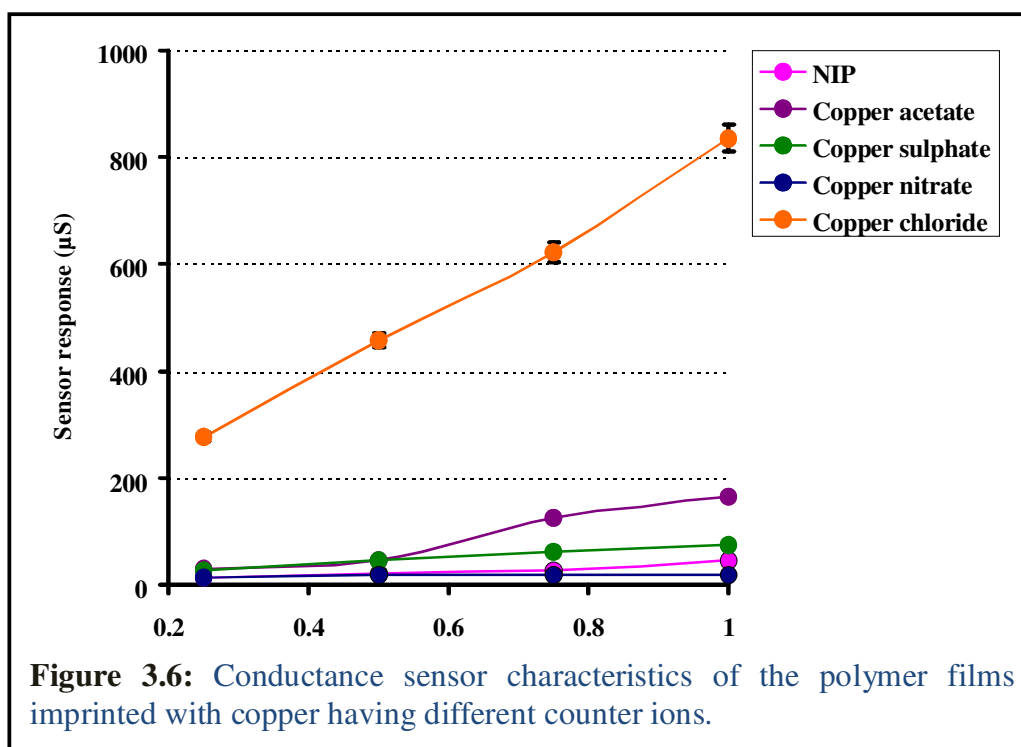
Table 3.1: UV/VIS absorption data against acetonitrile at room temperature.

<i>Test Mixture</i>	<i>Peak I</i>		<i>Peak II</i>	
	λ (nm)	ε ($M^{-1}cm^{-1}$)	λ (nm)	ε ($M^{-1}cm^{-1}$)
Cu(II)-NVP complex	462	3337	309	13182
Pre-polymer solution	463	3838	309	12959

It is evident in Figure 3.5 that N-vinyl-2-pyrrolidone and ethylene glycol dimethacrylate do not absorb in the spectral region between 280nm and 530nm. However, the mixing of Cu(II) with N-vinyl-2-pyrrolidone yields a brownish yellow solution that indicates the existence of a complex absorbing in the respective wavelength region and resulting in two corresponding absorption bands at 309nm and 462nm. The former one can be assigned to $\pi \rightarrow \pi^*$ transitions of the ligand¹⁰⁸ while the later is the consequence of ligand metal charge transfer (LMCT).^{109,110} Thus the spectra verifies the presence of coordinative bonds between copper ion and NVP when mixed. The comparably high extinction coefficient of $13182 M^{-1}cm^{-1}$ also confirms the formation of a complex while LMCT at lower λ_{max} of 462nm suggests its polar nature.¹¹¹ The spectrum of pre-polymer mixture shows the same peaks revealing that metal-ligand complexes are not distorted upon addition of the crosslinker and radical initiator.

3.3.3 Influence of Counter Ion on Imprinting

Sensor properties were observed utilizing copper templates as $Cu(CH_3COO)_2$, $CuSO_4$, $Cu(NO_3)_2$, and $CuCl_2$. Figure 3.6 shows the conductance responses of microelectrodes device coated with the above mentioned templates against different concentrations of their solutions except for the acetate salt (it was

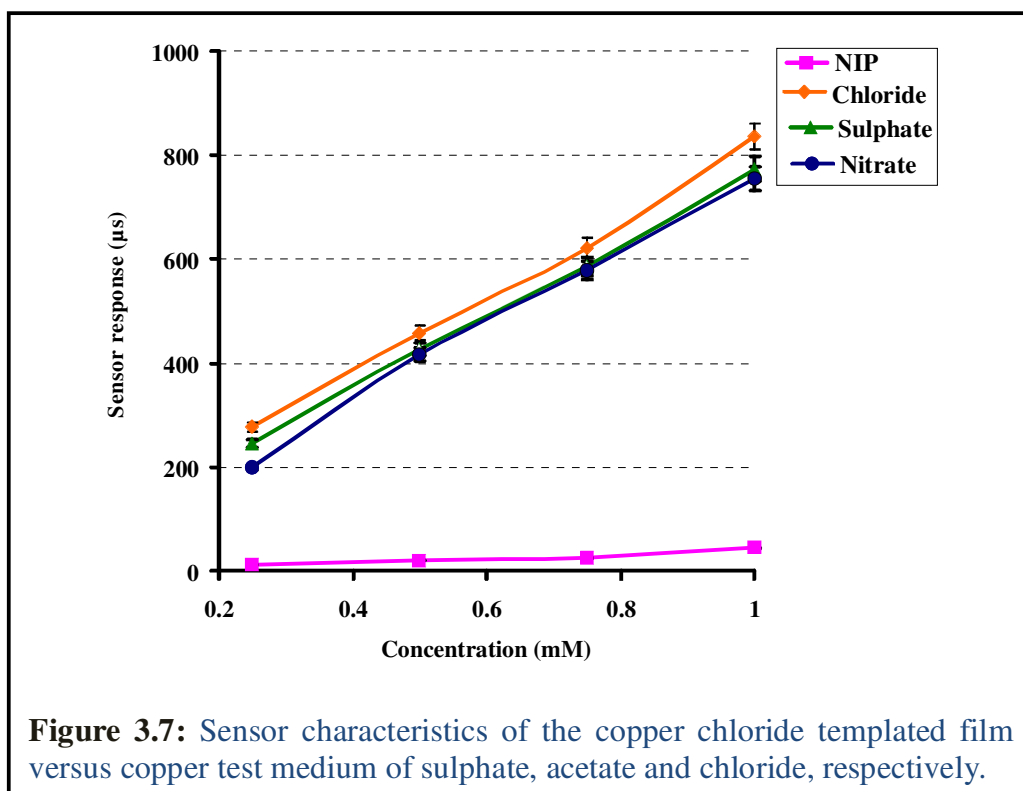


not dissolved freely in de-ionized water and its responses were recorded against chloride solution). It is observed that acetate, sulphate and nitrate of copper lead to the faster polymerization yielding clearer gels but finally exhibit smaller conductance values as compared to the chloride anion. The rationale behind this behavior lies in the varying solubility of all these salts in N-vinyl-2-pyrrolidone. The imprinting is carried out dissolving the copper salt directly into the monomer to prevent copper ions binding by the solvent molecules that may produce non-specific interaction responses. Thus NVP not only acts as a complexing agent, but also as a solvent in this case. Acetate is sparingly and sulphate, nitrates are moderately soluble in NVP as compared to the respective chloride that is instantly dissolved in it. This also correlates well with the quality of chloride as a ligand. Thus the imprinting of former three compounds leads to very small number of interaction sites for the incorporation of copper, rather their response are closer to the non-imprinted polymer coating as can be observed in Figure 3.6. Considering the high sensor

response of copper chloride-templated materials, all further experiments were carried utilizing this template for the imprinting.

3.3.4 Influence of Counter Ion on Sensor Response

To further elucidate sensor binding behavior, the effect of counter ion on the sensor response was also observed. The observed conductance shifts are displayed in Figure 3.7.

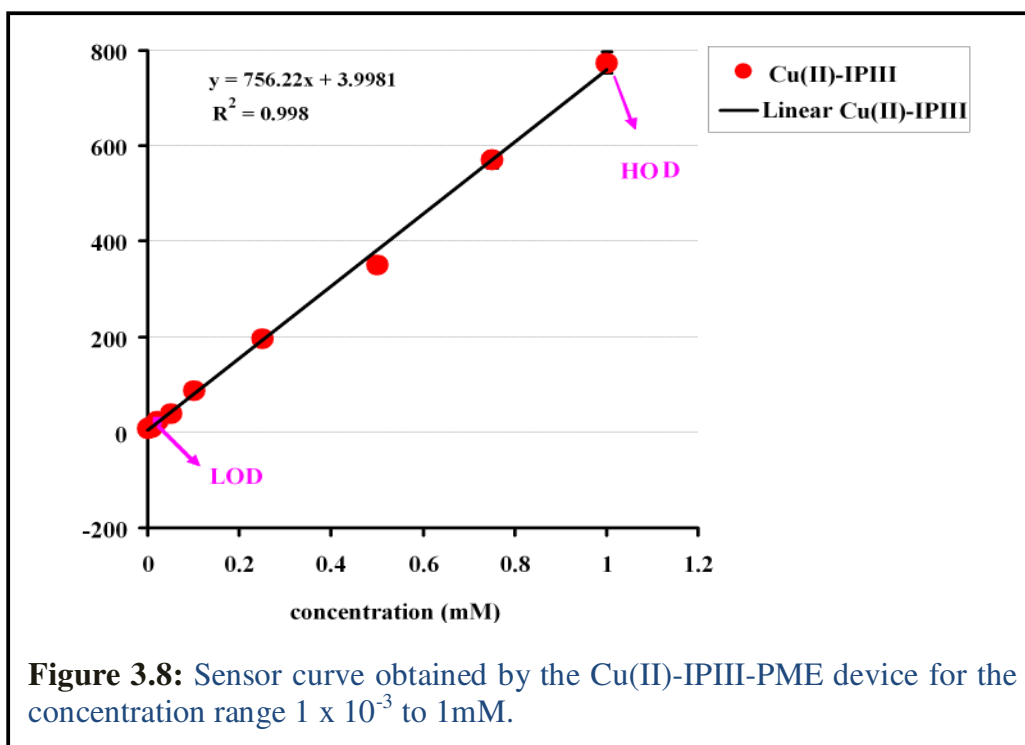


The copper chloride imprinted microelectrodes devices are exposed to copper solutions with sulphate, nitrate and chloride anions as counter ions, respectively. Generally, the imprinted polymer film exhibits enhanced conductance with the increase of concentration of all three copper solutions. The sensor characteristics are linear executing less than 3% error hence it can be concluded that the polymer film indeed contains cavities affine to the copper ions. Furthermore, the counter ion obviously plays only minor role for

sensitivity, where only the chlorides that can form mixed complexes with copper and NVP yield slightly larger signals.

3.3.5 Dynamic Range

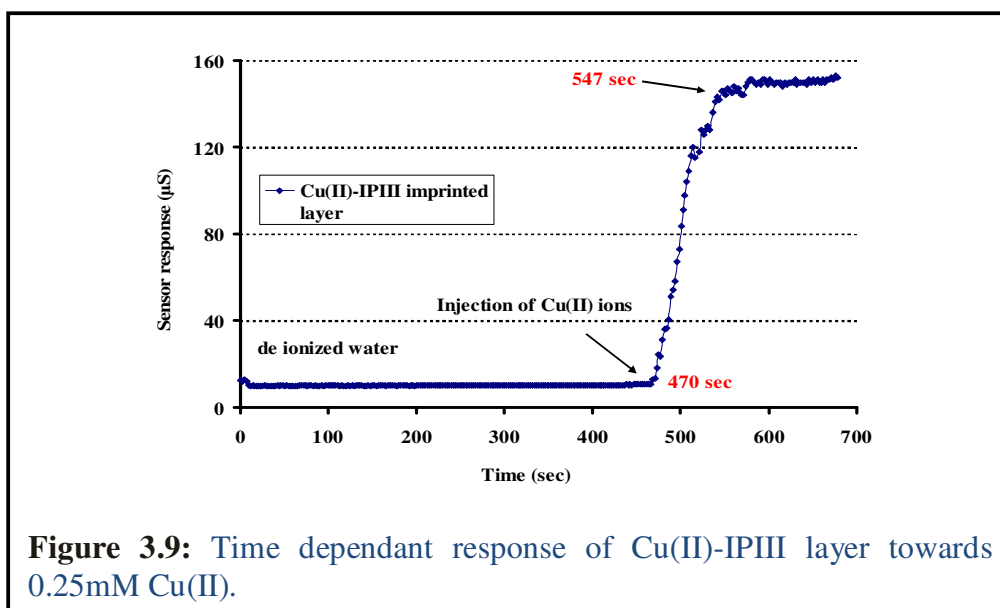
Sensitivity plays a key role for any analytical strategy therefore, the sensor characteristics of copper-imprinted PME device in the concentration range 1×10^{-3} to 1mM were observed. The resulting conductance responses are displayed in Figure 3.8.



The response of the device increases linearly ($R^2 = 0.998$) with increasing the analyte concentration. This is logical as increasing the concentration results in to more availability of copper for the given number of interaction sites present in the imprinted film. The imprinted device exhibited $25 \pm 5\mu\text{S}$ response in the background electrolyte i.e. de-ionized water so, 0.02mM concentration is assigned as the lower and 1mM as the higher limit of detection.

3.3.6 Response Time of Sensor Layer

Further, the response time of imprinted layers was investigated. To avoid any effects caused by switching from one solution to the other, the device was fully immersed in water and the conductance response was measured. After achieving a stable signal, a known amount of copper ions was pipetted into the solution to achieve a total concentration of 0.25mM. A typical conductance change with time is shown in Figure 3.9.



The imprinted-PME device responds quickly to the presence of copper and hence proves stable and robust. Equilibrium is achieved within less than 80 seconds after the addition of aliquot of copper solution. Given the fact that the layer height in this case is about 400nm, this is appreciably fast sensor response.

3.3.7 Stoichiometric Assessment of Imprinting

The optimal sensor performance is directly correlated with the polymer composition i.e. an appropriate amount of the functional and crosslinking

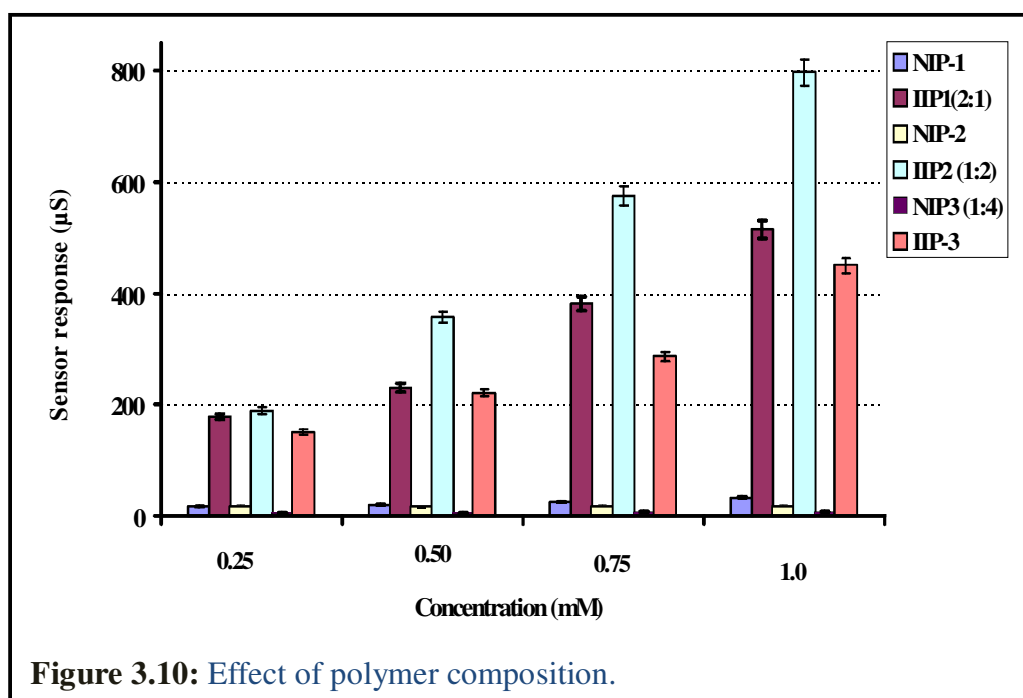
3. Characterization of Copper-Imprinted NVP Polymer

monomers. Table 3.2 shows stoichiometric variation to optimize the copper imprinted polymer (i.e. Cu(II)-IPIII containing NVP).

Table 3.2: The varying compositions of ion-imprinted polymer.

<i>Stoichiometry</i>	<i>Cu(II)-VP Complex (mg)</i>	<i>EGMA (mg)</i>	<i>AcN (μl)</i>	<i>AIBN (mg)</i>
<i>Cu(II)-IPIII-1</i>	60	30	500	3
<i>Cu(II)-IPIII-2</i>	30	60	500	3
<i>Cu(II)-IPIII-3</i>	30	120	500	3

Figure 3.10 summarizes the respective sensor responses revealing significant influence of the polymer stoichiometry. Two main trends can be recognized:



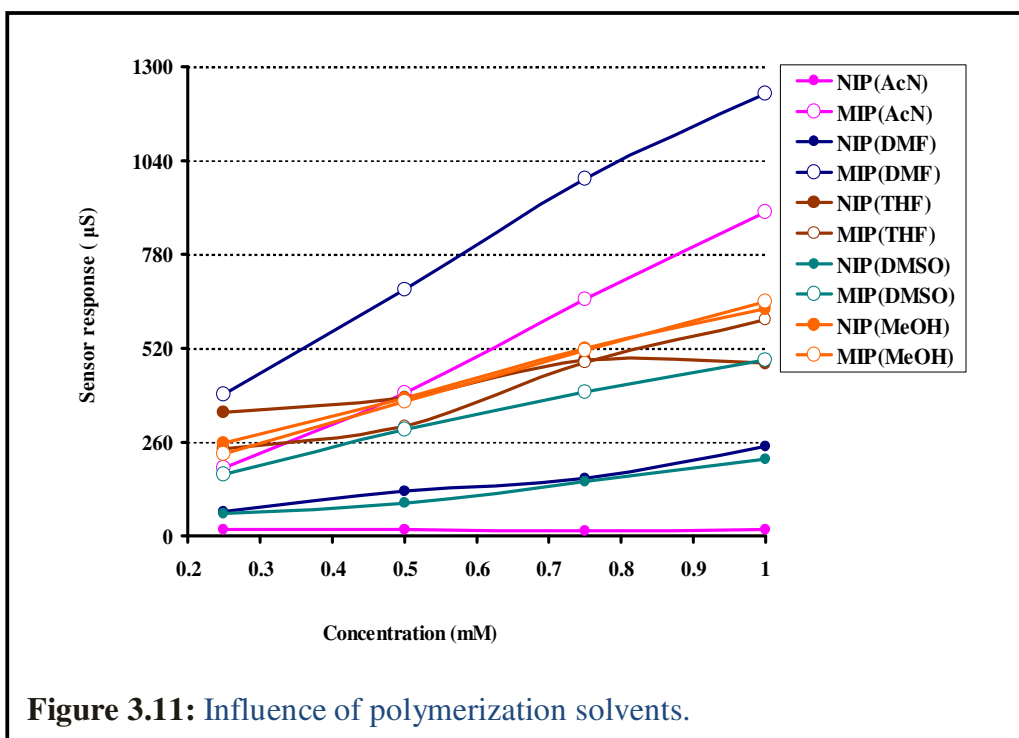
Firstly, irrespective of the polymer composition, the non-imprinted layers contribute negligible responses in contrast to the imprinted layers. This manifests the absence of any type of recognition centers in the non-imprinted

polymer networks. Secondly, among the imprinted polymers, IIP2 (1:2), where the amount of crosslinker is twice as large as the amount of functional monomer, exhibits the most favorable response. The ratio of monomer and cross linker has a direct influence on the structure and the number of interaction sites produced in the imprinted polymer, polymerization time, and the stability of MIP coating. In the cases of IIP1 (2:1) and IIP3 (1:4), obviously recognition sites are present in the matrix that lead to the concentration-dependent sensor signals. However, their sensitivities are about 30% lower than for the optimal material. In the former case the polymer layer lacks required rigidity due to the insufficient amount of crosslinking monomer whereas in later case the high amount of crosslinker leads to a dense polymer network. Nonetheless, the polymer with the low content of cross-linker offers surprisingly high responses consolidating that the polymer chains rearrange themselves upon interaction.

3.3.8 Influence of Polymerization Solvent

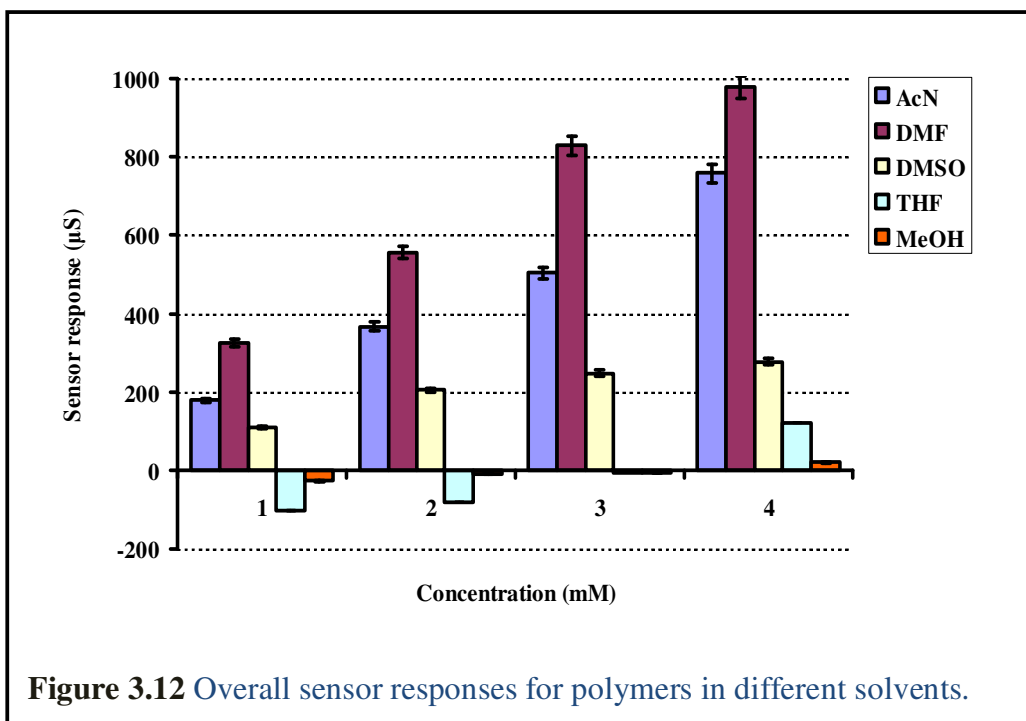
Especially in the case of pre-organizing compounds via non-covalent interactions, the solvent plays a seminal role. For assessing this influence, the polymerization was carried out choosing typical protic, aprotic, polar, apolar solvents, and with no solvent at all. Acetonitrile (AcN), N,N-dimethylformamide (DMF), dimethylsulfoxide (DMSO), n-heptane, methanol (MeOH), tetrahydrofuran (THF), and water were chosen for probing the solvent effects. The results are summarized in Figure 3.11. In the absence of a solvent, when reactants are simply mixed and exposed to UV light, both the reference- and ion-imprinted matrices do not polymerize. This clearly reflects the necessity of a solvent that dissolves and homogenizes the reactants. In **heptane**, the monomers and template are insoluble (resulting in a phase separation) thus preventing the formation of a homogenous system. The pre-polymer mixtures with **water** as the solvent lead to white precipitates that

3. Characterization of Copper-Imprinted NVP Polymer



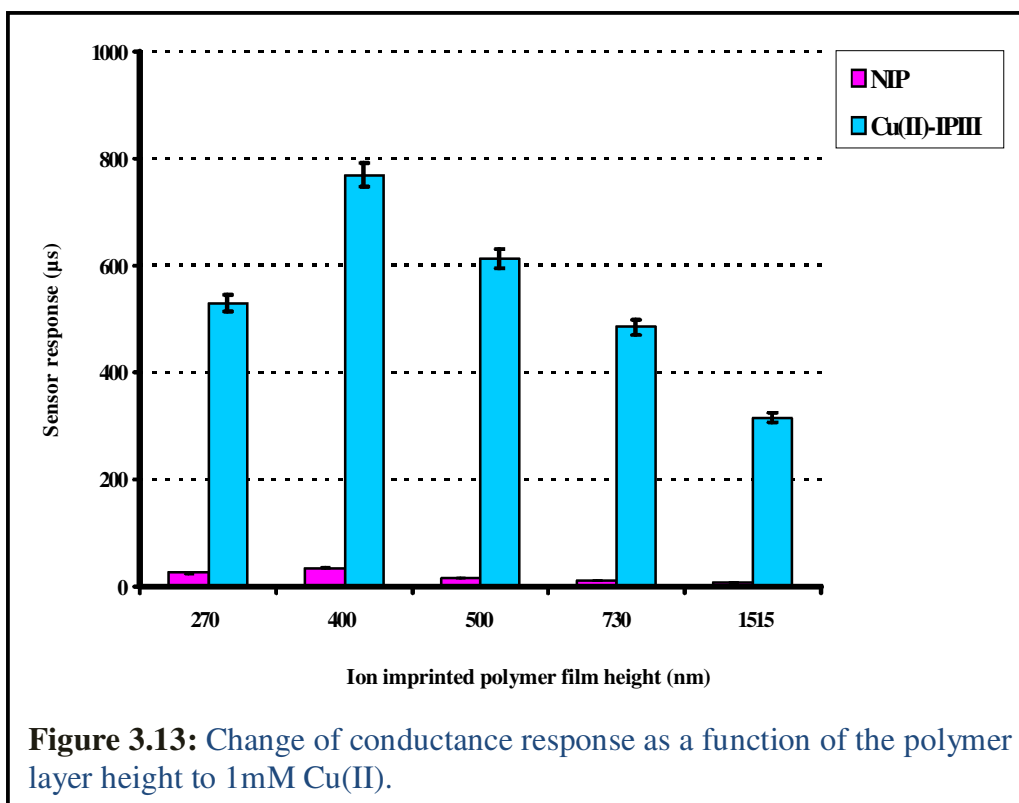
settle down in the reaction vial. One reason may be the comparative hydrophobicity of the Cu(II)-vinyl pyrrolidone adduct. In the case of **MeOH** and **THF**, the non-imprinted layers show almost same amount of the conductance as the respective ion imprinted polymer films. This means that in the presence of these solvents the reactants are polymerized, but metal ions do not bind inside the polymer matrix. In the case of other solvents, the response of non-imprinted polymer is larger than the reference polymers indicating substantially increased porosity of the systems. The sensor response with **DMSO** exhibits moderate concentration dependence both for the reference and imprinted films, whereas with **DMF** overall sensor activity is considerably high. This sensor effect may be due to the polar nature of DMF solvent. In case of **AcN**, the non-imprinted film shows negligible conductance effect whereas the imprinted one yields linear response. Overall, protic and apolar solvents seem to disturb the interaction of metal ions with monomers while polar aprotic solvents tend to stabilize the Cu(II)-VP complex. To better

understand the role of solvent during imprinted procedure, the net sensor effects are depicted in Figure 3.12. It can be seen that AcN produces polymer films generating a linear net response. Moreover, these films also bear superior stability. In contrast to this, DMF leads to significant sensor responses but imprinted films gradually dissolve after continuous exposure to water.



3.3.9 Effect of Coated Layer Height

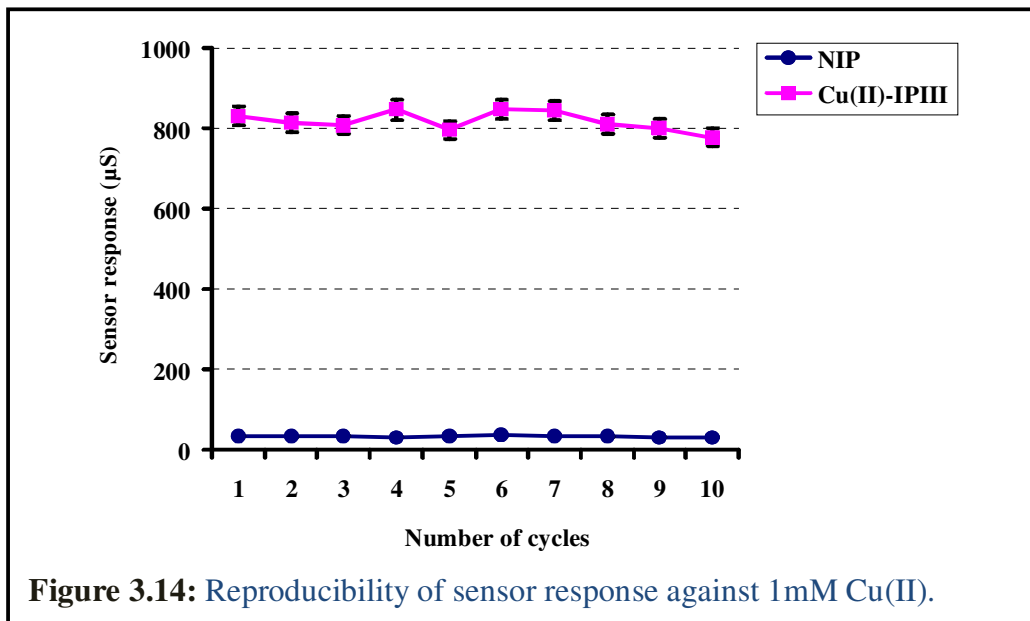
Layer height has direct influence on the resulting signals, if the interaction sites are distributed within the entire polymer matrix rather than only on the surface. To test this in the concrete case, 5μl, 10μl, 20μl, 50μl and 100μl were drop-coated onto the surface of devices and hardened under UV. Then layer heights were determined by AFM. The respective sensor response against 1mM Cu(II) are summarized in Figure 3.13. Generally, changing the layer heights leads to variation in the conductance signal. This effect is



substantially larger for the imprinted film than for the non-imprinted one because the latter contains no cavities to endorse ion binding. However, after going through a maximum at 400nm, further increase of the layer height leads to decreasing sensor responses. This clearly points out the importance of optimizing this parameter. First of all, it influences the rate at which the moieties are saturated with the target analyte. Hence, the thicker the polymer coating, the longer it takes for the analyte to approach the interaction site. It can be deduced from Figure 3.13 that increasing the layer height above 400nm hinders ions to access the inner regions of the polymer matrix, where field line density is maximal, as diffusion is getting increasingly difficult. Additionally, the conductance responses of NIP layers suggest that thicker polymer layers shield the device from the influence of the respective ions and therefore, the actual measuring effects are hindered.

3.3.10 Reproducibility

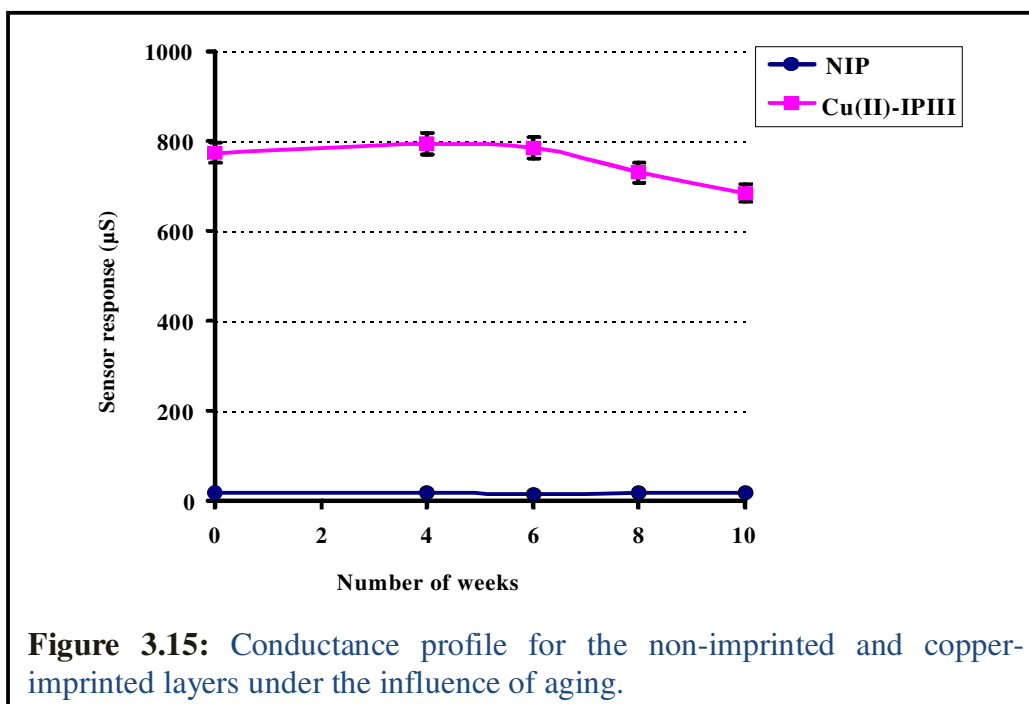
The practical application of a sensor strictly demands for the sensor signal being reproducible. For Cu(II)-IP111 coated microelectrodes this was studied by measuring the sensor signal ten times against 1mM Cu(II) concentration leading to the results presented in Figure 3.14.



Each time, a fresh solution was prepared and the device was exposed to it till equilibrium was attained. The sensor response was calculated as the average of thirty conductance readings on the LCR bridge. It can be seen in Figure 3.14 that conductance values have shown satisfactory signal reproducibility: when calculating the average of first and last two cycles, respectively, and comparing them, the total loss of signal is 3.87% of the original conductance value. This appreciable reproducibility of the sensor signal clearly indicates that ion-imprinted coated microelectrodes device is indeed suitable for the detection of copper ions.

3.3.11 Aging of Sensor Device

To study aging effects, the devices were exposed to 1mM Cu(II) after defined periods of time, and the respective conductance changes were recorded. The results are displayed in Figure 3.15.



Aging of a chemical sensor is a prime parameter that qualifies its marketability. The sensor response should be stable not only when operated from time to time but also after the longer periods of storage. For these tests, the reference and imprinted polymer coated devices were kept at room temperature, if not in use. It can be seen in Figure 3.15 that the ion-imprinted layer responded in a stable manner for eight weeks as it lost only 5.05% of the initial sensitivity of fresh layer. However, after twenty weeks a considerable loss of sensitivity was observed, namely 31.2%. Although this is not fully understood however it can be due to the swelling of MIP coating in water over the time. Interestingly, the reference layer did not undergo any

considerable loss of sensor signal. The layer was intact to mask microelectrodes efficiently even after twenty weeks preventing copper ions from interacting with these and causing the conductance change.

3.3.12 Selectivity Studies

(i) QCM Sensors:

Highly specific substrate recognition is one of the fundamental features of a wide range of biological functions governing life, including immune reactions, catabolic and anabolic enzymatic processes etc., to name the most important ones. This consummating of specificity by the imprinted materials fulfils the basic parameter of a chemical sensor required for the practical detection of the analytes. In this background the selective uptake of Cu(II) ions by QCM device coated with all the three polymer systems was studied in detail. In this group of experiments, Ni(II), Co(II) and Zn(II) ions were chosen as the interfering and competing ions. These are transition metal ions neighboring Cu(II) ions and possessing very minute difference in their radii.

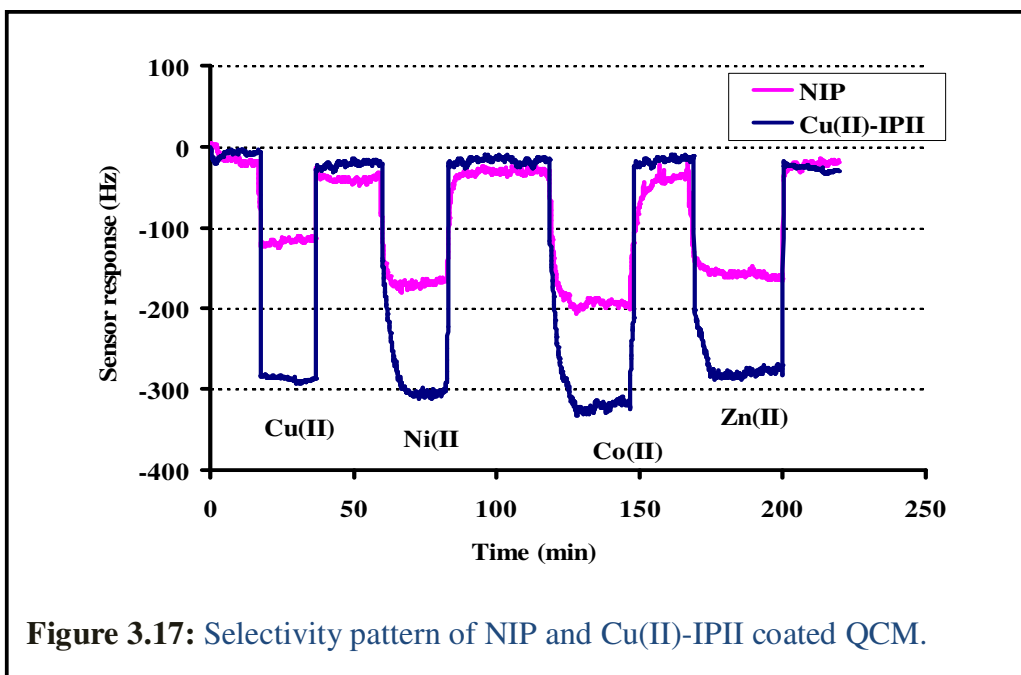
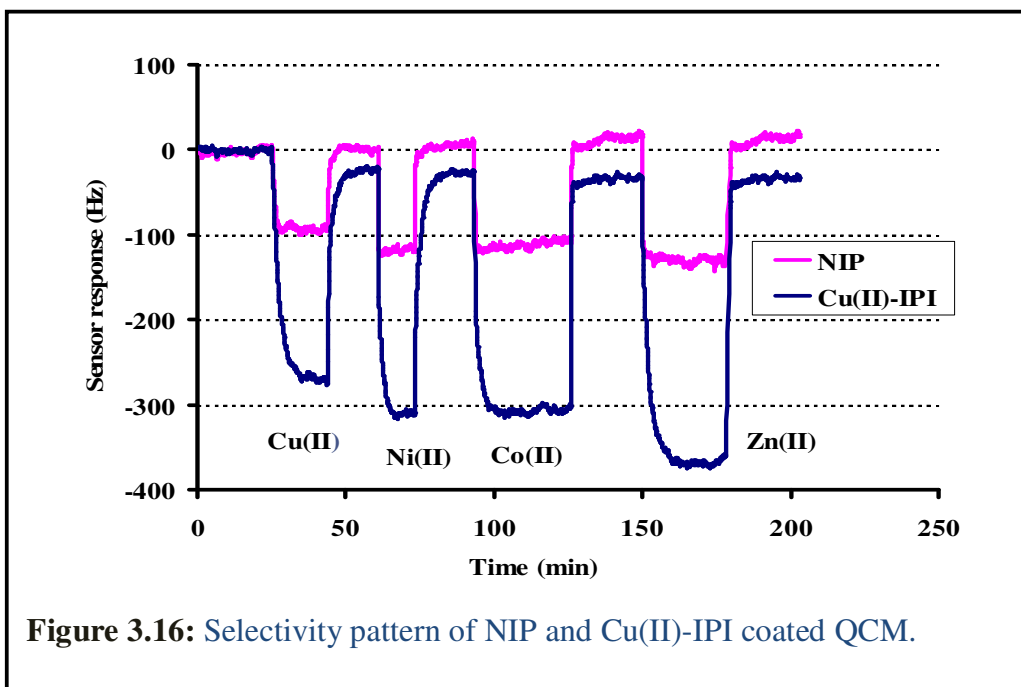
Their ionic radii are provided in Table 3.3

Table 3.3: Ionic radii of cations in question.

<i>Sr. no.</i>	<i>Metal ion</i>	<i>Ionic radius (pm)</i>
1	Co(II)	79
2	Ni(II)	83
3	Cu(II)	87
4	Zn(II)	88
5	Na(I)	166

3. Characterization of Copper-Imprinted NVP Polymer

The mass sensitive sensor responses versus time for the three copper imprinted systems described in section 2.2.4 are displayed in Figure 3.16-18, respectively.



3. Characterization of Copper-Imprinted NVP Polymer

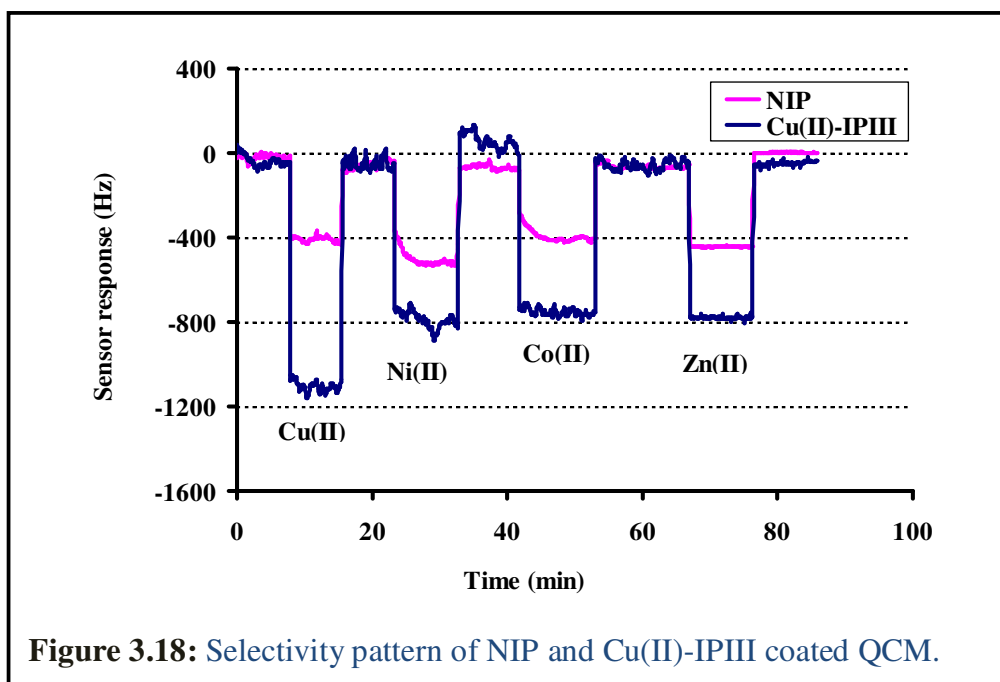


Figure 3.18: Selectivity pattern of NIP and Cu(II)-IPIII coated QCM.

The net sensor responses are summarized in Figure 3.19.

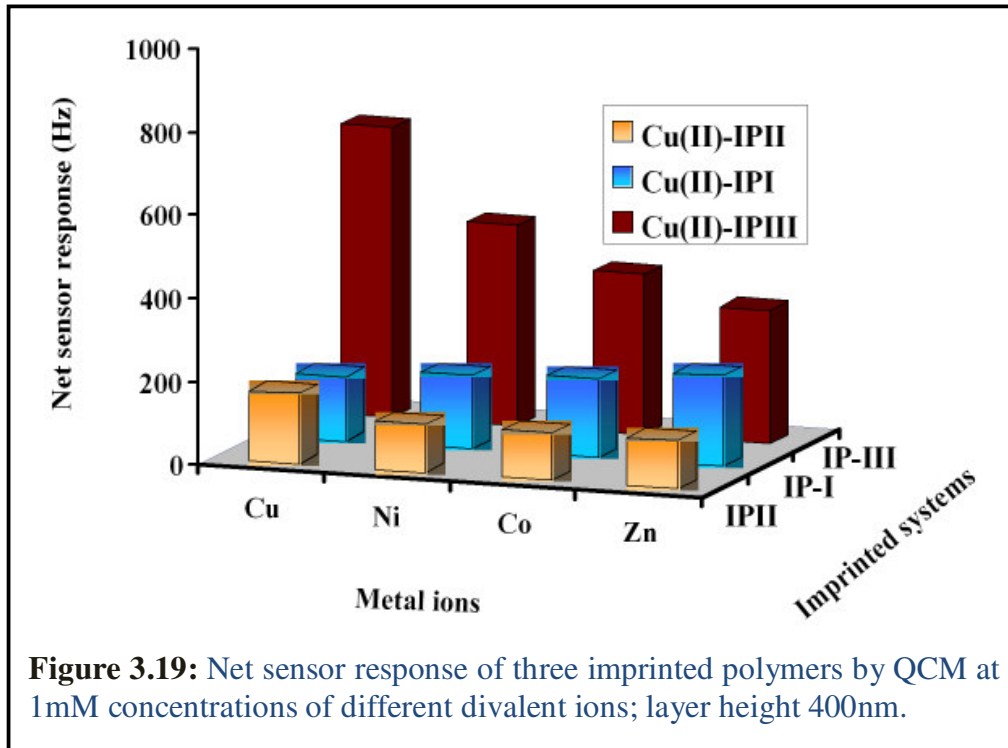


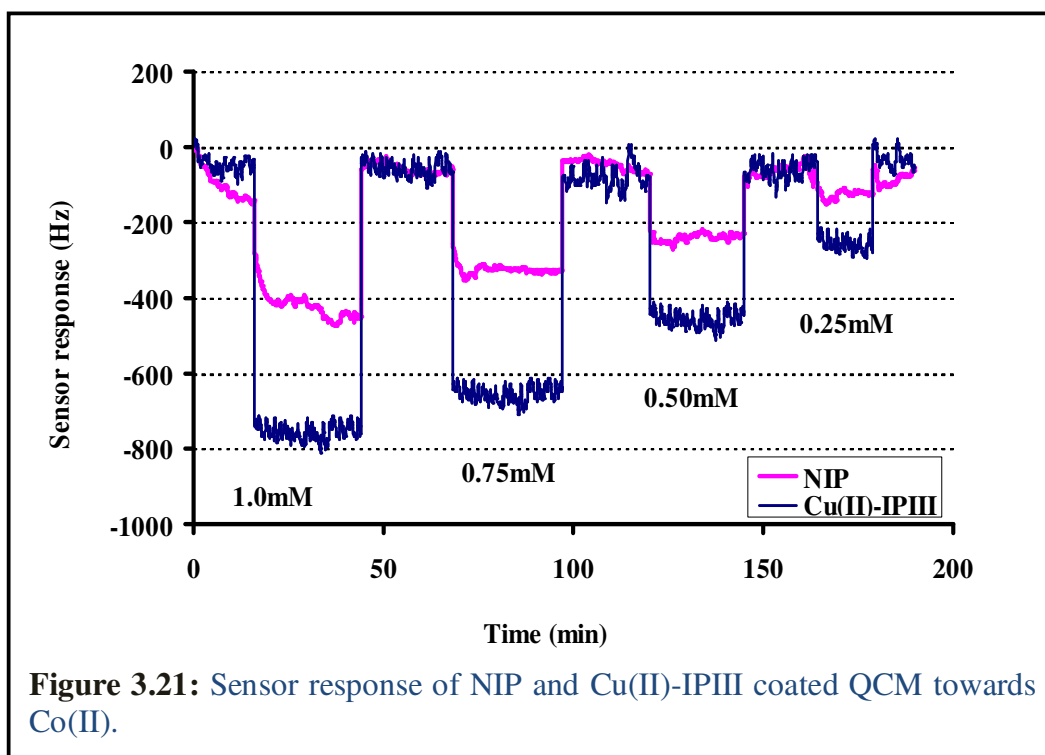
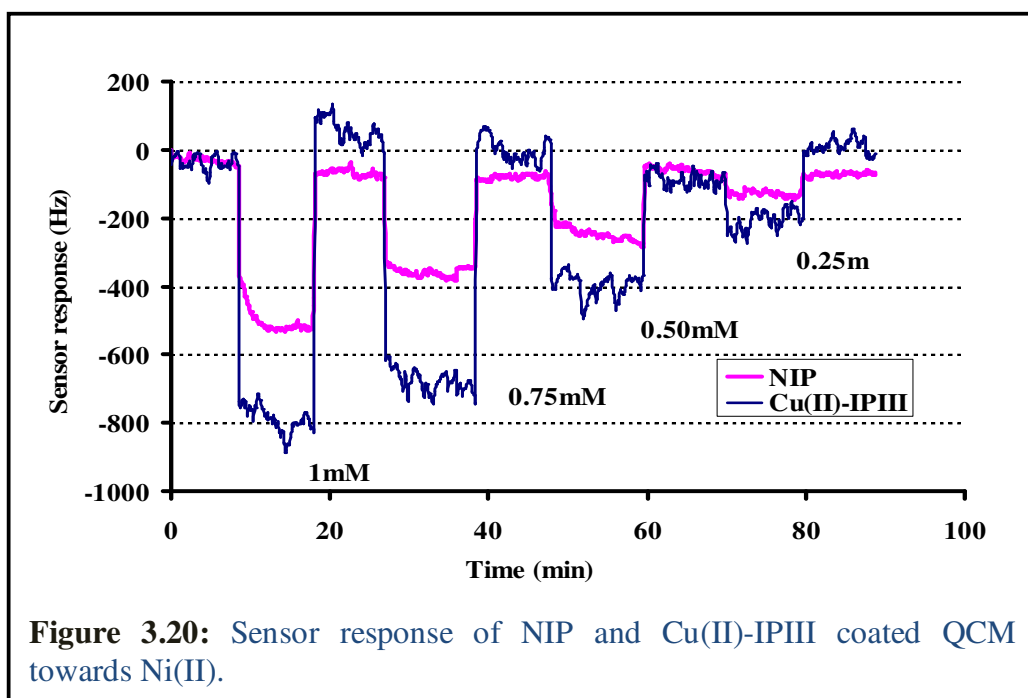
Figure 3.19: Net sensor response of three imprinted polymers by QCM at 1mM concentrations of different divalent ions; layer height 400nm.

3. Characterization of Copper-Imprinted NVP Polymer

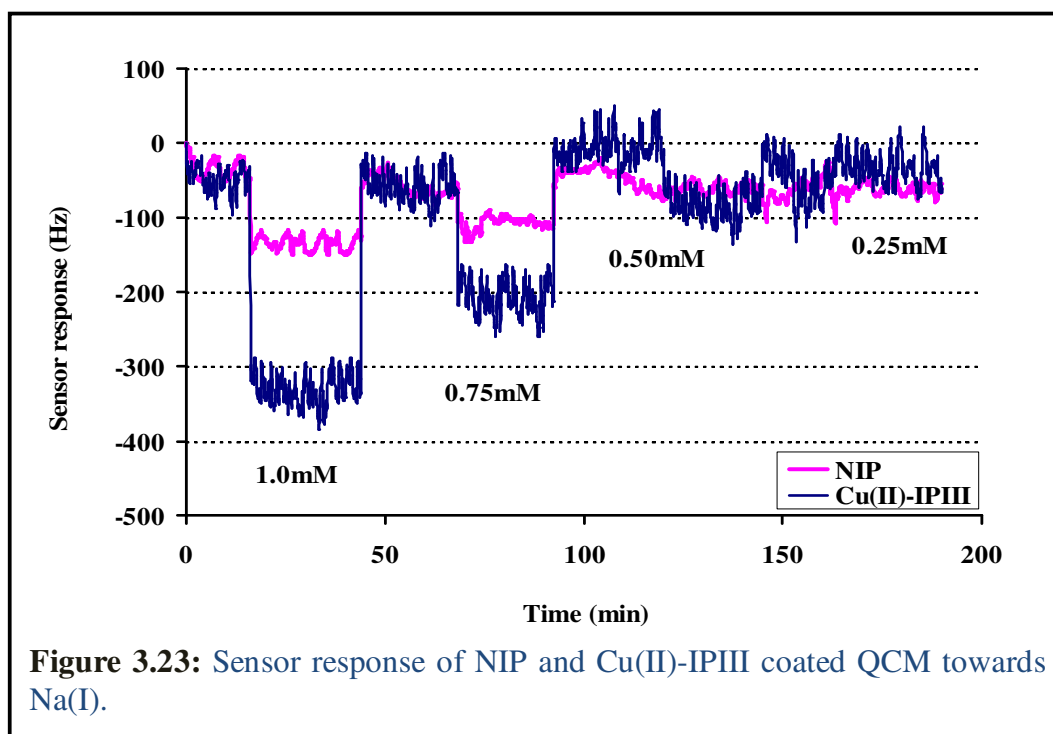
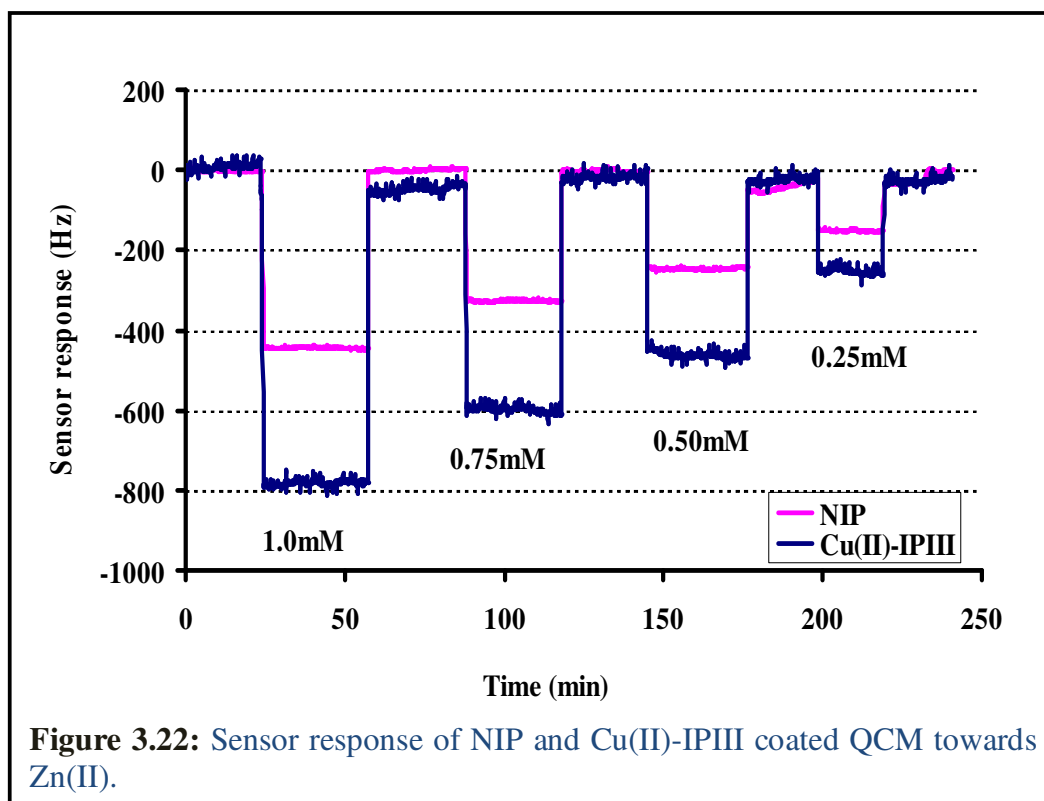
Obviously, IP-I yields the higher sensor response for Zn(II) and the lowest for Cu(II) i.e. the actual template. For the better understanding of selectivity patterns, responses are expressed in terms of the ratio in frequency change of Cu(II):Ni(II):Co(II):Zn(II). This ratio for IP-I is calculated to be 1:1.41:1.217:1.39 manifesting very broadband behavior of the imprinted polymer. This is logical as β -cyclodextrin is a large molecule with a large number of free hydroxyl groups bearing electron lone pairs. The IP-II film yields better selectivity; at least the signals caused by the other competing ions do not exceed those of Cu(II) ions: the normalized frequency change is calculated to be 1:0.687:0.680:0.684 showing preferential re-incorporation of Cu(II) ions. Thus omitting cyclodextrin and such modifying the polymer nanostructure results in a lower number of free hydroxyl groups hence improving selectivity. Bulky cyclodextrin obviously leads to the denser materials that are less accessible to the ions as indicated by the lower signals of the respective NIP sensors. However, the IP-III ion-imprinted layer shows best selectivity for Cu(II) as can be seen in Figure 3.19. For this polymer system the ratio of frequency shifts is determined to be 1:0.404:0.479:0.458. This polymer thus exhibits twofold larger selectivity for the Cu(II). Furthermore, it ascertains the suitability of N-vinyl-2-pyrrolidone in contrast to β -cyclodextrin and polyvinylphenol to generate recognition sites. Hence, this further corroborates that the coordinative interactions between Cu(II) and either the oxygen or nitrogen of N-vinyl-2-pyrrolidone can be regarded as the driving force for the copper recognition in these materials.

To discriminate the size and concentration effects from one another, IP-III polymer coatings were exposed to varying concentrations of all above mentioned ions and additionally to Na(I). The sensor response for Cu(II) concentration is displayed in chapter two (Figure 2.23) while time versus frequency changes profiles for other ions are depicted in Figure 3.20-23.

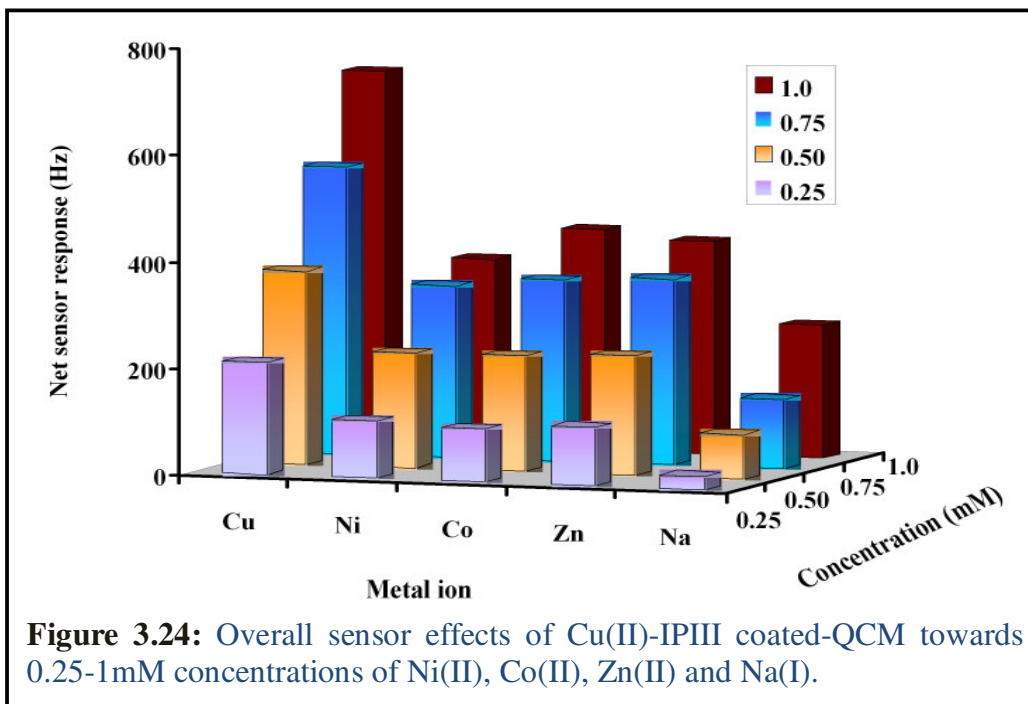
3. Characterization of Copper-Imprinted NVP Polymer



3. Characterization of Copper-Imprinted NVP Polymer



The calculated net sensor effects are summarized in Figure 3.24.



Evidently, at each concentration the polymer preferentially adsorbs cupric ions irrespective of its size being close to that of competing ions. The designed cavities are not only sensitive to the size of the ions but also their properties as a central atom in coordination. Thus, sodium ions with oxidation state +1, possessing poor complexibility, and larger ionic radius i.e. 166 pm lead to smaller frequency shifts for all concentrations. This sensor effect displays remarkable selective binding of the copper especially in virtue of the smaller and very closer radii of competing ions. Furthermore, this selectivity can also be regarded as highly appreciable, because ion imprinting does not offer geometric fit that could benefit substrate specificity.

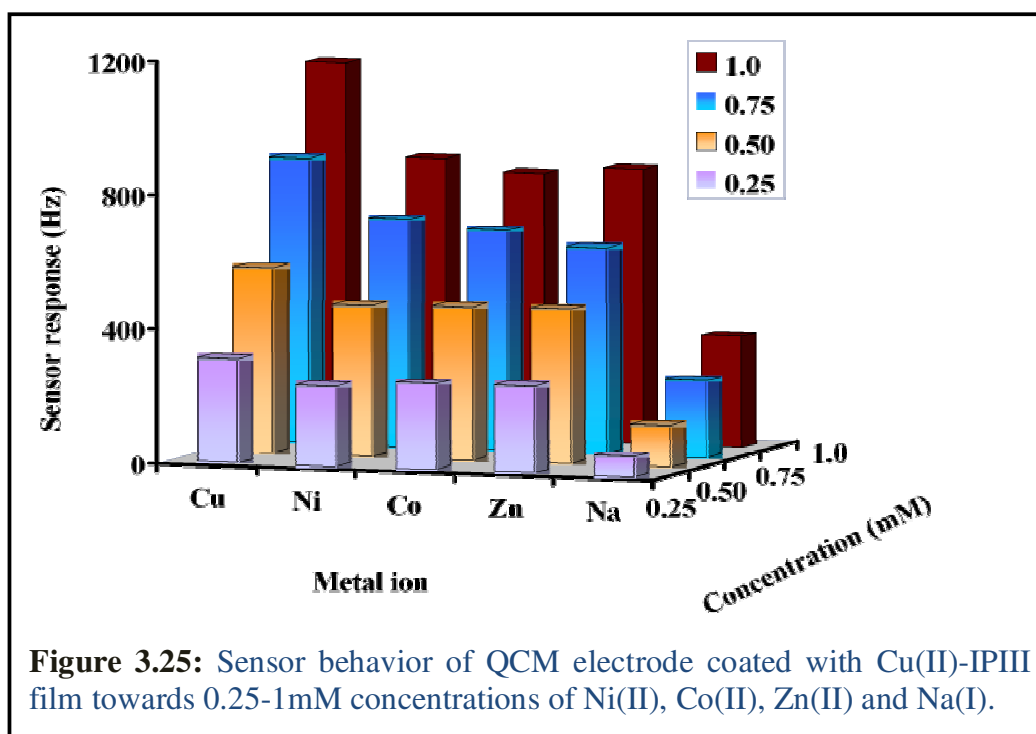
To extract further information out of this pattern, the normalized sensor responses are calculated and are displayed in Table 3.4. It is obvious from this table that lower concentration produces better selective recognition of the template ion. It can be explained considering the sorption of analyte in to the

Table 3.4: Normalized frequency shifts for three imprinted polymer systems

Conc. (mM)	Cu(II)	Ni(II)	Co(II)	Zn(II)	Na(I)
1	1	0.52	0.60	0.60	0.35
0.75	1	0.61	0.63	0.64	0.23
0.50	1	0.60	0.60	0.62	0.22
0.25	1	0.51	0.47	0.51	0.02

interaction site as an enthalpy controlled reaction. At higher concentration, the higher amounts of binding sites are occupied thus higher interfering effects are observed. Furthermore, changes in the conductivity around a QCM may lead to a frequency shift without actual changing the mass of imprinted layer.¹¹² This effect is less pronounced for lower concentration so it can be concluded that dealing with ion-imprinted polymer coated QCM device, it is advantageous to work with lower ionic strength to avoid potential speculations.

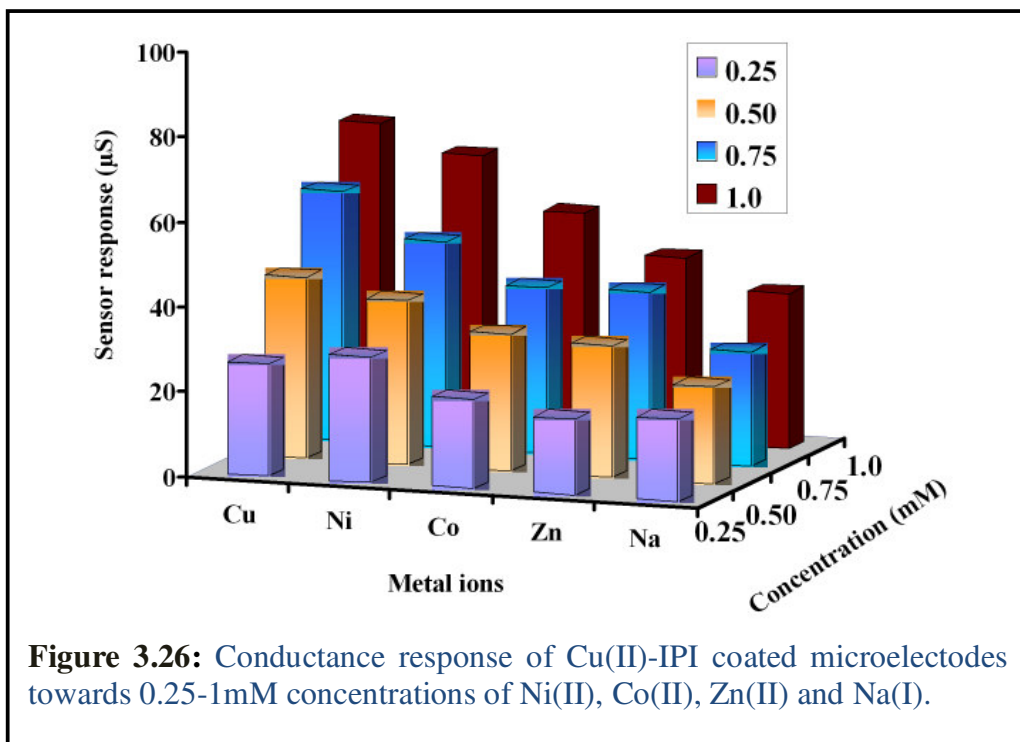
The QCM responses of only IIP electrodes are shown in Figure 3.25. Another



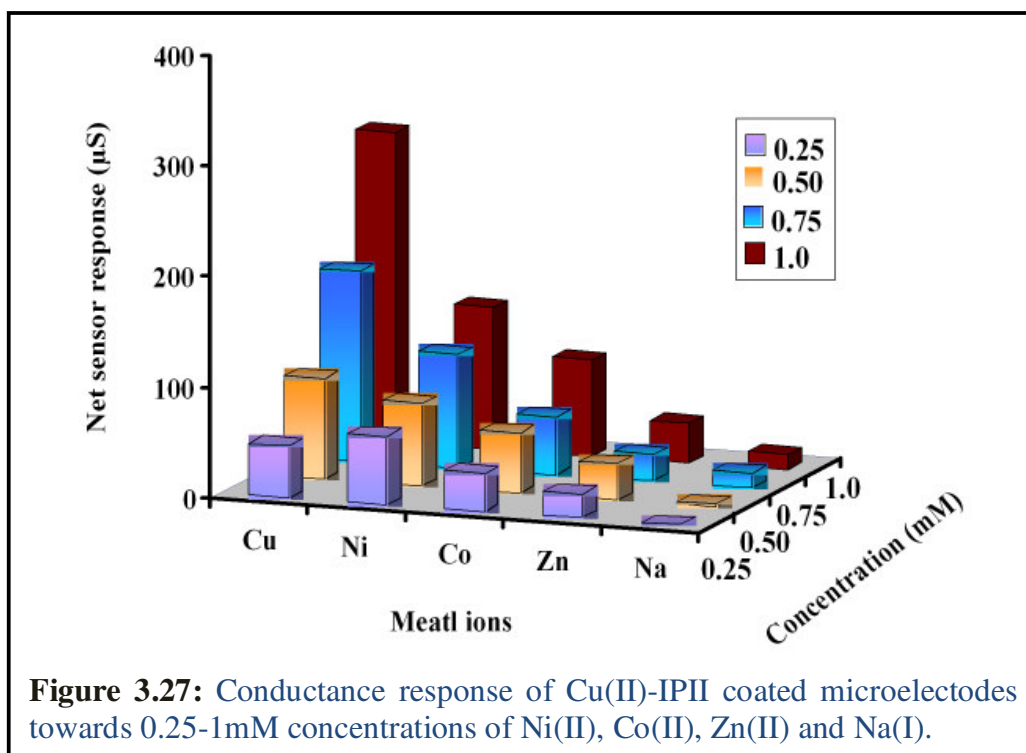
important point can be observed in this case. The overall sensor responses (i.e. the differences in frequency shifts between MIP and NIP) lead to such selectivity pattern. If Figure 3.25 is compared with Figure 3.24 then the less selectivity trend could be easily observed.

(ii) PME Sensors:

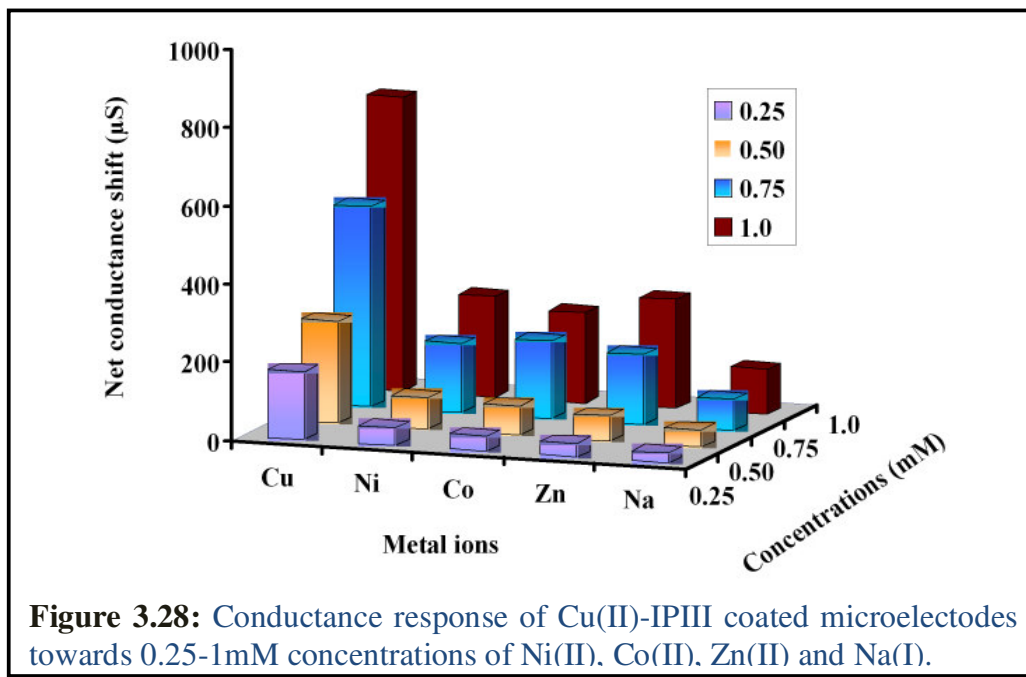
The selectivity patterns shown by the QCM sensors were cross checked by the periodic microelectrodes device. The conductance responses for Cu(II)-IPI, II, and III are summarized in Figure 3.26-28. Interestingly, this transducer yields different results in the case of IP-I and IP-II. For IP-I, the response of PME



device is presented in Figure 3.26. Even this layer shows insignificant but evident selectivity pattern in contrast to IP-I coated QCM electrode where Zn(II) shows larger effect (Figure 3.18). In the case of Cu(II)-IPII, similar behavior was observed (Figure 3.27) the polymer film shows selective inclusion of copper ions, whereas on QCM this effect is much less pronounced (Figure 3.17). Finally, in the case of Cu(II)-IPIII the selectivity



trend is more explicit for the periodic microelectrodes (Figure 3.28) than with QCM (Figure 3.24). These differences have to be regarded in the light of how



the two transducers interplay with the ionic species. The frequency shift of QCM in the liquid media does not only depend on the mass changes, but among others is influenced also by the conductivity of the medium,^{113,114} which needs to be considered.¹¹⁵ However, to a larger extent this can be overcome by exposing only one face of the quartz to the surrounding liquid sample. The ionic solutions further complicate this situation and demand for the readjustment of measurement electronics, proximal and distal electrodes geometry, etc. However, the use of PME device for the ionic species is an established protocol and successful data has been reported for a range of environments.^{116,117}

3.3.13 Real Water Samples

Finally, the rebinding of copper ions from natural water was investigated to obtain first information on real-life applicability of such systems. The obtained sensor results are summed in Table 3.5.

Table 3.5: Sensor response of microelectrodes device coated with Cu(II)-IPIII towards real water specimen spiked to 1mM concentration of Cu(II).

<i>Sr. no.</i>	<i>Water sample</i>	<i>Conductance shift (μS)</i>
1	De-ionized	691.45 ± 2.14
2	Tap (I)	699.18 ± 5.17
3	Tap (II)	696.08 ± 2.57
4	Mineral	752.2 ± 15.12

For this purpose three water samples from different sources were spiked with 0.1M Cu(II) solution to make final concentrations of 1mM. Two samples were of tap water (Ca^{+2} 43-58mg/l, Mg^{+2} 6-16mg/l and for anions Cl^{-1} 1-5mg/l, NO_3^{-1} 4-8mg/l, SO_4^{-2} 9-24mg/l, respectively). The third one was

mineral water containing a comparatively high ionic background (K^{+1} 1.80mg/l, Na^{+1} 13.20mg/l, Ca^{+2} 115.10mg/l, Mg^{+2} 39.40mg/l, for anions Cl^{-1} 18.90mg/l, SO_4^{-2} 223.50mg/l, HCO_3^{-} 256.50mg/l, H_2SiO_3 15.40mg/l, respectively).

In the spiked tap water samples, the imprinted layer shows almost same response as with de-ionized water. On the other hand, in mineral water it shows only 8% larger response owing to the presence of high electrolyte, of course added to the background signals. This is even more astonishing given the fact that the ionic background of the mineral water is ten times higher than the one for tap water. The matrix influence in terms of analytical quality could be considered only minor. This appreciable selectivity shows that it is possible to measure copper ions in natural water samples.

3.4 Conclusion

Molecular imprinting with the metal cations proves a substantial challenge due to their small size and the lack of pronounced geometrical features. The screening of suitable functional monomers by FT-IR and UV-VIS reveal that the main recognition mechanism between the analyte and the polymer in this case involves coordinative bonds. Hence, N-vinyl-2-pyrrolidone proved an optimal monomer, because it acts as a bidentate ligand for the copper ions. When applied as a sensor coating, the fabricated device responds quickly to the presence of copper (ca.1min) and leads to linear sensor response over a wide concentration range (1×10^{-6} to $1 \times 10^{-3}M$) with 20 μ M being the lower limit of detection. The power of the imprinting approach can also be seen by the fact that the resulting materials prefer copper over other bivalent metal ions with similar ionic radii e.g. Ni(II), Co(II), Zn(II). If the metal is not suitable to undergo coordinative binding, such as in the case of Na(I), sensor responses are much lower further corroborating the coordinative approach. The materials also allow for the selective detection in real life samples, where

3. Characterization of Copper-Imprinted NVP Polymer

tap water spiked with copper yields sensor signals that are not more than 1% different from the de-ionized water samples. For the mineral water with containing 686 mg/l salt, the sensor signals are shifted by less than ten percent further underpinning the excellent selectivity of the systems.

4. Titanium Dioxide Nanoparticles Imprinting

4.1 Introduction

Nanoparticles are of substantial scientific interest being a bridge between the bulk materials and atomic/molecular structures. A bulk material regardless of its size should have constant physical properties, but as its size approaches nanoscale and the percentage of atoms on the surface of the material becomes significant, the properties of material also change accordingly. The interesting and unexpected properties of nanoparticles are therefore mainly due to the larger surface area of the material that dominates over the contribution of the small bulk.¹¹⁸

Many metals are able to form oxides that can exhibit structural features with either the metallic, semiconductor or insulator character enabling them to play pivotal roles in many areas of science^{119,120} e.g. being used in the fabrication of microelectronic circuits, sensors, piezoelectric devices, fuel cells, coatings for the passivation of surfaces against corrosion, and as catalysts, etc. More recently, metal oxide nanoparticles have received increased attention due to the characteristic, size dependent physical and chemical properties.¹²¹

Titanium dioxide (TiO₂) is one of the most prominent metal oxides being widely applied e.g. as a catalyst in organic synthesis¹²² and stationary production,¹²³ as photocatalyst for the removal of pollutants,¹²⁴ and as the source of white pigments in paints.¹²⁵ It is an essential part of the photovoltaic devices,¹²⁶ electrochromic devices,¹²⁷ sensors,¹²⁸ food additives,¹²⁹ cosmetics,¹³⁰ and recently it has been used as the potential tool for cancer treatment.¹³¹

4.1.1 Problem Statement

The application of nanoparticles in human life has burgeoned to the extent that consciousness arises about health risk factors they may impart. The effects of nanoparticles on human health are yet to be established but they can certainly interfere with human life if entering the human body via lungs, intestines or skin depending on their size and surface properties.¹³² There are indications that the smaller the size of particle, the more toxic it could be.¹³³ Furthermore, distribution of the particles in the body strongly depends on their surface characteristics. To establish a standard study about nanoparticle toxicity, its extent, its relation with the size of particle, and the nature of application, there should be a robust, straightforward, and simple method for their sensing. Molecularly imprinted polymers could prove as a valuable tool in this regard along with a suitable imaging technique e.g. atomic force microscope (AFM),¹³⁴ electron energy loss spectroscopy (EELS),¹³⁵ energy dispersive x-ray spectroscopy (EDS),¹³⁶ field emission scanning electron microscopy (FESEM),¹³⁷ modified rapid expansion of supercritical suspension (RESS),¹³⁸ scanning electron microscopy (SEM),¹³⁹ or transmission electron microscopy (TEM).¹⁴⁰ Among these techniques, AFM is the most popular as it is ideally suited for the characterization and offers the capability of 3D visualization, as well as the qualitative and quantitative information on a range of physical properties including size, morphology, surface texture, and roughness.¹⁴¹ Moreover, the statistical information including size, surface area, and volume distributions can be determined as well. AFM can characterize a wide range of particle sizes from 1nm to 8 μ m.¹⁴² In addition; AFM can characterize NPs in multiple media including ambient air, controlled environments, and even liquid dispersions.¹⁴³

4.2 Methods and Strategies

All chemicals and reagents used in this work were purchased either from Merck or Sigma Aldrich & Co. These were of highest purity and used as received. Two types of polymeric substrates were evaluated; polyurethane and titania sol gel to develop surface imprints of titanium dioxide nanoparticles. All characterization studies by AFM were carried out by coating nanoparticles/polymer films on glass slides roughly $\sim 1.50\text{cm}^2$ in size. Prior to this, slides were thoroughly cleaned with acetone and heated at 60°C to remove any impurities from the surface.

4.2.1 Synthesis of Titania Nanoparticles

Titanium dioxide nanoparticles were prepared by a standard co-precipitation method developed in the group, $178\mu\text{l}$ of titanium tetra chloride (TiCl_4) were added to 6.5ml of carbon tetrachloride (CCl_4). This reaction mixture was heated for 30 minutes at 60°C . After this, it was kept at room temperature till cooled. Then $100\mu\text{l}$ of 1M NaOH were added drop wise to the solution while stirring vigorously to obtain white precipitates of TiO_2 .¹⁴⁴ Here it is worth to mention that slow addition of 1M NaOH droplets by strong and continuous stirring substantially influence the particle size and its distribution; the more vigorous the stirring; the smaller the nanoparticles and the more uniform the size distribution. This suspension was centrifuged at 4000rpm for 30 minutes to obtain white TiO_2 nanoparticles powder and calcined in an oven at 110°C to evaporate solvent residues. Afterwards, nanoparticles were annealed in two steps; at first they were heated at 400°C for 60 minutes and then at 800°C for 120 minutes. The first annealing step completely removes the organic materials and the second one helps optimizing the morphology.¹⁴⁵ Finally, the ultrafine powder was stored at room temperature in a plastic vial within a desiccator.

4.2.2 Synthesis of Ti Sol Gel Thin Films

Titanium dioxide sol-gel was synthesized by dissolving 67 μ l of tetrahydroxy titnate ($\text{Ti}(\text{OBU})_4$) as monomer in 970 μ l of isopropanol (IPA). Further, 10 μ l of titanium tetrachloride (TiCl_4) were added to this mixture as a reagent to initiate and propagate hydrolysis and condensation of the titanates. The mixture was then allowed to polymerize at 60°C for 30 minutes with continuous stirring till gel point was reached. During this synthesis, no water was added for carrying out hydrolysis, as the isopropanol already contains 0.5% water, which is sufficient for this purpose. This sol gel was directly employed for coating polymer films without any further dilution.

4.2.3 Synthesis of Polyurethane

For polyurethane synthesis, 100mg of diphenyl 4-4, diisocyanate (DPDI), 197mg of bisphenol A (BPA) and 22mg of phloroglucinol (PG) were dissolved in 200 μ l of tetrahydrofuran (THF). The ratio of isocyanate to hydroxyl group remained 1:2 in this mixture. This pre-polymer solution was heated at 70°C with stirring till its gel point. This solution was further diluted by THF in the ratio of 1:4 to obtain the required polymer layer heights.

4.2.4 Preparation of Nanoparticle Suspension

The samples of nanoparticles for AFM characterization were prepared dispersing 5mg of nanoparticles in 400 μ l of IPA with strong and continuous stirring. Out of this suspension, 5 μ l were coated on a glass slide spinning at a speed of 3000rpm for 5 minutes. It was directly employed for recording AFM image without any further surface treatment.

4.2.5 Imprinting Strategies

Two types of imprinting procedures were evaluated to generate titanium dioxide nanoparticles imprints on the polymeric layers; stamp imprinting and direct imprinting. A general schematic diagram that helps understanding the basic principles of these imprinting strategies can be seen in Figure 4.1.

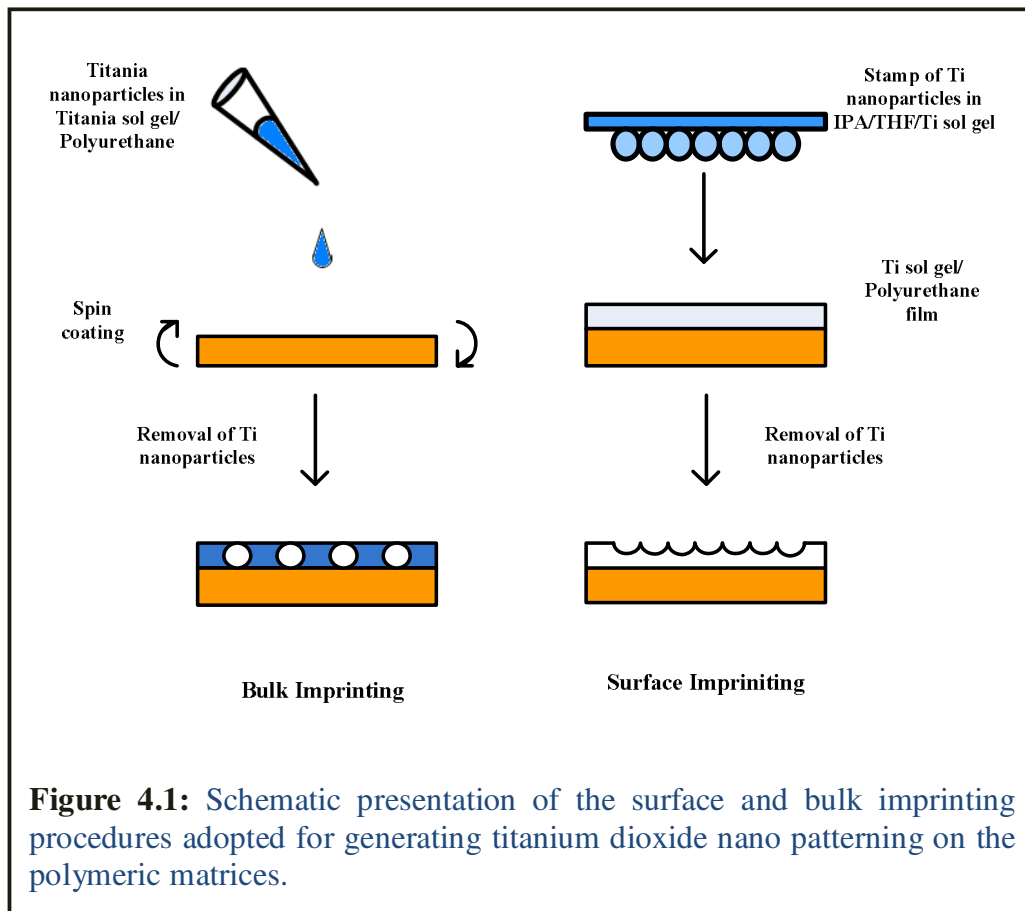


Figure 4.1: Schematic presentation of the surface and bulk imprinting procedures adopted for generating titanium dioxide nano patterning on the polymeric matrices.

During surface imprinting the stamp of analyte is pressed against a pre-polymer which is then allowed to cure in the presence of analyte. It results in the imprints of analyte on the polymer surface when the stamp is removed. In direct imprinting the pre-polymer mixture is prepared in the presence of analyte and then it is allowed to cure. When the analyte is washed off, it produces the desired interaction sites on the surface. These imprinting

techniques are assessed employing polyurethanes and titanium sol gel materials as the substrate matrix.

Stamp Imprinting of Titania Nanoparticles

The synthesized titanium dioxide nanoparticles were suspended in 400 μ l of IPA. The stamp of nanoparticles was prepared by spin coating 10 μ l of the above mentioned suspension at a speed of 3000rpm for about one minute and dried in the air at room temperature. On another glass slide, a thin layer of polymer (polyurethane/titania sol gel) was spin-coated by depositing 5 μ l of pre polymer solution and spinning at 3000rpm for 30 seconds. Then the stamp and the glass slide both were clamped together and kept overnight at room temperature.

Direct Imprinting of Titania Nanoparticles

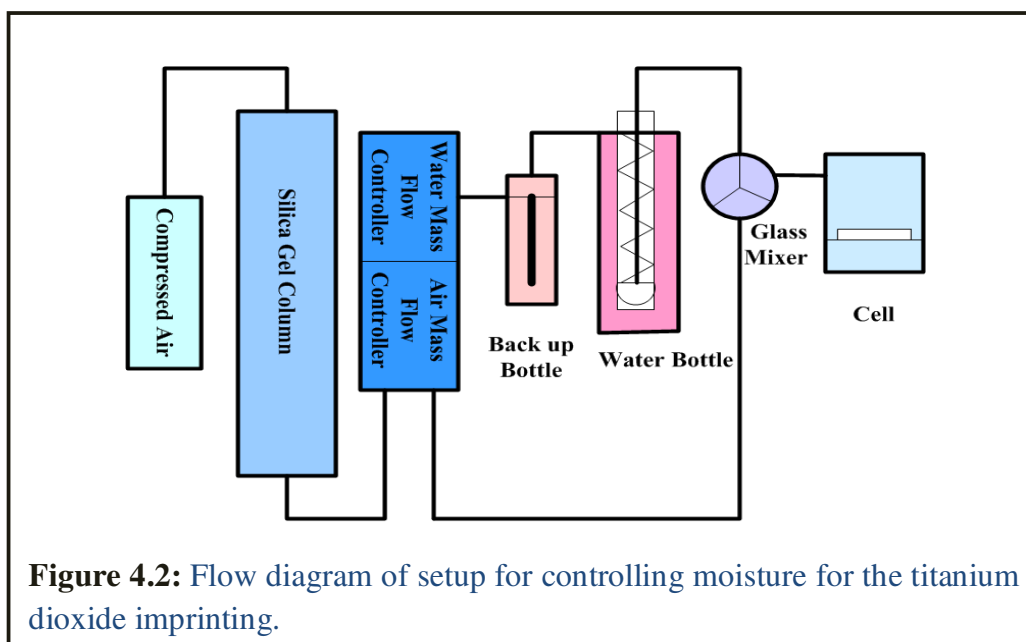
For the direct (i.e. stamp free) imprinting, following procedure was adopted:

- (i) First, 5mg of nanoparticles were dispersed in 100 μ l of titania sol gel precursor and 400 μ l of IPA. This suspension was stirred vigorously for 30 minutes to evenly distribute the nanoparticles. Out of this suspension, 10 μ l were spun on a glass slide at a speed of 2000-3000rpm for about 1-2 minutes. The polymer layer prepared in this way was cured at room temperature for 4-5 hours. Finally, the samples were directly employed for recording AFM images.
- (ii) To synthesize polyurethane MIP layer endorsing titanium dioxide nanoparticles, 5mg of nanoparticles were suspended in 20 μ l of Polyurethane and 300 μ l of THF. Out of this dispersion, 10 μ l were spun at 2000-3000 rpm for 1-2 minutes to obtain a polymer layer. The samples were cured at room temperature for 4-5 hours followed by recording AFM images.

In order to observe the influence of humidity on the polymer substrates supporting nanoparticles, a setup was built that allowed to control this parameter in the reaction chamber.

4.2.6 Moisture Control Setup

To observe the effect of humidity, the level in air was maintained by a constant source of dry air, mass flow controllers (Tylan-Model FC 2900V) and a circuit board model RO7031 for controlling and supplying the required amount of air (for the schematic see Figure 4.2). One mass flow controller



was connected to a gas washing bottle filled with water. By mixing defined streams of dry and humidity-saturated air, respectively, the desired target humidity could be achieved.

4.2.7 AFM Characterization Protocol

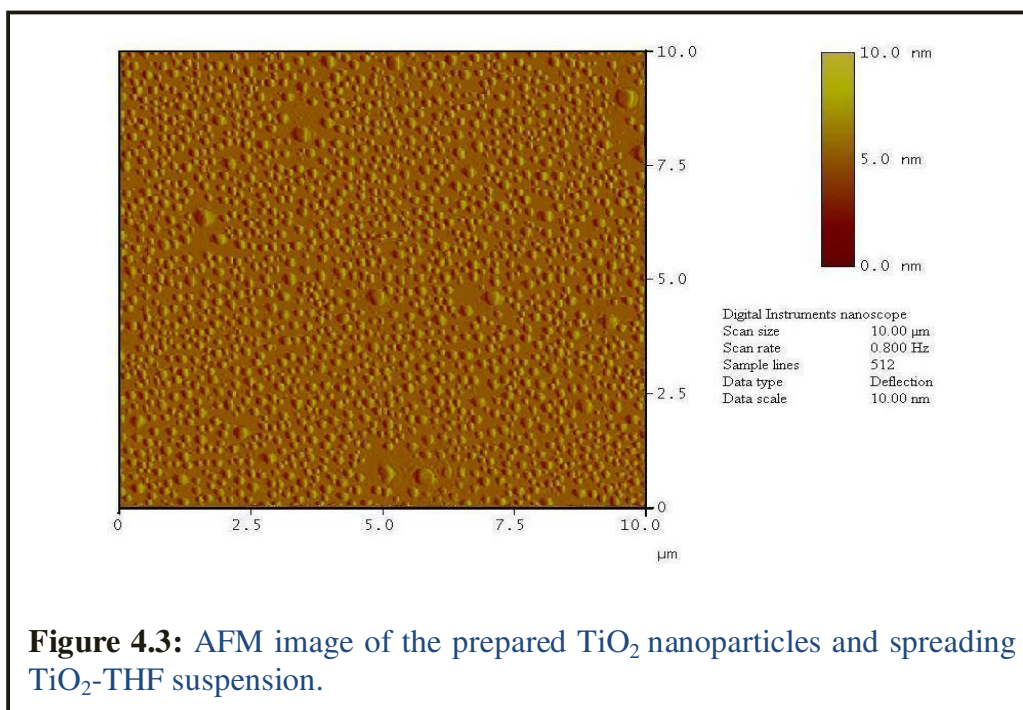
VEECO Nanoscope IVa AFM/STM system was utilized for recording the AFM images of titanium dioxide nanoparticles and imprinted polymer layers.

For acquiring scans, silicon nitride AFM probes (Model NP-S10 from Veeco) having cantilever spring constants of 0.58-0.06 N/m were used. All scans were recorded at ambient temperature ($24 \pm 2^\circ\text{C}$) in the air via contact mode. Three samples of each experiment were prepared and imaged at three distinct areas using the same tip. From these images, one representative each is displayed in this dissertation. The image data was analyzed by AFM system software to extract surface related features e.g. the root mean square roughness RMS (standard deviation of the z value within the given area), R_{max} (the difference in highest and lowest points on the surface relative to the mean plane), etc.

4.3 Results and Discussion

4.3.1 Titanium Dioxide Nanoparticles (Ti NPs)

First of all, titanium dioxide nanoparticles were characterized by AFM. One of the images is displayed in Figure 4.3. Evidently, particle diameters are



distributed over a larger range. Section analysis allows more in-deep assessment revealing that nanoparticles height and size dimension are between 50-120nm on the average, whereas the surface roughness related parameter (R_{\max}) is 67.4nm.

Strategies for Removal of Template

The following sections discuss different approaches adopted for removing nanoparticles from the polymeric matrices.

4.3.2 Surface Imprinting and Washing with Acidic Medium

The stamps of titania nanoparticles over polyurethane layer were dipped in 50ml of 0.01M HCl for 5-6 hours in order to detach stamps and nanoparticles from the polymer layer. After drying in the air at room temperature, AFM images were recorded. A representative picture is displayed in Figure 4.4

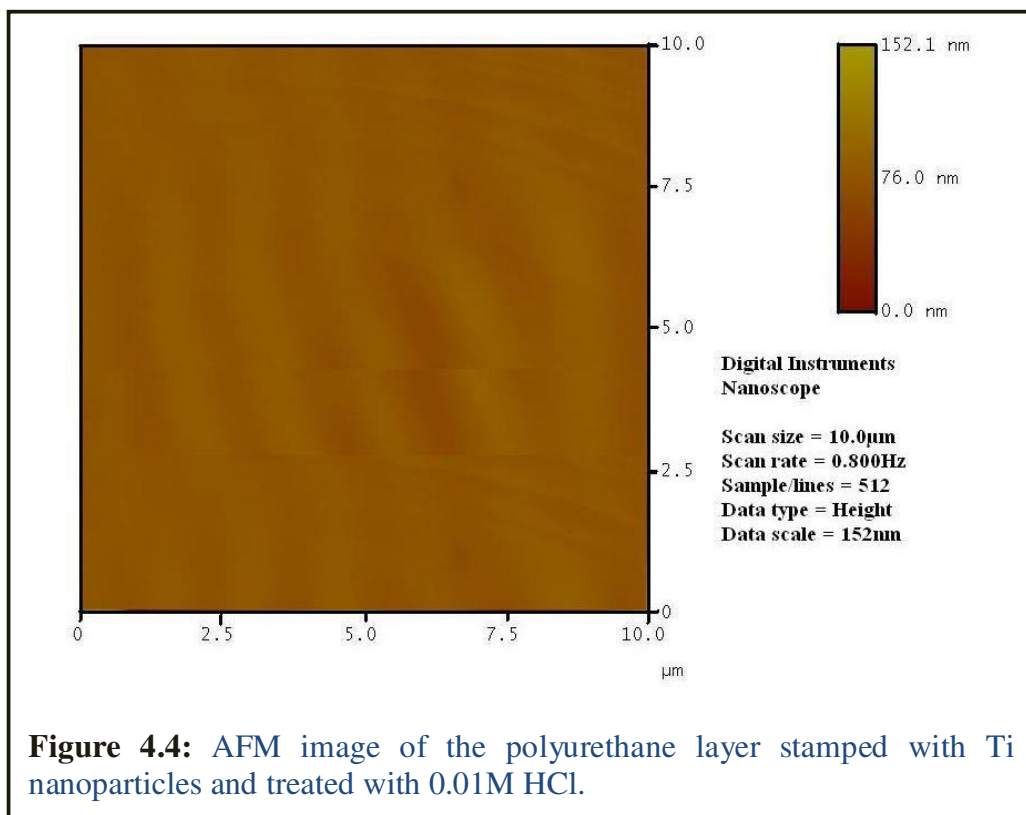
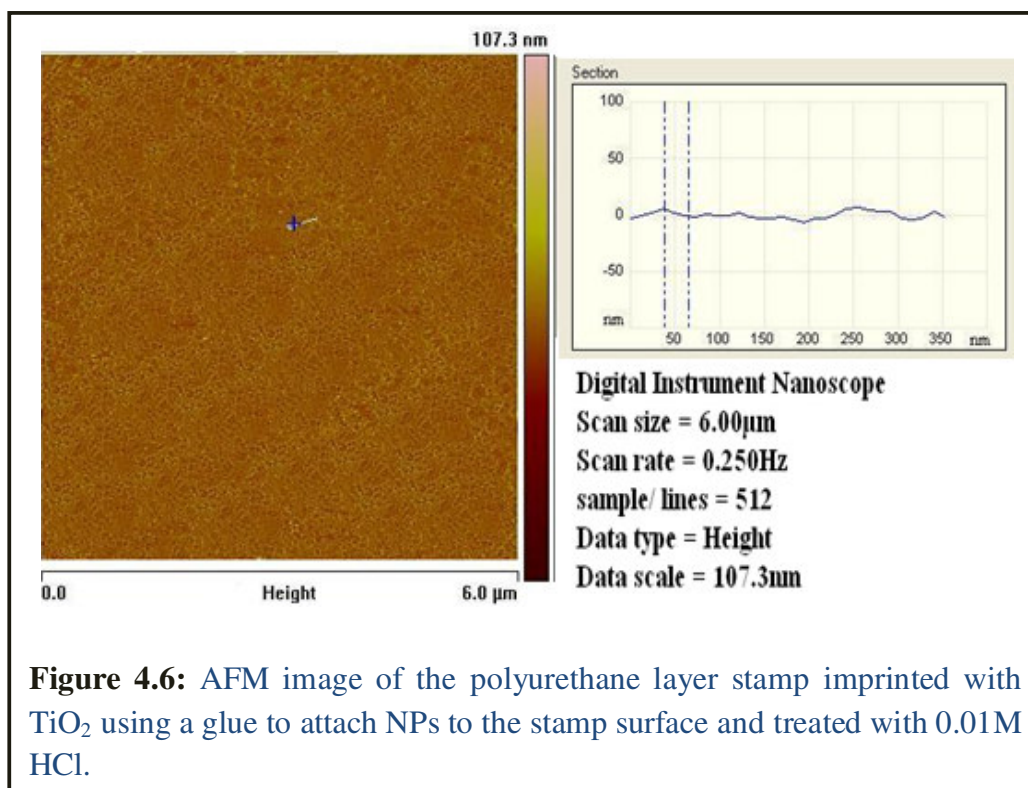
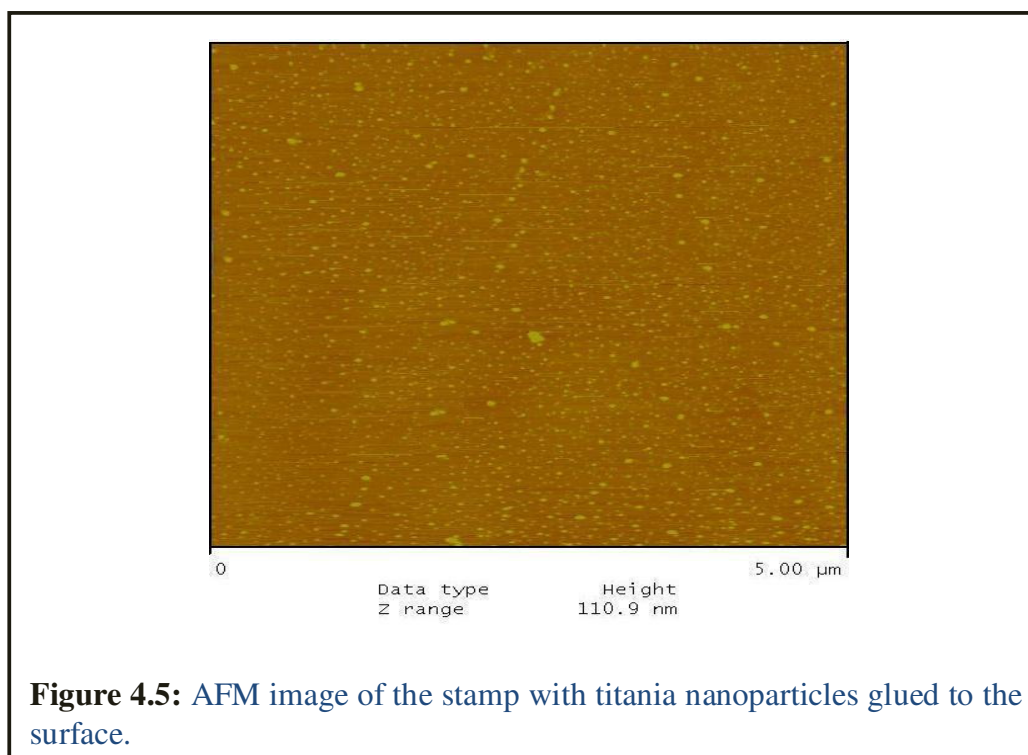


Figure 4.4: AFM image of the polyurethane layer stamped with Ti nanoparticles and treated with 0.01M HCl.

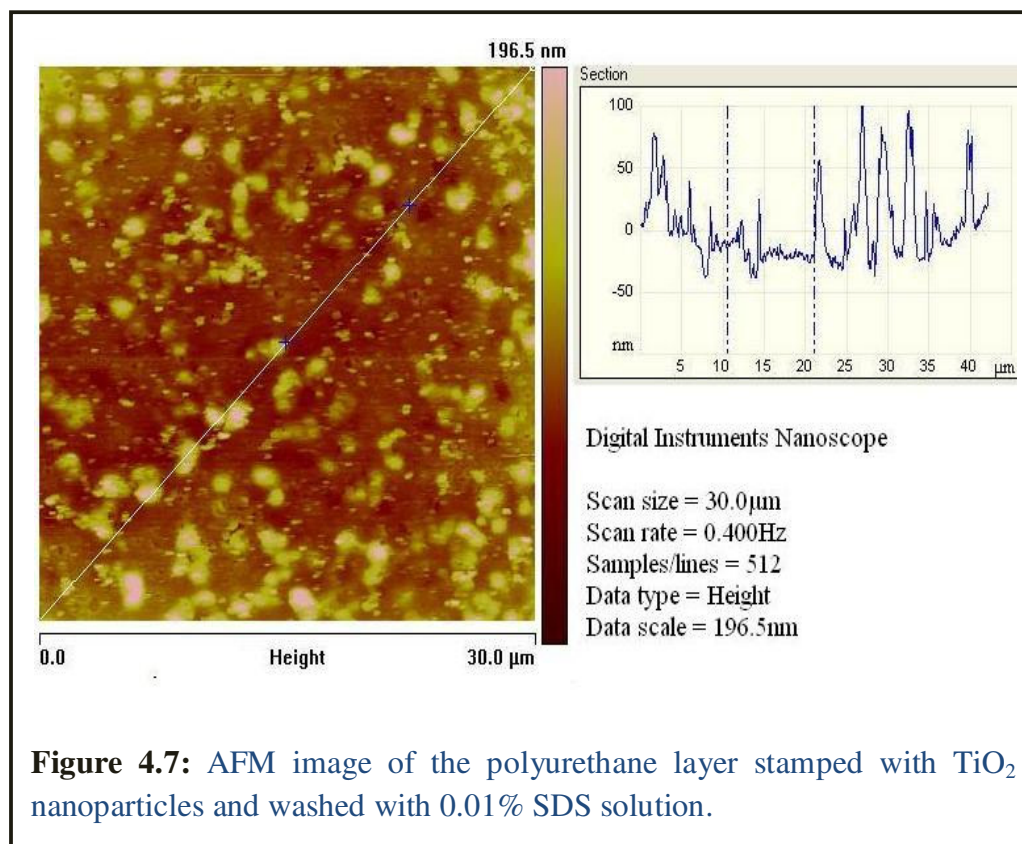
revealing a planar polymer surface without generating imprinted cavities. The section analysis also does not reveal any significant surface projections, but shows that RMS parameter is around 1.6nm that corroborates nanoparticles are washed off. The rationale behind the elution of nanoparticles by solvation with HCl is that a solvent can modify the interface between a nanoparticle and the polymer matrix by surface modification/passivation.¹⁴⁶ The effect of different acids upon the morphology of nanoparticles is also documented¹⁴⁷ which makes it logical to assume that this approach is suitable for the template removal. Applying acid may either results in the surface decomposition of nanoparticles¹⁴⁸ or it adsorbs on the particle surface resulting in the reduction of surface tension. HCl is chosen for its weaker affinity¹⁴⁹ towards titanium thus obtaining hydrogenation of O at surface. To avoid possible deterioration of polymer layers, a concentration of 0.01M was used, but nonetheless Figure 4.4 does not reveal surface imprints of nanoparticles. Another possible conclusion, however, is that when titania nanoparticles are stamped on the polyurethane layer these only adhere to the polymer surface and thus are washed off by acid without leaving behind any cavity on the polymer surface.

To ensure that TiO₂ nanoparticles indeed adhere on the stamp surface, the particles were suspended in 400μl IPA that contained 100μl of titanate sol. This was then used for coating and made sure that the particles were “glued” to the surface. Figure 4.5 shows the AFM image of the stamp before actually applying it for the imprinting. One can clearly see that the nanoparticles are ideally distributed. After imprinting and removing the stamps in 0.01M HCl, the polymer yields the surface structures as summarized in Figure 4.6. In this case clearly patterns can be seen, however, the cavities are only about 1-5nm deep and the surface and RMS parameter is 2.6nm. Compared to the results shown in Figure 4.5, the polymer surface indeed exhibits imprints even though they do not yet perfectly reproduce the template.



4.3.3. Surface Imprinting and Washing with Sodium Dodecyl Sulfate Solution

To exclude that HCl leads to modification of the surface after imprinting, other washing solutions were tested, one of which contains 0.01% (m/v) sodium dodecyl sulfate resulting in the surface structures shown in Figure 4.7. It is observed that SDS solution causes dissolving of the polymer surface.

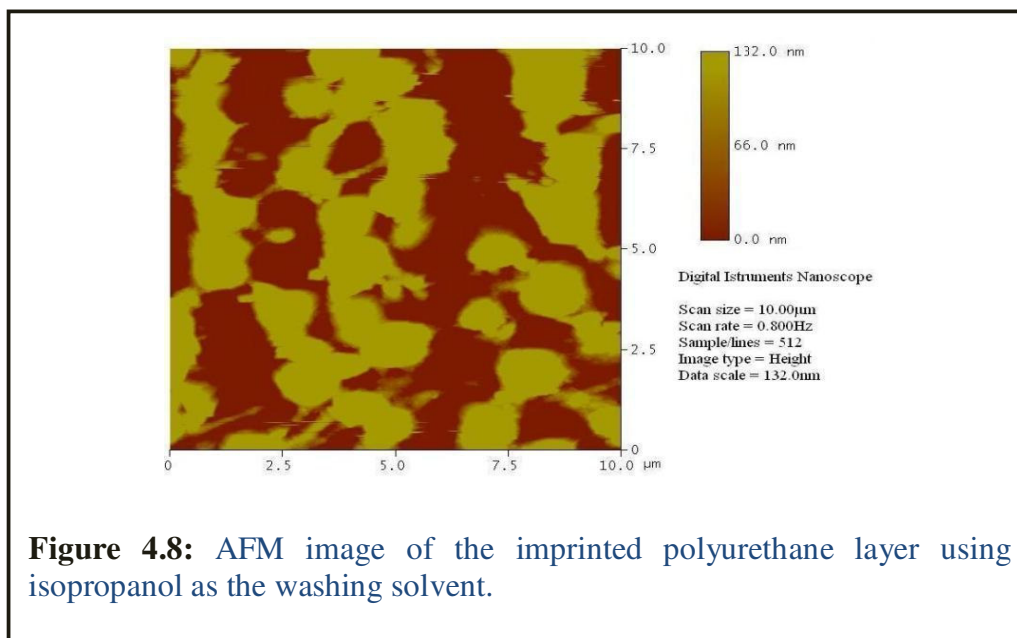


Furthermore, section analysis reveals micrometer dimensions of the particles indicating clustering on the surface.

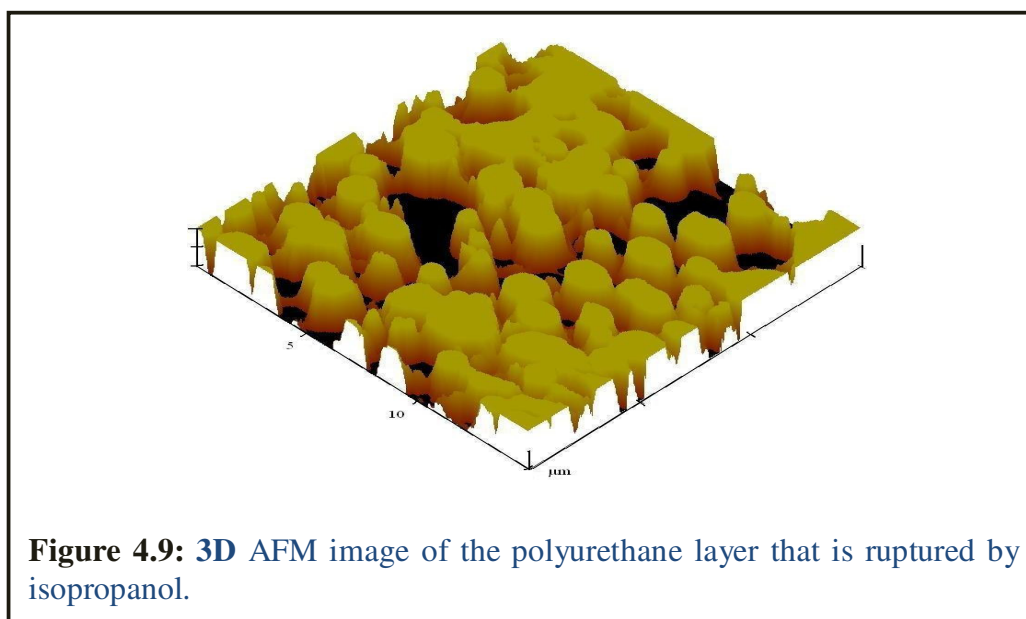
4.3.4. Surface Imprinting and Washing with Isopropanol

The acidic medium causes leveling of the polymer surface while SDS solution produces clustered structures. Therefore an organic solvent was assessed after

the acid (inorganic medium) and SDS (amphiphilic aqueous medium), namely IPA to remove the template, and resulting in surfaces as depicted in Figure 4.8. It shows that IPA being organic partly dissolved the polymer surface.



The RMS value is found to be 112.6 nm indicating agglomeration of the particles to μm dimension. The 3D image of another scan is shown in Figure 4.9 that confirms the depletion of polymer layer by IPA.



4.3.5 Direct Imprinting and Washing with Acidic Medium

In the view of the observations following surface imprinting of titania nanoparticles and their solvation by different solvents, experimental strategies were changed and titania nanoparticles were coated directly on the respective polymer substrate. The nanoparticles were suspended in tetrahydrofuran and then a small amount of polyurethane precursor solution was added following the procedures summarized in section 4.2.5(ii). This mixture was then directly coated on the glass substrate and cured overnight. The respective AFM image can be seen in Figure 4.10. It reveals that the polyurethane monomer mixture

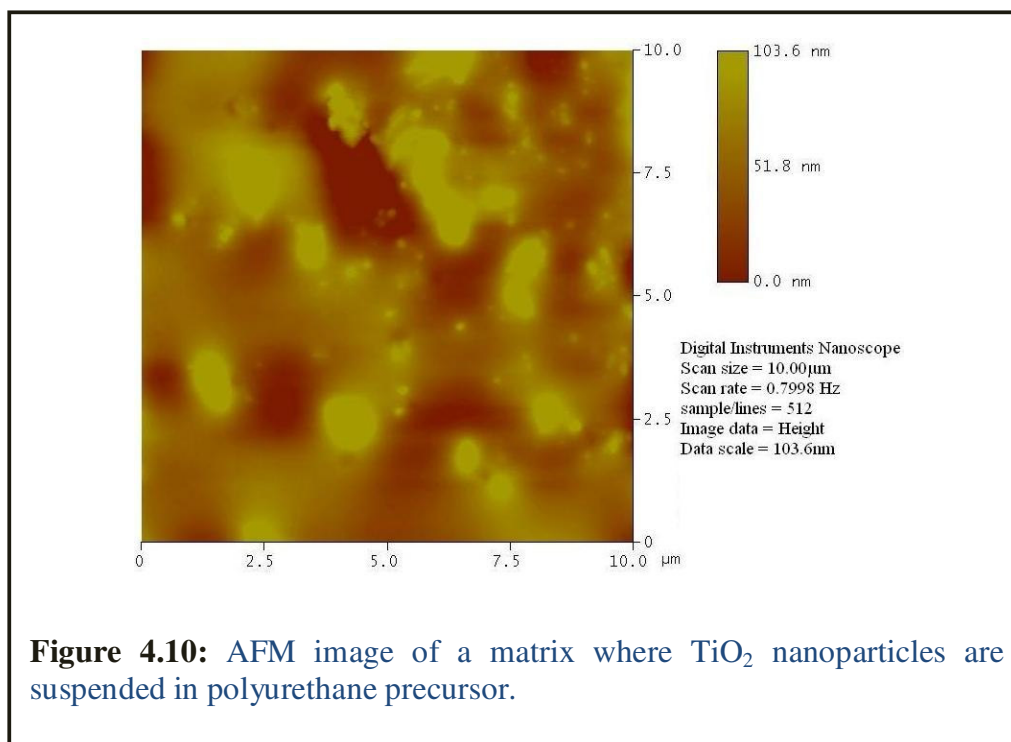
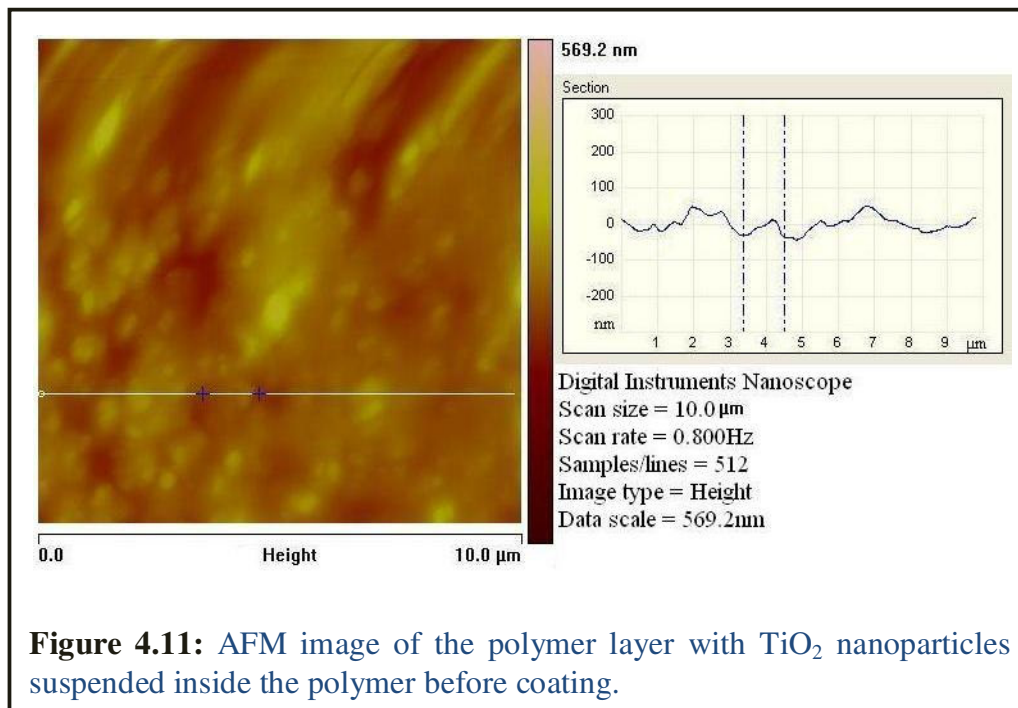


Figure 4.10: AFM image of a matrix where TiO_2 nanoparticles are suspended in polyurethane precursor.

obviously is not suitable as a dispersing medium for titania nanoparticles, as the image contains larger clusters having several μm lateral dimensions and more than 100nm height. It appears that despite sufficient stirring for the sake of uniform distribution, fine particles (50-100nm in Figure 4.3) adhere to one another yielding agglomerates ($>1\mu\text{m}$).

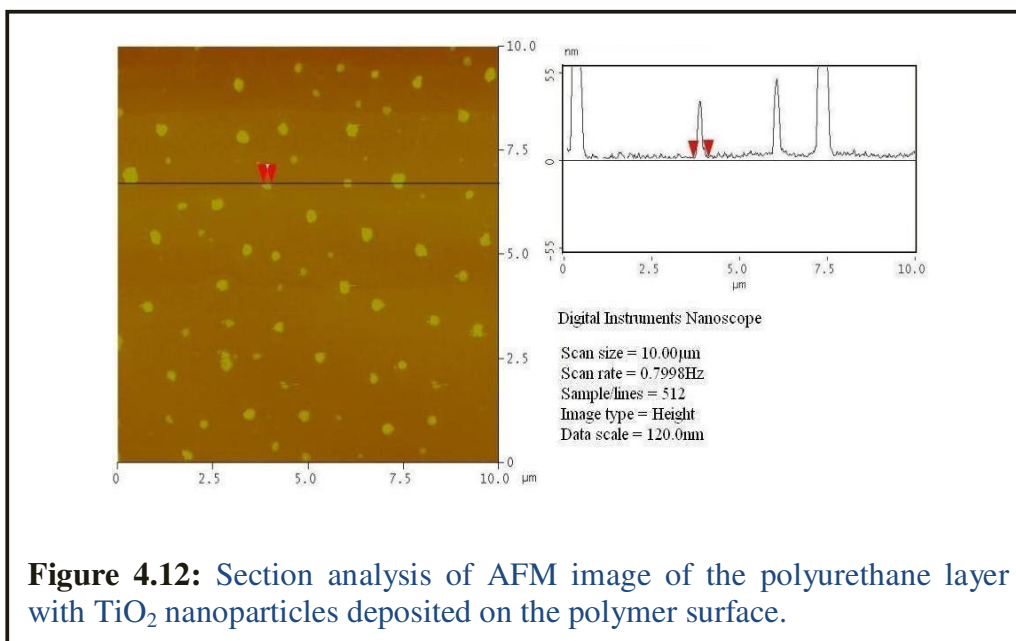
Nonetheless, this layer was subjected to 0.01M HCl to test template removal. Figure 4.11 shows the resulting surface. Apparently, nanoparticles have not



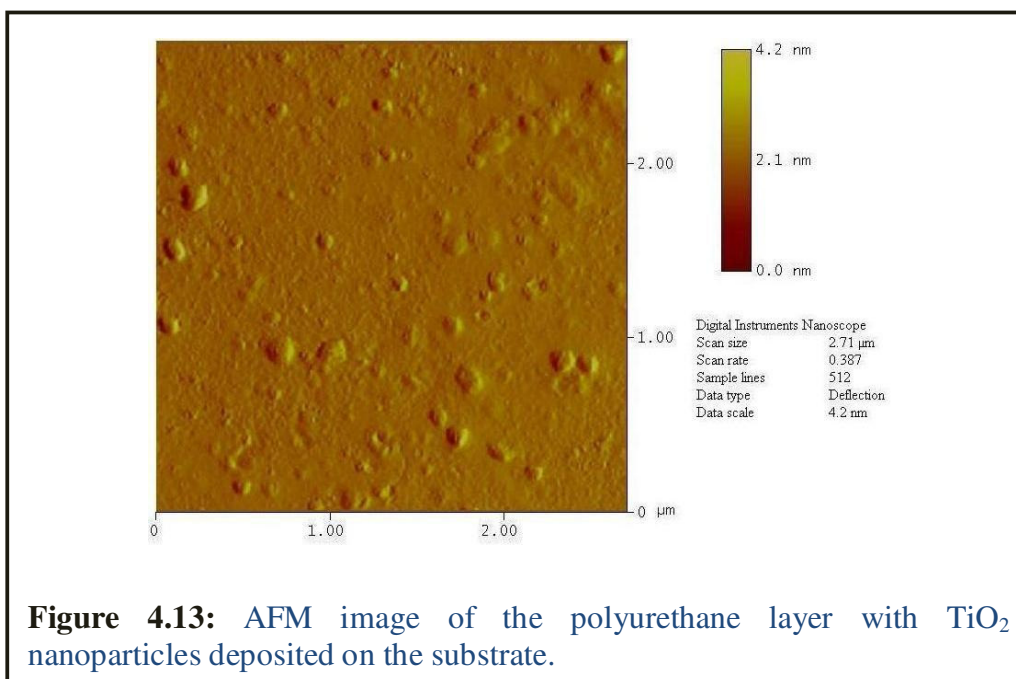
been removed by treating with acid. Contrary to Figure 4.4 with its flat surface, here the particles appear to be buried under a polymer layer. Section analysis reveals surface structures that correspond to nanoparticles covered by a polymer layer instead of the sharp projections of individual particles. Therefore, the particles are obviously irreversibly buried within the polymeric matrix and hence completely “immobilized”. Thus the template nanoparticles have to be spread on the top of the polymer substrate. In pursuing this course an interesting result was obtained when titania nanoparticles/THF suspension was coated on top of ca. 350nm layer of polyurethane. The result can be seen in Figure 4.12 along with section analysis.

It reveals swelling of titania nanoparticles to larger dimensions with even distribution. The shape of peaks in section analysis indicates that these cannot

4. Titanium Dioxide Nanoparticles Imprinting



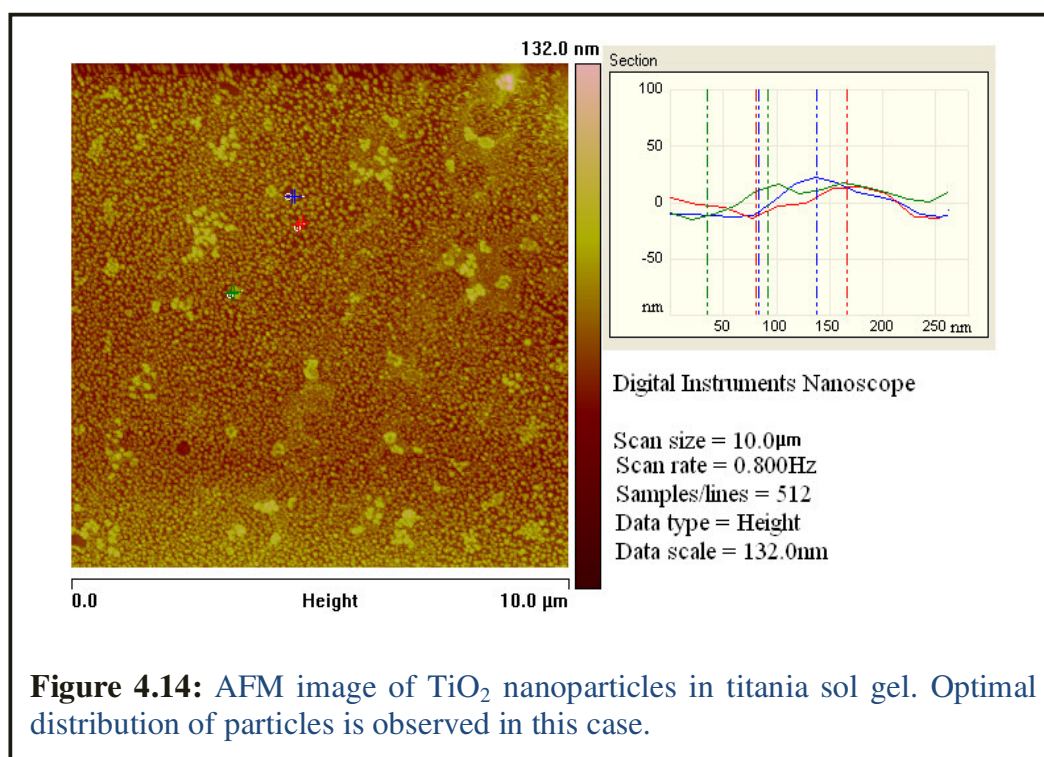
be regarded as clusters but their size has increased to ~400nm. These polymer layers were exposed to 0.01M HCl that was now in direct contact with the nanoparticles in contrast to the previous situation (Figure 4.11) leading to the



4. Titanium Dioxide Nanoparticles Imprinting

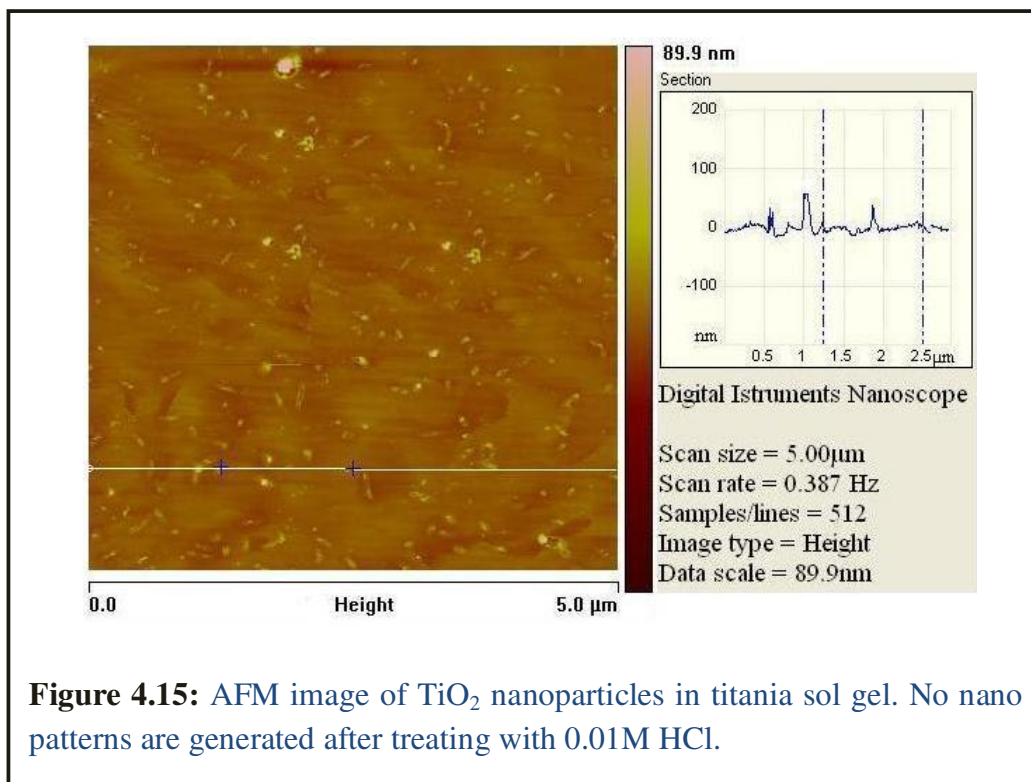
AFM image shown in Figure 4.13. The procedure does not generate a specific pattern, additionally; the large particles are not affected by the acid.

In the light of all results described so far, another polymer system has to be chosen on the basis that titania nanoparticles should have affinity towards titania sol gel as both consist of a Ti-O network similar in the chemical structure. Considering this affinity relation Ti sol gel coatings were considered. For this purpose TiO_2 nanoparticles were dispersed in titanate sol gel plus IPA and dried in the air overnight after coating, resulting in AFM images as shown in Figure 4.14. Obviously, nanoparticles are optimally



dispersed on the surface. They are less than 50 nm high and have a diameter of 50-100 nm thus indicating that the particles are indeed submersed in the forming film.

This layer was treated with 0.01M HCl to achieve the image displayed in Figure 4.15 that again reveals leveling off the whole polymer surface together with removing nanoparticles.



Regarding the RMS parameter that was 7.30nm after treatment with acid as compared to 13.21nm (Figure 4.14) for initial polymer layer further confirms leveling of the surface. At this point it can be concluded that acidic medium is not a suitable agent for removing titania nanoparticles. However, the experiment also shows that the nanoparticles remaining on the surface do not change their size. This means that titania sol gel is an efficient gluing and dispersion medium for nanoparticles, in which it clearly exceeds polyurethane. One of the possible reasons is that the polyurethane matrix is not suitable to suspend particles leading to clustering, while the titania matrix is chemically much more similar to the particles thus overcoming agglomeration.

4.3.6 Mechanical Agitation Employing Surface Imprinting

Another option for removing the nanoparticles may be given by sonication and therefore mechanical agitation. This was applied to both polymer systems i.e. polyurethane and Ti sol gel. One representative picture showing the outcome of this approach is shown in Figure 4.16. Obviously, mechanical agitation results in damaging the polyurethane layer.

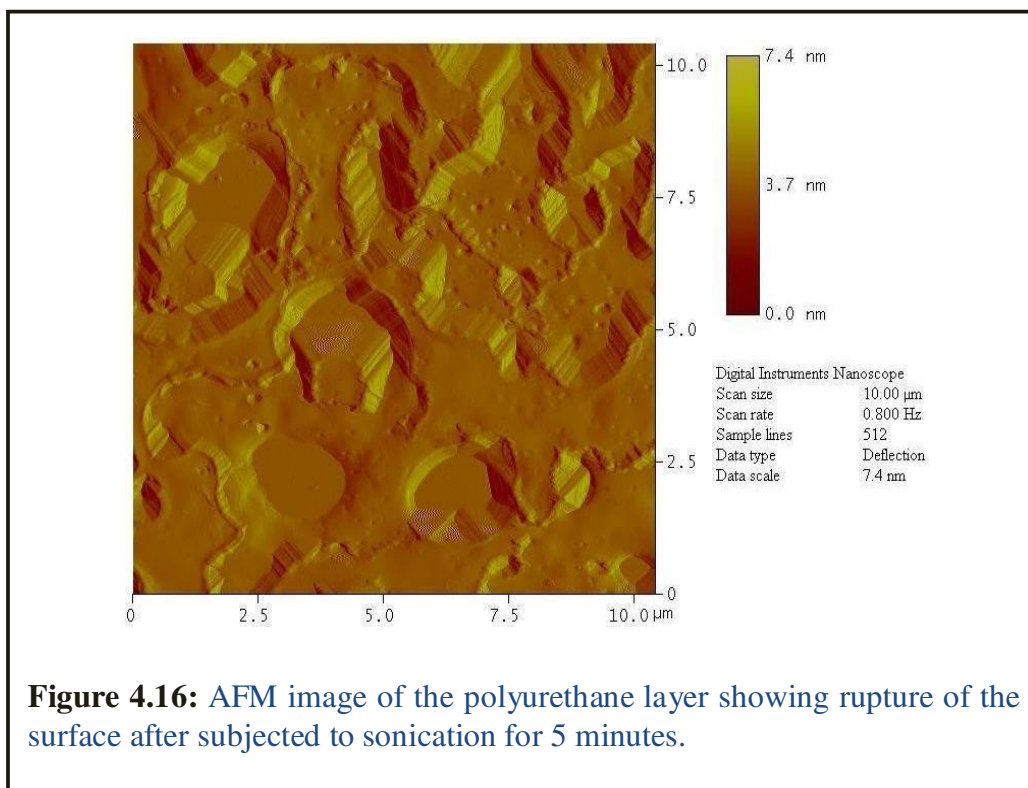
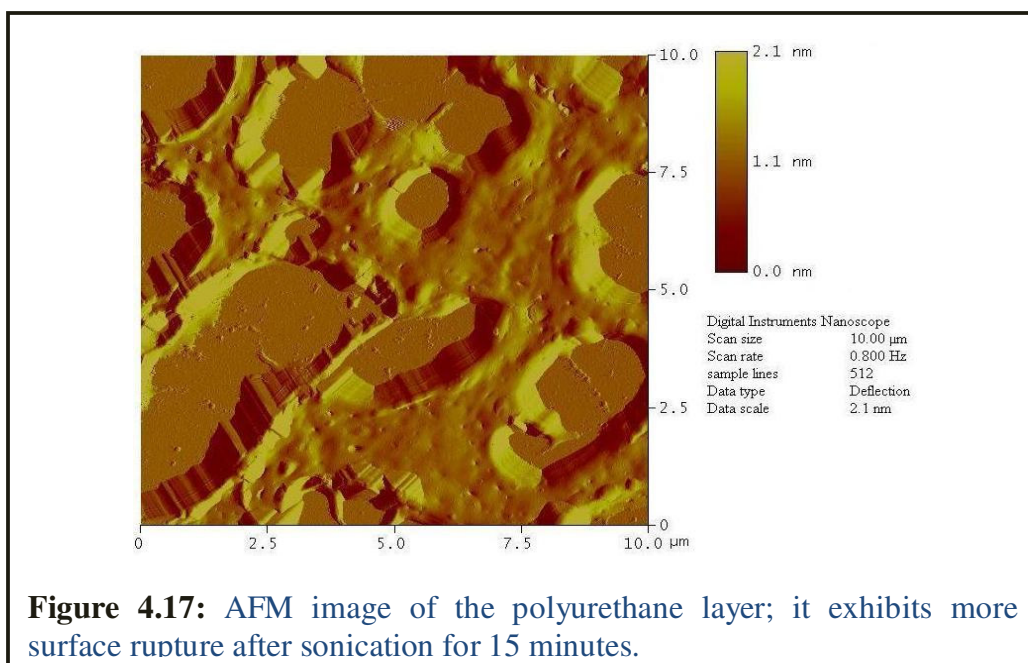


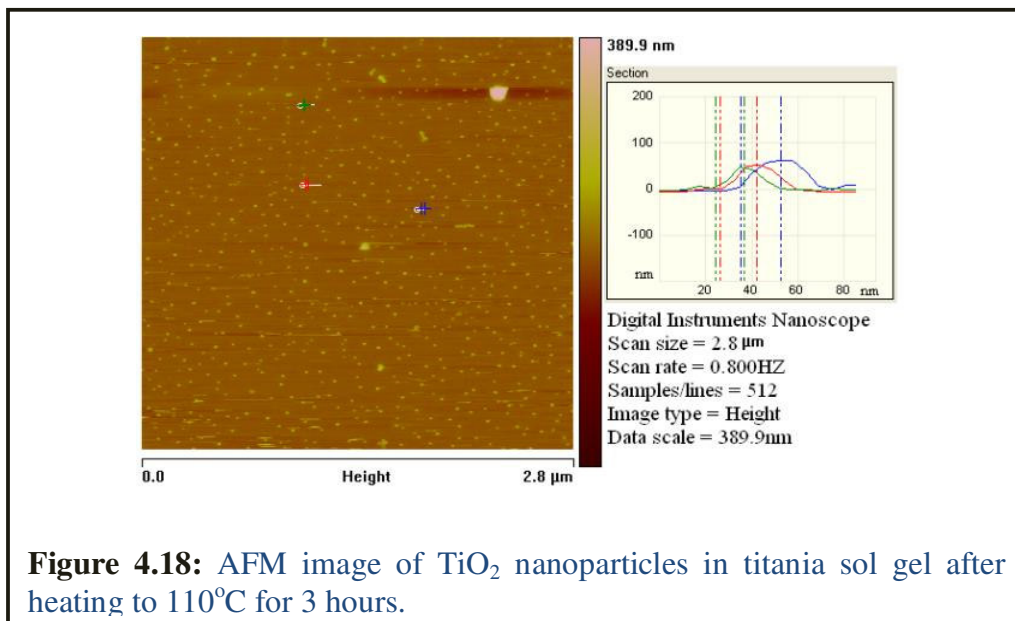
Figure 4.16: AFM image of the polyurethane layer showing rupture of the surface after subjected to sonication for 5 minutes.

To confirm whether sonication indeed leads to destruction of the layer, stamps were removed by sonication for 15 minutes. The resulting polymer surface is depicted in Figure 4.17. Increasing sonication time obviously further ruptures the polymer layer. This implies that mechanical agitation is not suitable for removing nanoparticles after surface imprinting.

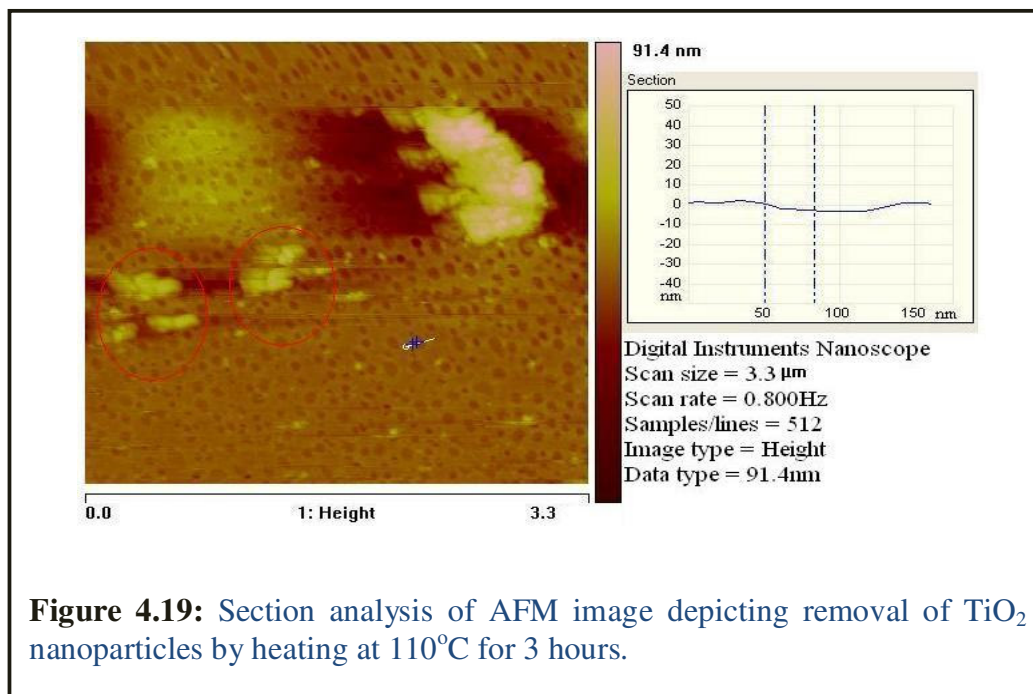


4.3.7 Influence of Heat

To remove nanoparticles from the polymer surface heat treatment was tested. The titania sol gel layers having titania nanoparticles were cured for 12 hours and these were heated to 110°C for three hours. The AFM image 4.18 shows



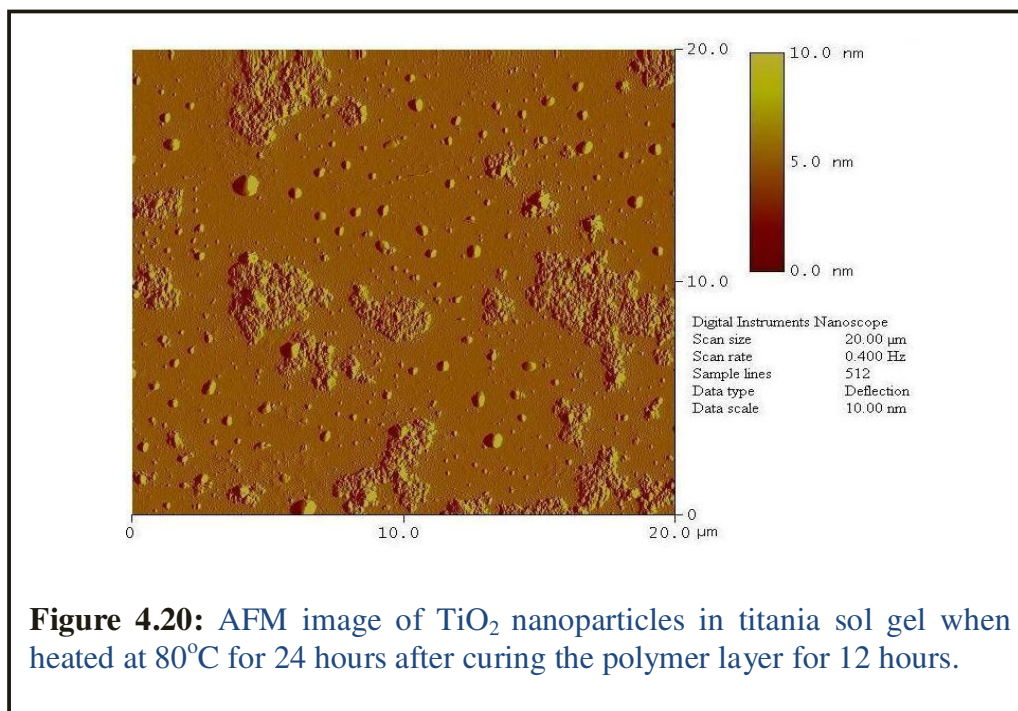
that this sudden exposure of the polymer layers to heat causes the particles to shrink (40-50nm in diameter). Further samples were dried at room temperature for only one hour and then exposed to 110°C for the same three hours. The results are summarized in Figure 4.19.



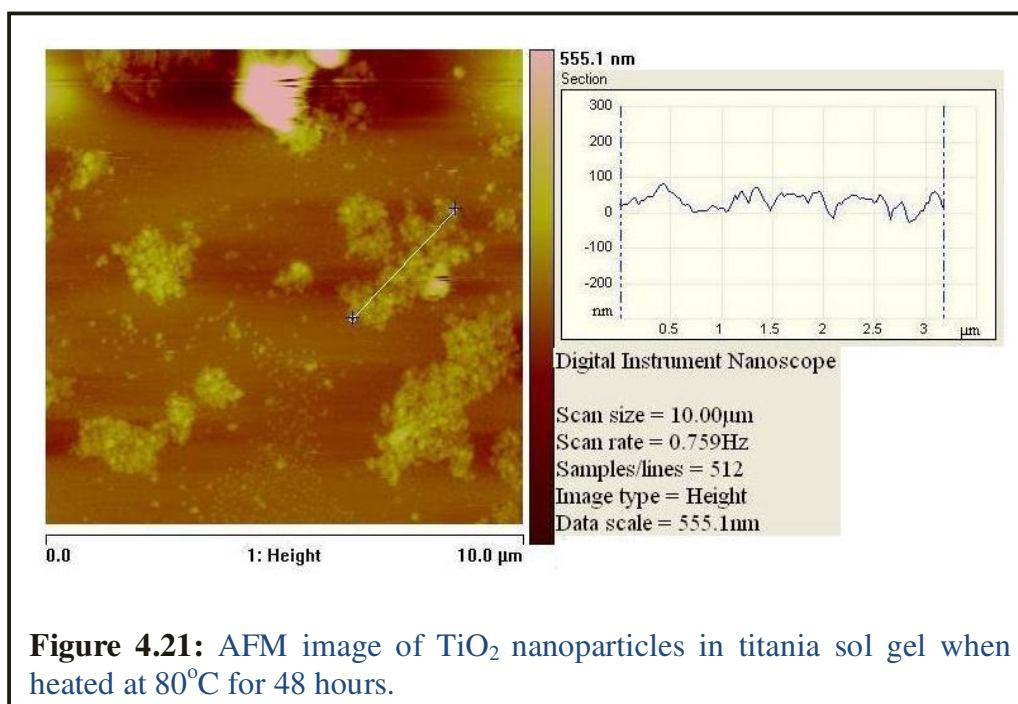
All titania nanoparticles could be removed from the titania thin film. Section analysis shows that the cavities are approximately 10nm deep and 100nm wide. The surface roughness parameter RMS is found to be 0.94nm that manifests the removal of nanoparticles. One thus can assume heating first leads to the shrinking of nanoparticles followed by their disintegration. To further study the heating effect on nanoparticles that itself seems a promising strategy, samples were prepared in the same way. After hardening overnight they were subjected to lower temperatures over extended periods of time, namely 80°C for 24 hours and 48 hours, respectively. After 24 hours, images the one shown in Figure 4.20 could be obtained. The nanoparticles remains at the sol gel layer surface as in the first case (Figure 4.19) however, they have agglomerated together to form patches or islands ranging from 0.1 to more

4. Titanium Dioxide Nanoparticles Imprinting

than $1.37\mu\text{m}$ in size. The RMS value is also increased to 33.3nm that shows enhanced roughness of the polymer surface.

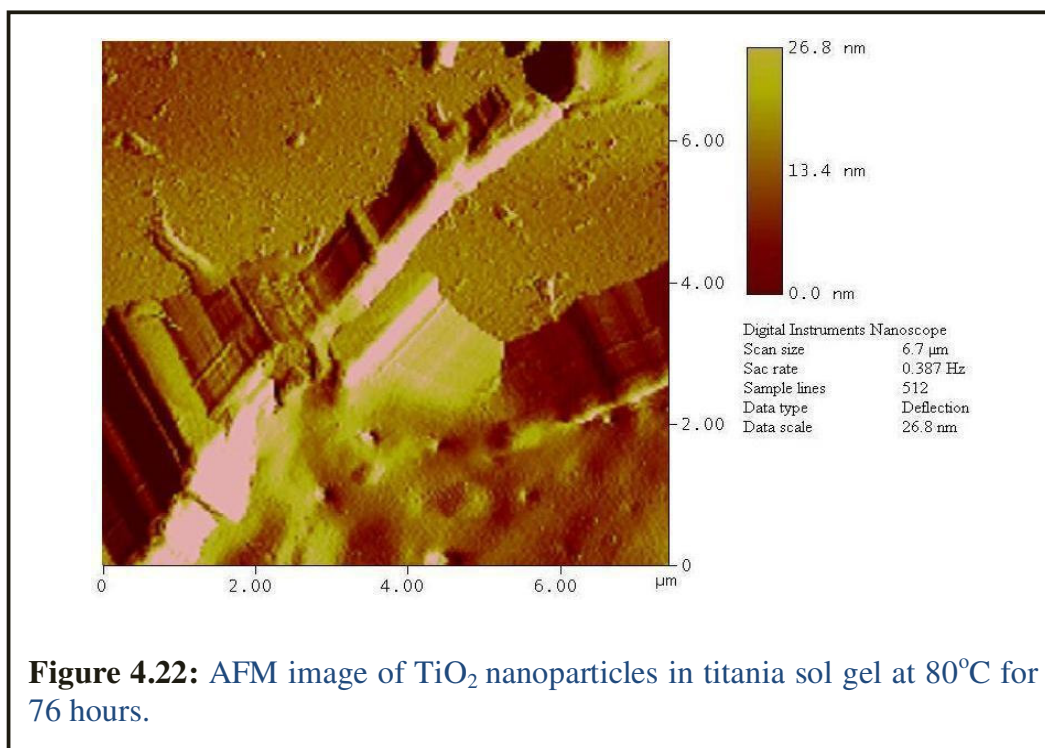


After 48 hours another AFM image was again recorded (Figure 4.21).



Obviously, further heating increases the size of these islands up to 3-2 μm and nearly 100nm in height. The RMS value is 52.4nm depicting enhanced surface roughness.

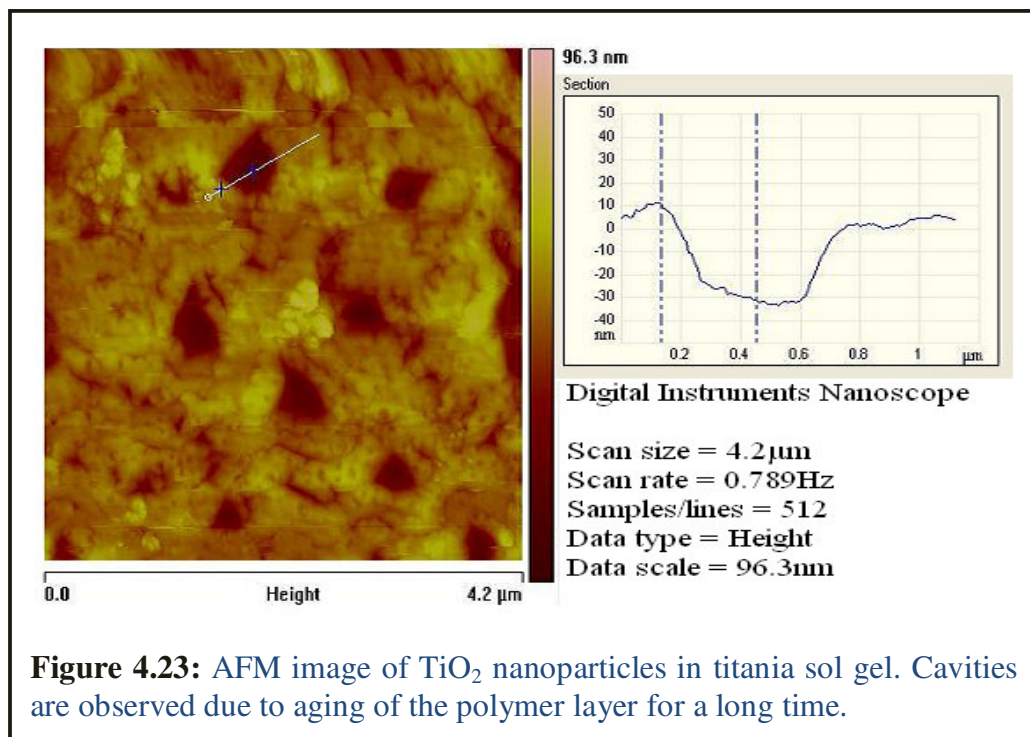
Further heating for even longer a period of time e.g. 76 hours at 80°C causes damage and rupture of the polymer layer as shown in Figure 4.22 instead of revealing further structural changes.



4.3.8 Influence of Humidity

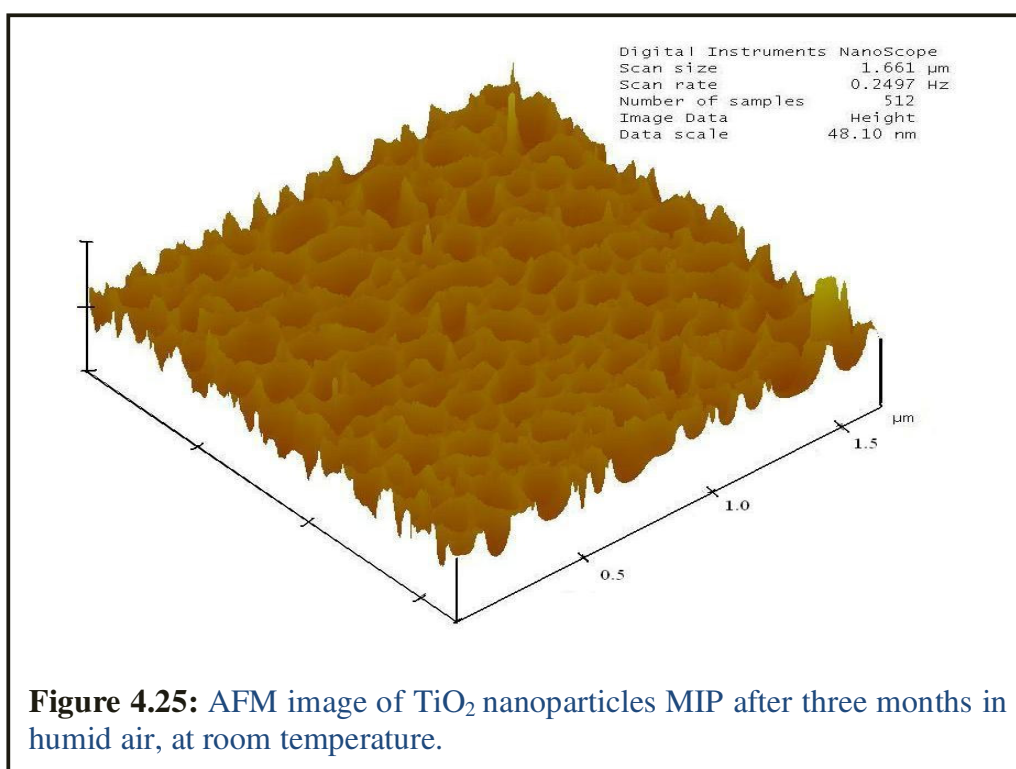
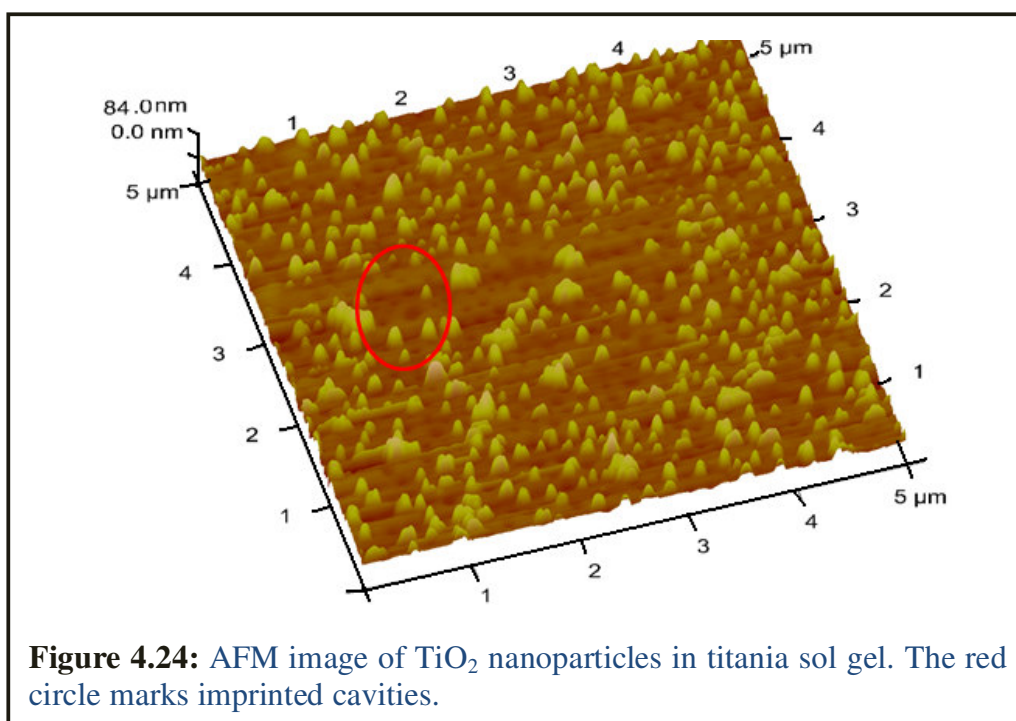
The titania MIPs left at room temperature for several months revealed the AFM image depicted in Figure 4.23. Rather unexpectedly the polymer layer exhibited cavity-like structures that although are too large to stem from individual particles. These structures could have been the result of nanoparticle clusters. Given the storage conditions, relative humidity of air could be regarded being the prime parameter behind this phenomenon.

Section analysis Figure 4.23 further corroborates this observation. The dimensions of the cavities were found to be larger than those of the original



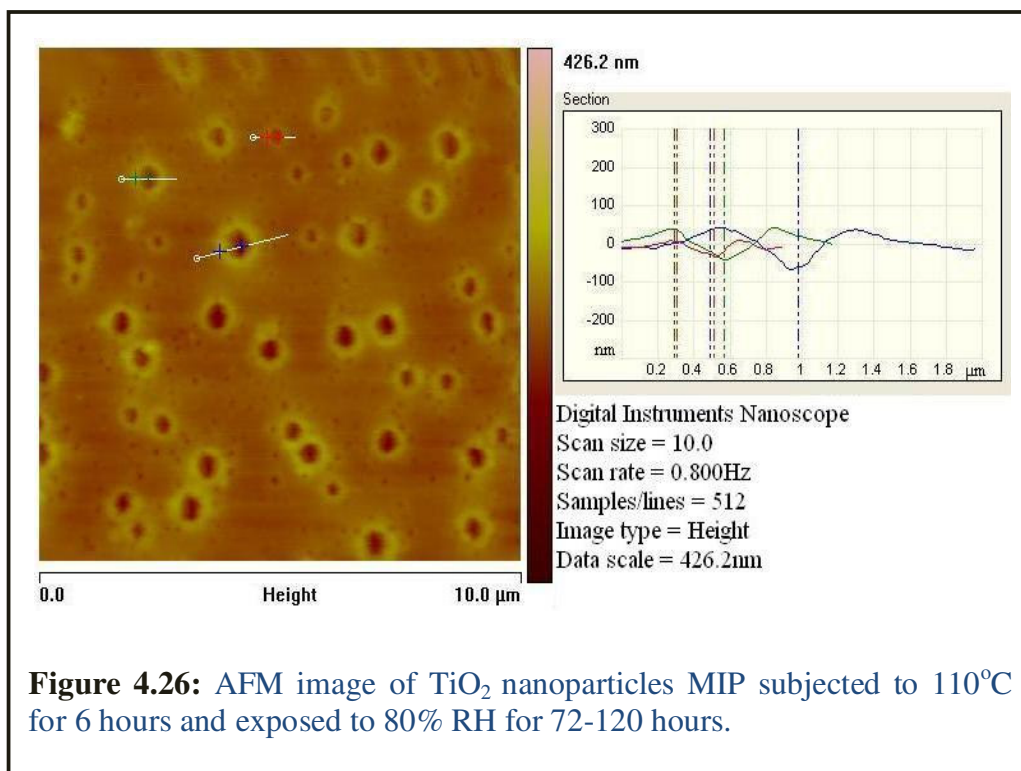
ones particles i.e. from $\sim 100\text{nm}$ to 300nm - 600nm . This can be ascribed to the presence of humidity. Slowly and gradually water molecules continue to deposit on these agglomerates till nanoparticle morphology disintegrates, as has been found in literature.¹⁵⁰ Thus the cavities found in the aged polymer layer are greater in size than originally dispersed particles. The effect of aging was observed as the function of time. Figure 4.24 and 4.25 display the images of Ti nanoparticles on sol gel after 15 days and three months, respectively. In former picture the onset of aging is clearly manifested and after three months hardly any particles is left on the surface. The cavities are $30\text{-}150\text{nm}$ wide and $20\text{-}25\text{nm}$ deep.

4. Titanium Dioxide Nanoparticles Imprinting

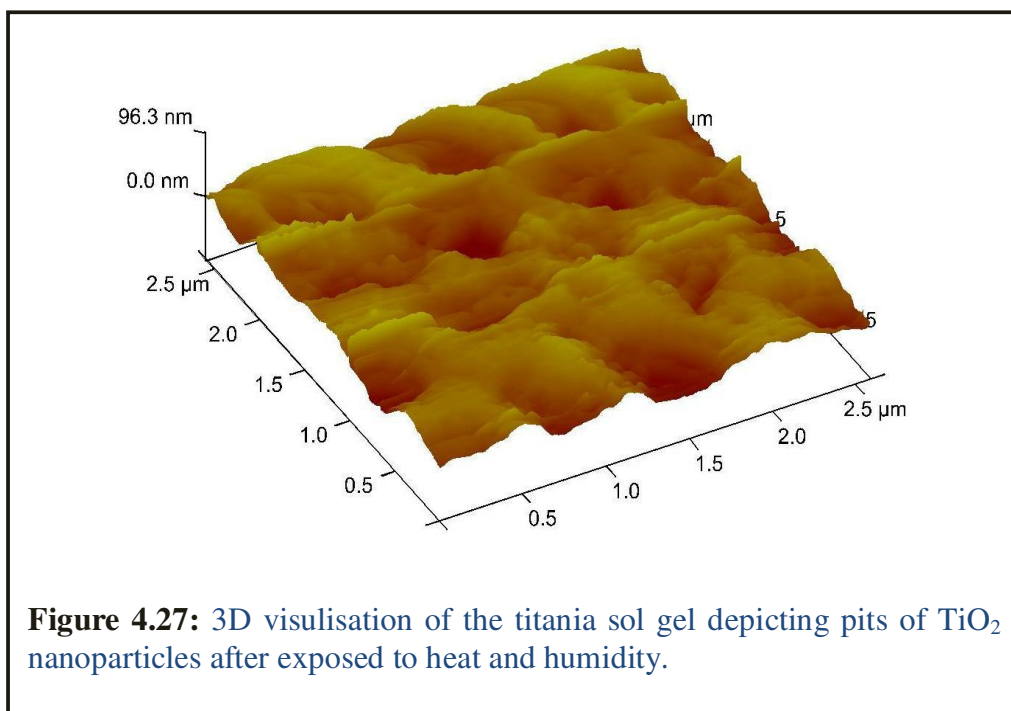


4.3.9 Designing Titanium Dioxide Template Cavities

Two conclusions can be drawn from the nanoparticles imprinting experiments: titania nanoparticles are sensitive to the heat and humidity. Both factors thus are combined for generating the nanoparticle-templated cavities on the polymer surface by first keeping the layers at 110°C for 6 hours following synthesis. After cooling, the substrates are exposed to the air containing 80% relative humidity for 72-120 hours. After this period, the surface of the layers was observed under AFM (Figure 4.26) revealing the



presence of cavities on the polymer surface. Section analysis shows that the lateral dimensions of the structures range from 50-400nm, whereas the depth is found from 50-100nm. For further clarification, Figure 4.27 gives a 3D image showing cavities in the polymer surface.

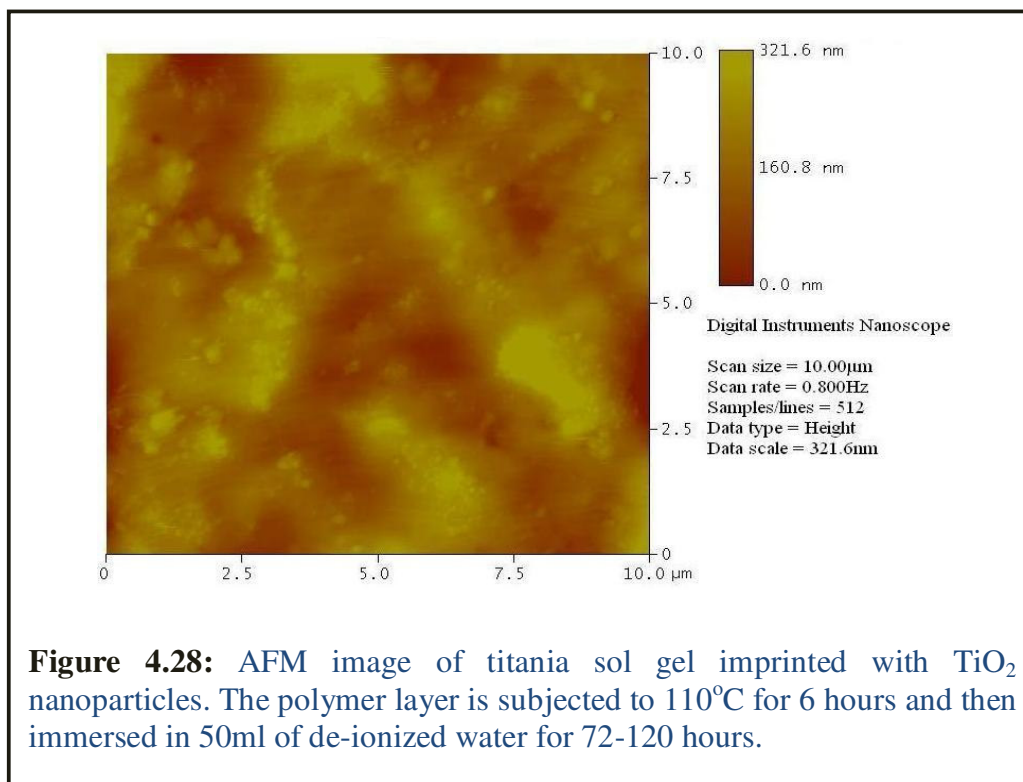


A previous study has confirmed such a transformation of the morphology of primary particles¹⁵¹ under the influence of temperature. The influence of humidity on nanoparticles is more straightforward to understand. At conditions close to the ambient air when relative humidity exceeds 30%, a multilayer of water molecules covers the particle surface.¹⁵² A nanoparticle is instable after fluctuations of the surface area if its surface free energy becomes higher than the critical free energy of particle, which ultimately results in its decay.

4.3.10 Behavior of Nanoparticles in Water

To finally discriminate between the influence of humidity and water, respectively, the polymer layers were dried for 3 hours and heated at 110°C for 6 hours as in previous experiments. Finally, these were immersed in 50ml of de-ionized water for the 3-4 days, which is the same duration as for the

exposure to humid air in previous experiments. The resulting AFM image is displayed in Figure 4.28 and shows that nanoparticles are still embedded in



the polymer matrix. Under the influence of aqueous medium, nanoparticles at some places form agglomerates and the polymer layer shows swelling due to hydration resulting in the overall increased roughness (RMS parameter = 57.88nm). In this case, obviously water molecules enter the interstitial spaces of nanoparticles in bulk. Thus increased their volume but retained their shape.

4.4 Conclusion

The imprinting of titania nanoparticles on polyurethane and Ti sol gel is investigated by AFM. This study reveals and confirms a range of morphological changes. Titania nanoparticles of $50\text{-}120\text{nm}$ in size and polyurethane, Ti sol gel as the substrate matrices are synthesized. When

dispersed in polyurethane, nanoparticles form clusters being $<1\mu\text{m}$ in size. However, after surface imprinting instead of clustering they show swelling reaching diameters up to 400nm. Ti NPs exhibits optimal distribution in Ti sol gel about 50-100nm in diameter. Stamp imprinting of Ti NPs suspension in Ti sol gel, over polyurethane and washing with acid generates cavities about 1-5nm deep. However, direct deposition of NPs on polyurethane/Ti sol gel and washing with acid results in to the leveling of the polymer surface. Heating of NPs at 110°C for 3 hours leads to nanoparticles with diameters of 40-50nm, whereas increasing the heating time to 24 hours induces clustering of these particles to aggregates being 0.1- $2\mu\text{m}$ in diameter. Further heating causes the size of clusters to increase to more than $2\mu\text{m}$ and later to the rupture of polymer layer. The deposition of NPs over Ti sol gel and immediate heating to 110°C produces imprints 10nm deep whereas aging of the polymer layer shows cavities 30-150nm in size. Additionally, heating titania sol-gel drop-coated with titania nanoparticles to 110°C and then keeping them in an atmosphere containing 80% relative humidity produces template cavities 50-400nm in diameter. The polymer layers bearing titanium dioxide nanoparticle cavities prepared in this study can be potentially employed as a transducer for fabricating a titanium dioxide chemical sensor.

Abstract

English: The sensing material plays a pivotal role in the development and successful implementation of a chemical sensor. Molecular imprinting techniques have developed into highly appreciated strategy to actually generate them.

The first part of this dissertation describes the development of artificial receptors for the detection of copper in liquid media. Copper-imprinted polymers are synthesized using β -cyclodextrin, polyvinylphenol and N-vinyl-2-pyrrolidone as the functional monomers. Mass sensitive measurements are carried out with 10MHz quartz crystal microbalances (QCMs), whereas conductance behavior is investigated after drop-coating the polymers on periodic microelectrodes (PME) devices. N-vinyl-2-pyrrolidone, among the three, proved to be the seminal monomer for the imprinting of Cu(II) due to its coordination properties. The coated PME devices respond rapidly to the presence of copper yielding linear sensor characteristics over a wide concentration range (1×10^{-6} to 1×10^{-3} M). $20\mu\text{M}$ is assigned as the lower limit of detection whereas the device exhibits selectivity coefficient of 1:0.31:0.30:0.29:0.15 in the presence of Ni(II), Co(II), Zn(II), and Na(I), respectively as competing ions. This makes the sensor suitable for the determination of copper in natural water samples.

The second part of the dissertation deals with the imprinting of titanium dioxide nanoparticles for the rational designing of surfaces with templated nano moieties. Titania nanoparticles (50-100nm), polyurethane, and titania sol gel as the substrates are synthesized. Two strategies are evaluated for imprinting nanoparticles on the polymer substrates, namely direct and surface imprinting and the morphology is observed by atomic force microscopy. The influence of solvent, heat and humidity on titania nanoparticles imprinted

polymer surfaces has been investigated in detail. Heating of the imprinted titania sol gel polymer surface to 110°C for 6 hours and later keeping at 80% relative humidity for 72-120 hours result in to titanium dioxide template cavities in the dimension of 50-400nm.

Deutsch: Während der Entwicklung und für die erfolgreiche Anwendung von chemischen Sensoren spielt das Sensormaterial eine entscheidende Rolle. Molekulares Prägen stellt dabei eine hoch leistungsfähige Technik für dessen Herstellung dar.

Im ersten Teil dieser Dissertation wird die Entwicklung künstlicher Rezeptoren zur Detektion von Kupfer in flüssiger Phase beschrieben. Hierfür werden Kupfer-geprägte Polymere hergestellt, welche β -Cyclodextrin, Polyvinylphenol und N-Vinyl-2-pyrrolidon als funktionelle Monomere enthalten. Massensensitive Messungen mit diesen Materialien werden mit 10MHz Quarzmikrowagen (engl. quartz crystal microbalances QCMs) durchgeführt, wohingegen Leitfähigkeitsmessungen nach dem Beschichten mit Polymer durch Auftragen eines Tropfens der vorpolymerisierten, verdünnten Lösung auf Periodische Mikroelektroden (engl. periodic microelectrodes PME) realisiert werden können. Unter den drei untersuchten funktionellen Monomeren, hat sich N-vinyl-2-pyrrolidon für das molekulare Prägen mit Cu(II) als das bestgeeignete herausgestellt, was auf seine koordinativen Eigenschaften zurückzuführen ist. Beschichtete PME Bauteile reagieren schnell auf die Anwesenheit von Kupfer und liefern lineare Sensorantworten über einen weiten Konzentrationsbereich (1×10^{-6} bis 1×10^{-3} M). Als unteres Detektionslimit wurde eine Konzentration von 20 μ M bestimmt, wohingegen der Sensor in der Gegenwart der konkurrierenden Ionen Ni(II), Co(II), Zn(II) und Na(I) Selektivitätskoeffizienten von 1:0,31:0,30:0,29:0,15 aufweist. Somit kann dieser Sensor auch zur Bestimmung von Kupfer in realen Wasserproben eingesetzt werden.

Der zweite Teil der vorliegenden Dissertation beschäftigt sich mit der Prägung mittels Titandioxid Nanopartikeln zur gezielten Beeinflussung von Oberflächen mit Templaten im nano-Bereich. Als Substrate werden Titandioxidnanopartikel (50 - 100 nm Durchmesser), Polyurethan und Titandioxid Sol-Gel synthetisiert. Für das Prägen der Nanopartikel auf den Polymersubstraten kommen zwei Strategien zum Einsatz, nämlich die direkte Prägung und die Prägung der Oberfläche. Die Morphologie wird mittels Rasterkraftfeldmikroskop (engl. atomic force microscopy AFM) untersucht. Der Einfluss von Lösungsmitteln, Wärme und Feuchtigkeit auf mit Titandioxid Nanopartikel geprägte Polymerschichten wurde bestimmt. Das Erhitzen der geprägten Titandioxid Sol-Gel Polymer Oberfläche auf 110 °C für sechs Stunden und das anschließende Aufbewahren unter 80 %iger relativer Feuchtigkeit für 72 bis 120 Stunden führt zu Titandioxid Templat Kavitäten in der Größenordnung von 50 - 400 nm.

Abbreviations

AFM	Atomic Force Microscope
AIBN	Azobisisobutyronitrile
ATR	Attenuated total reflection
BAW	Bulk acoustic wave
Cu(II)-IPI	Bivalent copper imprinted polymer system I
Cu(II)-IPII	Bivalent copper imprinted polymer system II
Cu(II)-IPIII	Bivalent copper imprinted polymer system III
DC	Direct current
DMF	Dimethylformamide
DPDI	Diisocyanate diphenylmethane
FT-IR	Fourier transform infra red
IIP	Ion imprinted polymer
IR	Infra red
IUPAC	International Union of Pure and Applied Chemistry
MIP	Molecularly imprinted polymer
NBS	National Bureau of Standards (US)
NIP	Non-imprinted polymer
NPs	Nanoparticles
NVP	N-vinyl-2-pyrrolidone
PDMS	Polydimethylsiloxane
PME	Periodic microelectrodes
PME-IP	Ion-imprinted polymer layer coated periodic microelectrodes device
PMMA	Polymethylmethacrylate
PU	Polyurethane
PVP	Polyvinylphenol

QCM	Quartz crystal microbalance
QCM-IP	Ion-imprinted layer polymer coated quartz crystal microbalance device
SAM	Self assembled monolayer
SAW	Surface acoustic wave
TEGMA	Triethylene glycol trimethacrylate
THF	Tetrahydrofurane
TMPTMA	Trimethylol propane trimethacrylate
TSM	Thickness shear mode

References

- 1 Simon, E. *Meas. Sci. Technol.* **2010**, *21*, 112002.
- 2 Guenther, M.; Gerlach, G. *Springer Series on Chemical Sensors and Biosensors (Hydrogel Sensors and Actuators)*, Springer-Verlag Berlin Heidelberg, **2009**, 165.
- 3 Kellner, R.; Mermet, J-M.; Otto, M.; Widmer, H.M. *Analytical Chemistry: The Authentic Text to the FECS Curriculum Analytical Chemistry*, Wiley-VCH, Weinheim, **1998**, 359.
- 4 Hulanicki, A.; Ingman, F. *Pure Appl. Chem.* **1991**, *63*, 1247.
- 5 Grüdler, P. *Chemical Sensors; An Introduction for Scientists and Engineers*, Springer-Verlag Berlin Heidelberg, **2007**, 3-12, 7.
- 6 Chiba, A. *Development of the TGS Gas Sensor in Chemical Sensor Technology*, S. Yamauchi (ed.), Tokyo, Kodansha Ltd. **1992**, *4*, 1.
- 7 Curie, P.; Curie, J. *Développement, par pression, de l'électricité polaire dans les cristaux hémiedres á faces inclinées*, C.R.T. **1880**, *91*, 294.
- 8 Bense, E.; Gröschl, M.; Burger, W.; Schmid, M. *Sens. Actuators A* **1995**, *48*, 1.
- 9 Drafts, B. *IEEE Transactions on Microwave Theory and Techniques* **2001**, *49*, 795.
- 10 Zhou, R.; Hierlemann, A.; Weimar, U.; Göpel, W. *Sens. Actuators, B* **1996**, *34*, 356.
- 11 Park, S.; Kang, J.; Park, J.; Mun, S. *Sens. Actuators, B* **2001**, *B76*, 322.
- 12 Narakathu, B. B.; Atashbar, M. Z.; Bejcek, B. *Sens Lettr.* **2011**, *9*, 872.

- 13 Shul'gas, A. A.; Soldatkin, A. P.; El'skaya, A. V.; Dzyadevich, S. V.; Patskovsky, S. V.; Strikha, V. I. *Biosens. Bioelectron.* **1994**, 9, 217.
- 14 Bottom, V.E. *Introduction to Quartz Crystal Unit Design*. Van Nostrand Reinhold, Newyork, **1982**, 3.
- 15 Lucklum R.; Eichelbaum F. Interface Ciruits for QCM Sensors, *Springer Series Chemical Sensors and Biosensors*, Springer-Verlag Berlin Heidelberg, **2006**, 5, 3.
- 16 Sullivan, D.B. *Time and Frequency Measurement at NIST: the First Hundred Years. IEEE International Frequency Control Symposium and PDA Exhibition* **2001**, 4.
- 17 Wulff, G.; Sarhan, A. *Angew. Chem. Int. Ed.* **11**, **1972**, 341.
- 18 Arshady, R.; Mosbach, K. *Macromol. Chem.* **1981**, 182, 687.
- 19 Yang, Z-P.; Zhang, C-J *Sens. Actuators, B* **2009**, 142, 210.
- 20 Malitesta, C.; Losito, I.; Zambonin, P. G. *Anal Chem.* **1999**, 7, 1366.
- 21 Dickert, F. L.; Tortschanoff, M.; Bulst, W. E.; Fischerauer, G. *Anal. Chem.* **1999**, 71, 4559.
- 22 Lee, S-W.; Kunitake, T. *Mol. Cryst. Liq. Cryst. Sci. Technol., Section A: Mol. Cryst. Liq. Cryst.* **2001**, 371, 111.
- 23 Dickert, F.; Hayden, O.; Lieberzeit, P.; Palfinger, C.; Pickert, D.; Wolff, U.; Scholl, G. *Sens Actuators. B* **2003**, B9, 20.
- 24 Lieberzeit, P. A.; Glanznig, G.; Jenik, M.; Gazda-Miarecka, S.; Dickert, F. L.; Leidl, A. *Sensors*, **2005**, 5, 509.
- 25 Dickert, F. L.; Hayden, O.; Lieberzeit, P.; Haderspoeck, C.; Bindeus, R.; Palfinger, C.; Wirl, B. *Synth. Met.* **2003**, 138, 65.
- 26 Das, K.; Penelle, J.; Rotello, V. M. *Langmuir* **2003**, 19, 3921.

- 27 Dickert, F.L. *Anal. Bioanal. Chem.* **2007**, 389, 353.
- 28 Feng, L.; Liu, Y.; Zhou, X.; Hu, J. *J. Colloid Interface Sci.* **2005**, 284, 378.
- 29 Matsuguchi, M.; Uno, T. *Sens. Actuators, B* **2006**, B113, 94.
- 30 Tan, Y.; Yin, J.; Liang, C.; Peng, H.; Nie, L.; Yao, S. *Bioelectrochemistry*, **2001**, 53, 141.
- 31 Kugimiya, A.; Takeuchi, T. *Electroanalysis* **1999**, 11, 1158.
- 32 Ersoz, A.; Denizli, A.; Ozcan, A.; Say, R. *Biosens. Bioelectron.* **2005**, 20, 2197.
- 33 Tai, D.-F.; Lin, C.-Y.; Wu, T.-Z.; Huang, J.-H.; Shu, P.-Y. *Clinical Chem.* **2006**, 52, 1486.
- 34 Whitcombe, M.J.; Rodriguez, M.E.; Villar, P.; Vulfson, E.N. *J. Am. Chem. Soc.* **1995**, 117, 7105.
- 35 Dickert, F.L.; Hyden, O. *Anal. Chem.* **2002**, 74, 1302.
- 36 Lieberzeit, P.A.; Afzal A.; Glanzing G.; Dickert, F.L. *Anal. Bioanal. Chem.* **2007**, 389, 41
- 37 Tai, D.F.; Lin, C.Y. Wu, T.Z. Chen, L.Y. *Anal Chem.* **2005**, 77, 5140.
- 38 Hill, S. J.; Arowolo, T. A.; Butler, O. T.; Chenery, S. R. N.; Cook, J. M.; Cressar, M. S.; Miles, D. L. *J. Anal. At. Spectrom.* **2002**, 17, 284.
- 39 Sreenivasa Rao, K.; Balaji, T.; Prasada Rao, T.; Babu, Y.; Naidu, G. *Spectrochim. Acta, Part B* **2002**, 57, 1333.
- 40 Kang, S. W.; Park, C. M.; Cho, K. H.; Han, H. S. *Bull. Korean Chem. Soc.* **1993**, 14, 59.
- 41 Janssen, L. J. J.; Koene, L. *Chem. Eng. J.* **2002**, 85, 137.
- 42 Rottmann, L.; Heumann, K. G. *Anal. Chem.* **1994**, 66, 3709.

- 43 Altenau, A. G.; Rogers, L. B. *Anal. Chem.* **1964**, *36*, 1726.
- 44 Starodub, N.; Kanjuk, N.; Kukla, A.; Shirshov, Y. M. *Anal. Chim. Acta* **1999**, *385*, 461.
- 45 Sarkar, M.; Das, M.; Datta, P. K. *J. Colloid Interface Sci.* **2002**, *246*, 263.
- 46 Zhu, X.; Xu, L.; Lou, Y.; Yu, H.; Li, X.; Blake, D. A.; Liu, F. *J. Agric. Food Chem.* **2007**, *55*, 7648.
- 47 Palacios, M. A.; Wang, Z.; Montes, V. A.; Zyryanov, G. V.; Anzenbacher, P. *J. Am. Chem. Soc.* **2008**, *130*, 10307.
- 48 Knecht, M.; Sethi, M. *Anal. Bioanal. Chem.* **2009**, *394*, 33.
- 49 Lee, J. S.; Han, M. S.; Mirkin, C. A. *Angew. Chem. Int. Ed.* **2007**, *46*, 4093.
- 50 Kim, Y.; Johnson, R. C.; Hupp, J. T. *Nano Letters* **2001**, *1*, 165.
- 51 Yoosaf, K.; Ipe, B. I.; Suresh, C. H.; Thomas, K. G. *J. Phys. Chem. C* **2007**, *111*, 12839.
- 52 Cathell, M. D.; Szewczyk, J. C.; Bui, F. A.; Weber, C. A.; Wolever, J. D.; Kang, J.; Schauer, C. L. *Biomacromolecules* **2007**, *9*, 289.
- 53 Li, G.; Zhang, L.; Li, Z.; Zhang, W. *J. Hazard. Mater.* **2010**, *177*, 983.
- 54 Huang, G.; *US Patent App.* 20,090/107, 217, **2008**.
- 55 Casilli, S.; Malitesta, C.; Conoci, S.; Petralia, S.; Sortino, S.; Valli, L. *Biosens. Bioelectron.* **2004**, *20*, 1190.
- 56 Kim, Y. S.; Kim, S. H.; Son, Y. A. *Mol. Cryst. Liq. Cryst.* **2010**, *519*, 90.
- 57 Egorov, V. M.; Smirnova, S. V.; Formanovsky, A. A.; Pletnev, I. V.; Zolotov, Y. A. *Anal. Bioanal. Chem.* **2007**, *387*, 2263.

- 58 Schauer, C. L.; Mu-San Chen; Price, R. R.; Schoen, P. E.; Ligler, F. S. *Environ. Sci. Technol.* **2004**, *38*, 4409.
- 59 Daniel, M. C.; Astruc, D. *Chem. Rev.* **2004**, *104*, 293.
- 60 Sun, Y.; Xia, Y. *Science* **2002**, *298*, 2176.
- 61 Ahmadi, T. S.; Wang, Z. L.; Green, T. C.; Henglein, A.; El-Sayed, M. A. *Science* **1996**, *272*, 1924.
- 62 Sun, S.; Murray, C.; Weller, D.; Folks, L.; Moser, A. *Science* **2000**, *287*, 1989.
- 63 Tang, Z.; Kotov, N. A.; Giersig, M. *Science* **2002**, *297*, 237.
- 64 Peng, T.; De Zhao; Dai, K.; Shi, W.; Hirao, K. *J. Phy. Chem. B* **2005**, *109*, 4947.
- 65 Liu, S.; Dai, Z.; Chen, H.; Ju, H. *Biosens. Bioelectron.* **2004**, *19*, 963.
- 66 Schubert, D.; Dargusch, R.; Raitano, J.; Chan, S. W. J. *Biochem. Biophys. Res. Com.* **2006**, *342*, 86.
- 67 Lu, Y.; Yin, Y.; Mayers, B. T.; Xia, Y. *Nano Letters* **2002**, *2*, 183.
- 68 Carnes, C. L.; Stipp, J.; Klabunde, K. J.; Bonevich, J. *Langmuir* **2002**, *18*, 1352.
- 69 Fernández-Urrusuno, R.; Calvo, P.; Remuñán-López, C.; Vila-Jato, J. L.; José Alonso, M. *Pharmaceut. Res.* **1999**, *16*, 1576.
- 70 Fujishima, A.; Honda, K. *Nature* **1972**, *238*, 37.
- 71 Antonelli, D. M.; Ying, J. Y. *Angew. Chem., Int. Ed.* **1995**, *34*, 2014.
- 72 Campbell, L.; Na, B.; Ko, E. *Chem. Mater.* **1992**, *4*, 1329.
- 73 Gu, Z. Z.; Kubo, S.; Qian, W.; Einaga, Y.; Tryk, D. A.; Fujishima, A.; Sato, O. *Langmuir* **2001**, *17*, 6751.

- 74 Wang, F.; Jiu, J.; Pei, L.; Nakagawa, K.; Isoda, S.; Adachi, M. *Mat. Lett.* **2007**, 61, 488.
- 75 Swamy, V.; Kuznetsov, A.; Dubrovinsky, L. S.; Caruso, R. A.; Shchukin, D. G.; Muddle, B. C. *Phys. Rev. Lett. B* **2005**, 71, 184302.
- 76 Frausto da Silva, J.J.R.; Williams, R.J.P. *The Biological Chemistry of the Elements*, Oxford University Press Inc. NewYork, **1991**.
- 77 Davis, C.D. *J. Nutr.* **2003**, 133, 522.
- 78 Institute of Medicine, *Dietary Reference Intakes for Vitamin A, Vitamin K, Arsenic, Boron, Chromium, Copper, Iodine, Iron, Manganese, Molybdenum, Nickel, Silicon, Vanadium, and Zinc*. National Academy Press: Washington DC, **2001**.
- 79 World Health Organization, *Guidelines for Drinking-Water Quality*, **2004**.
- 80 Saeed, M.M.; Bajwa, S.Z.; Ansari, M.S.; Ahmed, R. *J. Chin. Chem. Soc.* **2007**, 54, 173.
- 81 Guo, X.; Yun, Y.; Shanov, V. N.; Halsall, H. B.; Heineman, W. R. *Electroanalysis* **2011**, 23, 1252.
- 82 Kim, M. L.; Tudino, M. B. *Talanta* **2010**, 82, 923.
- 83 Sacmaci, S.; Kartal, S. *Microchim. Acta* **2010**, 170, 75.
- 84 Ichinoki, S.; Sasai, S.; Sugai, H.; Fujii, Y. *J. Liq. Chromatogr. Relat. Technol.* **2009**, 32, 3066.
- 85 He, L-J.; Zhang, K-G.; Wang, C-J.; Luo, X-L.; Zhang, S-S. *J. Liq. Chromatogr. A* **2011**, 1218, 3595.
- 86 Matoso, E.; Cadore, S. *Talanta* **2011**, 84, 335.
- 87 Eksperiandova, L. P.; Blank, A. B.; Makarovskaya, Y. N. *X-ray Spectrom.* **2002**, 3, 259.

- 88 Nishide, H.; Deguchi, J. *Chem. Lett.* **1976**, 169, 11.
- 89 Nishide, H.; Tsuchida, E. *Macromol. Chem.* **1976**, 177, 2295.
- 90 Efendiev, A.A.; Kabanov, V.A. *Pure Appl. Chem.* **1982**, 54, 2077.
- 91 Ohga, K.; Kurauchi, Y.; Yanase, H. *Bull. Chem. Soc., Jpn.* **1987**, 60, 444.
- 92 Kato, M.; Nishide, H.; Tsuchida, E. *J. Polym. Sci. (Polym. Chem. Ed.)* **1981**, 19, 1803.
- 93 Gupta, S.N.; Neckers, D.C. *J. Polym. Sci. Polym. Chem. (Polym. Chem. Ed.)* **1982**, 20, 1609.
- 94 Kuchen, W.; Schram, J. *Angew. Chem. Int. Ed. Engl.* **1988**, 27, 1695.
- 95 Yu, K.Y.; Tsukagoshi, K. ; Maeda, M.; Takagi, M. *Anal. Sci.* **1992**, 8, 701.
- 96 Birlik, E.; Ersöz, A.; Denizil, A.; Say, R. *Anal. Chim. Acta* **2006**, 565, 145.
- 97 Li, F.; Du, P.; Chen, W.; Zhang, S. *Anal. Chim. Acta* **2007**, 585, 211.
- 98 Rao, T.P.; Kala, R.; Daniel, S. *Anal. Chim. Acta* **2006**, 578, 105.
- 99 Etorki, A.M.; Hillman, A.R.; Ryder, K.S.; Glidle, A. *J. Electroanal. Chem.* **2007**, 599, 275.
- 100 Latif, U.; Mujahid, A.; Afzal, A.; Sikorski, R.; Lieberzeit, P. A.; Dickert, F. L. *Anal. Bioanal. Chem.* **2011**, 400, 2507.
- 101 Szejtli, J.; Osa, T. *Comprehensive Supramolecular Chemistry, Vol. 3, Pergamon, Oxford*, **1996**.
- 102 Jiang, Y.; Du, L.; Wu, Y.; Liu, X.; Gang, J.; Lu, F. *Polymer Preprints (American Chemical Society, Division of Polymer Chemistry)* **2006**, 47, 311.
- 103 Saks, N.S. *Solid State Electron.* **1975**, 18, 737.

104. Nicholls, I.A.; Adbo, K.; Andersson, H.S.; Anderson, P.O.; Ankerloo, J.; Hein-Dahlstrom J.; Jkela, P.; Karlsson, J.G.; Olofsson, I.; Rosengren, J.; Shoravi, S.; Svenson, J.; Wikman, S. *Anal Chim. Acta* **2001**, 435, 9.
- 105 Barbucci, R.; Casolaro, M.; Maguari, A. *Macromol Chem* **1989**, 190, 2627.
- 106 Hu, J-C.; Cao, Y.; Yang, P.; Deng, J-F.; Fan, K-N. *J. Mol. Catal. A: Chem.* **2002**, 85, 1.
- 107 Wiles, A. B.; Bozzuto, D.; Cahill, C.L.; Pike, R.D. *Polyhedron* **2006**, 25 776.
- 108 Downing, R.S.; Urbach, F.L. *J. Am. Chem. Soc.* **1969**, 91, 5977.
- 109 Amundsen, A.R.; Whelan, J. ; Bosnich, B. *J. Am. Chem. Soc.* **1977**, 99, 6730.
- 110 Parker, D.; Davies, E.S.; Wilson, C.; McMaster J. *Inorg. Chim. Acta* **2007**, 360, 203.
- 111 Murugesan, R.; Subramanian, E. *Mater. Chem. Phys.* **2002**, 77, 860.
- 112 Yu, G.Y.; Janata J *Anal. Chem.* **2008**, 80, 2751.
- 113 Shana, Z. A.; Josse, F. *Anal. Chem.* **1994**, 66, 1955.
- 114 Dunham, G. C.; Benson, N. H.; Petelenz, D.; Janata, J. *Anal. Chem.* **1995**, 67, 267.
- 115 Kanazawa, K. K.; Melroy, O. R. *IBM J. Res. Dev.* **1993**, 37, 157.
- 116 Yang, B.; Kong, J. *Chem. Lett.* **2009**, 38, 1072.
- 117 Lin, J.; Moeller, S.; Obermeier, E. *Sens. Actuators, B* **1991**, B5, 223.
- 118 Nanoparticle Technology handbook, edited by Masuo Hosokawa, Kiyaooshi Nogi, Makio Naito, Toyokazu Yokoyama, Elsevier, **2007**.

- 119 Kung, H.H. *Transition Metal Oxides: Surface Chemistry and Catalysis*; Elsevier: Amsterdam, **1989**.
- 120 Hensrich, V.E.; Cox, P.A. *The Surface Chemistry of Metal Oxides*; Cambridge University Press: UK, **1994**.
- 121 Ayyub, P.; Palkar, V. R.; Chattopadhyay, S.; Multani, M. *Physical Review B* **1995**, *51*, 6135.
- 122 Maldoti, A.; Molinari, A.; Amadeni, R. *Chem. Rev.* **2002**, *102*, 3811.
- 123 Forzatti, P. *Catal. Today* **2000**, *62*, 51.
- 124 Hoffman, M.R.; Martin, S.T.; Choi, W. Bahneman, D.W.; *Chem. Rev.* **1995**, *95*, 69.
- 125 Johnson, R.W.; Thieles, E.S.; French, R.H. *TAPPI. J.* **1997**, *80*, 233.
- 126 Kalyanasendevan, K.; Gratzel, M.; *Optoelectronics Properties of Inorganic Compounds*; p. 169-194; Roundhill, D.M.; Fackler, J.P. (Editors); Plenum, New York, **1999**.
- 127 Bonhole, P.; Gogniat, E.; Gratzel, M.; Ashrit, P.V. *Thin Solid Films* **1999**, *350*, 269.
- 128 Sheveglieri, G. (Editor); *Gas sensors*; Kluwer, Dordrecht, **1992**.
- 129 Phillips, L.G.; Barbeno, D.M. *J. Dairy Sci.* **1997**, *80*, 2726.
- 130 Selhofer, H. *Vacuum Thin Films* **1999**, *15*.
- 131 Fujishima, A.; Rao, T.N.; Tryk, D.A. *J. Photochem. Photobiol. C: Photochem.Rev.* **2000**, *1*, 1.
- 132 Watanabe, E.; Nishizawa, K.; Miki, T.; Taoda, H. *Skin Damage by Different Shapes of Photocatalyst Nanoparticles*; John Wiley & Sons, Inc., **2010**.

- 133 Liu R, Zhang X, Pu Y, Yin L, Li Y, Zhang X, Liang G, Li X, Zhang J. *J. Nanosci. Nanotechnol.* **2010**, *10*, 5161.
- 134 Caruso, F.; Möhwald, H. *Langmuir* **1999**, *15*, 8276.
- 135 Vickerman, J. C.; Gilmore, I. S. *Surface analysis: the principal techniques*; Wiley Online Library, **2009**.
- 136 Weinekötter, R.; Gericke, H.; *Mixing of Solids*, Kluwer Academic Publishers, Dordrecht, the Netherlands, **2000**, 15.
- 137 De Jonge, N.; Lamy, Y.; Schoots, K.; Oosterkamp, T. H. *Nature* **2002**, *420*, 393.
- 138 Tom, J.W.; Debenedetti, P.G. *Biotechnol. Prog.* **1991**, *7*, 403.
- 139 Caruso, F.; Furlong, D. N.; Ariga, K.; Ichinose, I.; Kunitake, T. *Langmuir* **1998**, *14*, 4559.
- 140 Wei, D.; Dave, R.; Pfeffer, R. *J. Nanopart. Res.* **2002**, *4*, 21.
- 141 Jalili, N.; Laxminarayana, K. *Mechatronics* **2004**, *14*, 907.
- 142 Scaif, J.; West, P. *Introduction to Characterization of Nanoparticles with AFM-Part I*, Pacific Nanotechnology, 3350 Scott Blvd., Santa Clara, CA 95054.
- 143 Hidehiro, K.; Iijima, M. *Sci. Technol. Adv. Mater.* **2010**, *11*, 044304.
- 144 Lieberzeit, P.A.; Afzal, A.; Glanzing, G.; Dickert, F.L. *Ana. Bioanal. Chem.* **2007**, 389, 441.
- 145 Mialon, G. G., M.; Gacoin, T.; Boilot, J-P. *Nano* **2008**, *12*, 2505.
- 146 Hongwei, G.; Ruixiang, P.; Shikui, H.; Xianhong, G.; Mingtai, W. *J. Elec. Mat.* **2010**, *39*, 2346.
- 147 Zhang, D.; Qi, L.; Ma, J.; Cheng, H. *J. Mater. Chem.* **2002**, *12*, 3677.

- 148 Kovalenko, G.A.; Vanina, M.P. *Zav. Labor (Diagnostika Materialov)* **1998**, 65, 43.
- 149 Wu, M.M.; Long, J.B.; Hung, A.H.; Luo, Y.J.; Feng, S.H.; Xu, R.R. *Langmuir* **1999**, 15, 8822.
- 150 Keller, K.K.; Wang, H.; Zhou, D.; Lenihan, H.S.; Cherr, G.; Cardinale, B.J.; Miller, R.; Ji, Z. *Environ. Sci. Technol.* **2010**, 44, 1962.
- 151 Oskam, G.; Nellore, A.; Penn, R.L.; Searson, P.C. *J Phys. Chem. B*, **2003**, 107, 1734.
- 152 Kozlov, D.V.; Panchenko, A.A.; Bavykin, D.V.; Savinov, E.N.; Smirniotis, P.G. *Russian Chem. Bull. (Int. Ed.)* **2003**, 52, 1100.

Curriculum Vitae

Name : **Sadia Zafar Bajwa**

Date of Birth: 11th July, 1977

Academic Profile

PhD Scholar in Chemistry (on going since July 2008) Department of Analytical Chemistry, University of Vienna, Vienna, Austria

Master of Philosophy (M.Phil) in Physical Chemistry (2002) Quaid-i-Azam University, Islamabad, Pakistan

Master of Science (M.Sc.) in Physical Chemistry (1999) Government College, Sargodha, in affiliation with The University of Punjab, Lahore, Pakistan

Bachelors of Science (B.Sc.) (1997) in Botany, Chemistry, and Zoology Government College for Women, Sargodha, in affiliation with The University of Punjab, Lahore, Pakistan

Higher Secondary School Certificate (HSSC) Examination (1995) Premedical Group Government College for Women, Sargodha, in affiliation with Sargodha Board, Pakistan

Secondary School Certificate (SSC) Examination Science Group(1993) Govt. Comprehensive Girls High School, Sargodha, in affiliation with Sargodha Board, Pakistan

Distinction:

- Merit Scholarship in FSc, BSC, MSC, and M.Phil
- First among all candidates of Botany, Chemistry, and Zoology group of B.SC. thought out Punjab, Pakistan
- Gold medal for first position among all M.Sc. candidates of The University of Punjab and science colleges of Punjab, Pakistan
- Higher Education Commission Overseas Scholarship for PhD studies